Tetraphenylporphyrin dimers

An optical and magnetic resonance study

Promotor: **dr. T. J. Schaafsma**
hoogleraar in de moleculaire fysica

L. Benthem

Tetraphenylporphyrin dimers

An optical and magnetic resonance study

Proefschrift

ter verkrijging van de graad van
doctor in de landbouwwetenschappen,
op gezag van de rector magnificus,
dr. C. C. Oosterlee,
in het openbaar te verdedigen
op vrijdag 12 oktober 1984
des namiddags te vier uur in de aula
van de Landbouwhogeschool te Wageningen

ISN = 154533-03

The author permitted to see the grand Academy of Lagado. The Academy largely described.

The first man I saw was of meagre aspect, with sooty hands and face, his hair and beard long, ragged and singed in several places. His clothes, shirt, and skin were all of the same colour. He had been eight years upon a project for extracting sunbeams out of cucumbers, which were to be put into vials hermetically sealed, and let out to warm the air in raw inclement summers. He told me, he did not doubt in eight years more, that he should be able to supply the Governor's gardens with sunshine at a reasonable rate; but he complained that his stock was low, and entreated me to give him something as an encouragement to ingenuity, especially since this had been a very dear season for cucumbers.

Jonathan Swift in GULLIVER'S TRAVELS.

Eigenlijk zijn er maar twee dingen
waar Foefje nooit aan zal wennen-
en dat zijn tweelingen.

De Bescheurkalender
Van Kooten & De Bie
Vrijdag 12 oktober 1984

STELLINGEN.

1. *De mogelijkheid van een kleine tunnelingsfrequentie voor de rotatie van de methylgroep in de laagste* $n\pi^*$ *triplet toestand van toluchinon is niet voldoende onderzocht. Deze mogelijkheid is niet in tegenspraak met ENDOR experimenten van het* $|-1,A\rangle$ *niveau.*

   J.H. Lichtenbelt and D.A. Wiersma, Chem.Phys., 39 (1979) 161-172

2. *De suggestie dat de CP-MAS techniek een bijdrage zou kunnen leveren bij de selectie van granen is ongerechtvaardigd. De interpretatie van MAS-NMR spectra met behulp van moleculaire interacties tussen verschillende graaneiwitten is sterk aan twijfel onderhevig.*

   I.C. Baianu and H. Förster, J.Appl.Biochem., 2 (1980) 347-354

   J.D. Schofeld and I.C. Baianu, Cereal Chemistry, 59 (1982) 240-245

3. *Het gebruik van gefluorideerde verbindingen biedt waarschijnlijk grotere mogelijkheden voor de studie van weefsel perfusie m.b.v. NMR dan het gebruik van de in het bloed aanwezige protonen.*

   B. Vinocur, Diagnostic Imaging, march 1984, p. 49-52

4. *De conclusie van Gückel et al. dat het excitonmodel op bis-zink-porfyrine dimeren mag worden toegepast, teneinde informatie over de geometrie te verkrijgen, is op grond van hun eigen experimentele gegevens onjuist.*

F. Gückel, D. Schweitzer, J.P. Collman, S. Bencosme, E. Evitt and J. Sessler, Chem.Phys., 86 (1984) 161-172

Dit proefschrift, hoofdstuk 4.

5. *Bij de berekening van de donor - acceptor afstand in gemengde dimeren, gebruiken Anton et al. irreële waarden voor de oriëntatiefactor van de donor en acceptor.*

J.A. Anton, P.A. Loach and Govindjee, Photochem.Photobiol., 28 (1978) 235-242

Dit proefschrift, hoofdstuk 4.

6. *Uit een oogpunt van vroegtijdige opsporing van complicaties tijdens een zwangerschap dient echodiagnostiek terminste éénmaal te worden uitgevoerd bij prenatale controle.*

7. *Het verschijnsel van de zure regen maakt het gebruik van regentonnen en andere commercieel verkrijgbare systemen voor de verzorging van kamerplanten minder aanbevelenswaardig.*

8. *Bij een dreigende vroeggeboorte lijkt een verblijf op een afdeling met de naam 'Verloskunde' geen goede verblijfplaats.*

L. Benthem - Tetraphenylporphyrin Dimers.

Wageningen, 12 oktober 1984

CONTENTS: Page

LIST OF ABBREVIATIONS AND SYMBOLS.

A	in formulae: arbitrary constant
a	outer radius of inner conductor
B	magnetic field vector
B-states	Soret absorption states
b	inner radius of outer conductor
CI	configuration interaction
c	velocity of light
c_i	amplitude of sublevel |i>
cw	continuous wave
D	zero field splitting parameter
DMF	dimethylformamid
DMSO	dimethylsulfoxide
E	energy
ΔE	difference in energy
E	zero field splitting parameter
EPR	electron paramagnetic resonance
ET	energy transfer
FDMR	fluorescence detected magnetic resonance
FF	fluorescence fading
FWHM	full width at half maximum
f	relative amplitude
g	g-factor of free electron
HOMO	highest occupied molecular orbital
ΔH_{pp}	peak-peak broadening in magnetic field units of EPR-lines
δH_{pp}	peak-peak broadening in magnetic field units of EPR-lines, due to spin-spin interaction
H_2-TPP	free-base tetraphenylporphyrin
h	Planck's constant
I	intensity
|i>	triplet sublevel in general i = x, y, z in zero field i = -1, 0, 1 in high magnetic field

I_0	excitation light intensity (in photons.cm^{-2}.s^{-1})
I_f	fluorescence intensity (in Einstein.cm^{-3}.s^{-1})
$I_f(t)$	time dependent fluorescence intensity
ΔI_f	change in fluorescence intensity
δI_f	relative change in fluorescence intensity
ISC	intersystem crossing
k_{ex}	rate constant for excitation, contains excitation light intensity (in s^{-1})
k_f	rate constant for fluorescence (in s^{-1})
k_i	decay rate constant of triplet sublevel $\|i\rangle$ (in s^{-1})
k_{ISC}	rate constant for intersystem crossing (in s^{-1})
k_T	mean decay rate constant of $T_0 \rightarrow S_0$ (in s^{-1})
LUMO	lowest unoccupied molecular orbital
M_i	transition dipole moment i
MO	molecular orbital
MTHF	3- methyl tetrahydrofuran
N	total number of molecules in a sample
N_{AV}	Avogadro's number
NMR	nuclear magnetic resonance
n	refractive index
n_i	relative population of denoted sublevel
ODMR	optically detected magnetic resonance
P	porphin
P	transition probability
P_i	populating rate of denoted sublevel (in mol.l^{-1}.s^{-1})
p_i	relative populating rate of denoted sublevel (dimensionless)
Q-states	Q_x and Q_y absorption states
r	distance
S	spin angular momentum of the electron
S_0	ground state
S_1	first excited singlet state
S/N	signal-to-noise ratio
T_0	lowest triplet state
THF	tetrahydrofuran
TLC	thin layer chromatography
TPP	meso tetraphenylporphyrin
TTP	meso tetratolylporphyrin
U	unit vector

V	exciton splitting
X, Y, Z	eigenvalues of zero field spin Hamiltonian
x, y, z	coordinates w.r.t. molecular frame of reference
$\|x\rangle, \|y\rangle, \|z\rangle$	triplet sublevels, in absence of magnetic field
Z_0	characteristic impedance
ZFS	zero field splitting
α	angle
γ	dimensionless parameter
γ	magnetogyric ratio
ε	extinction coefficient (in $l.mol^{-1}.cm^{-1}$)
ε_r	relative dielectric contant ($\varepsilon_{vacuum} = 1$)
Θ	angle
κ	orientation factor
λ	radiation wavelength
μ	transition dipole moment
μ_0	magnetic permeability of vacuum
μ_r	relative permeability ($\mu_{vacuum} = 1$)
υ	frequency
$\Delta\upsilon$	difference in frequency
τ	lifetime, defined as the time elapsed after a quantity has decreased to 1/e of its original value through exponential decay
ϕ	angle
ϕ_{ET}	quantum efficiency for energy transfer
ϕ_f	fluorescence quantum yield
ϕ_T	triplet yield
ψ	angle
Ω	overlap integral

Chapter 1.

INTRODUCTION.

1 INTRODUCTION.

1.1 GENERAL INTRODUCTION.

Magnetic resonance research on the organic triplet state has been increasingly become a field of interest since the first EPR experiments on photoexcited triplet states in the 50's by Hutchison and his group at the University of Chicago /1,2/. The emergence of optically detected magnetic resonance (ODMR) techniques over the past 15 years has further increased the accessibility of the properties of the organic triplet state, especially in the field of biology where the triplet state can be used to probe the environment and interactions experienced by the photoinduced paramagnetic centre in its natural surroundings.

Zero field magnetic resonance transitions among the electron-spin sublevels in the photoexcited triplet state can be detected using any optical transition, the choice being determined by practical considerations. Using optical photons instead of microwave photons for detection of the zero field transitions provides an improvement in sensitivity, due to the fact that the energy of an optical photon is 6 orders of magnitude larger than that of a microwave photon.

Clarke and Hayes demonstrated in 1972 the first non-phosphorescent optical magnetic resonance detection of an organic triplet state /3/. Fluorescence detected ODMR (FDMR) was used by van Dorp et al. to study the zero field transitions of free-base porphine /4/ and by Clarke and Hofeldt for chlorophyll /5/. Subsequently, it has been demonstrated that triplet state ODMR may even be detected on the ground state to the first excited singlet state absorbance ($S_1 \leftarrow S_0$) /6-8/ and very recently on Raman transitions /9/.

1.2 OPTICALLY DETECTED MAGNETIC RESONANCE.

For a non-phosphorescent molecule the microwave-induced changes in absorption or emission can be understood from fig. 1. This figure represents a situation where the top sublevel of T_0 is predominantly populated and depopulation occurs mainly from the lowest level. In general, $S_1 \rightarrow T_0$ as well as $T_0 \rightarrow S_0$ inter-

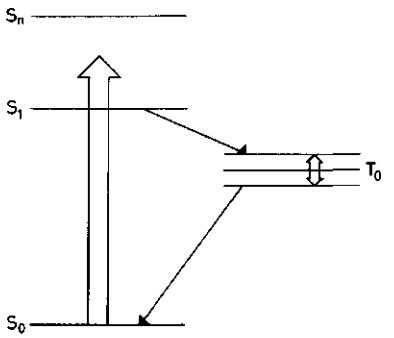

Fig. 1. A schematic example of optical pumping ($S_0 \rightarrow S_1$), intersystem crossing ($S_1 \rightarrow T_0$, $T_0 \rightarrow S_0$), and microwave saturation within the triplet state T_0 of an organic molecule.

system crossing occurs with different rates. At temperatures low enough to prevent spin-lattice relaxation between the sublevels of T_0 (usually $T \leq 4.2$ K) continuous optical pumping results in a large population in T_0 at the expense of S_0. Under these conditions the triplet state acts as a bottleneck in the pumping cycle. When we now apply microwaves at a frequency corresponding to the energy difference between both levels, the triplet bottleneck is short-circuited, the overall triplet population is reduced and the ground state population (and thus the S_1 population) increases. Thus, if the triplet state population is monitored by following the intensity of the ground state absorption, fluorescence or triplet-triplet absorption, a microwave-induced change in T_0 can be detected in the optical spectrum whenever the frequency of the microwave field is in resonance with a zero field transition in T_0.

1.3 PRINCIPLES OF FDMR.

The amplitude and sign of FDMR signals can be related to triplet sublevel populations, rate constants and other readily accessible experimental constants /10-14/. In this paragraph we want to calculate the FDMR spectrum, knowing these experimental constants, e.g. from a fluorescence fading experiment (see § 1.4).

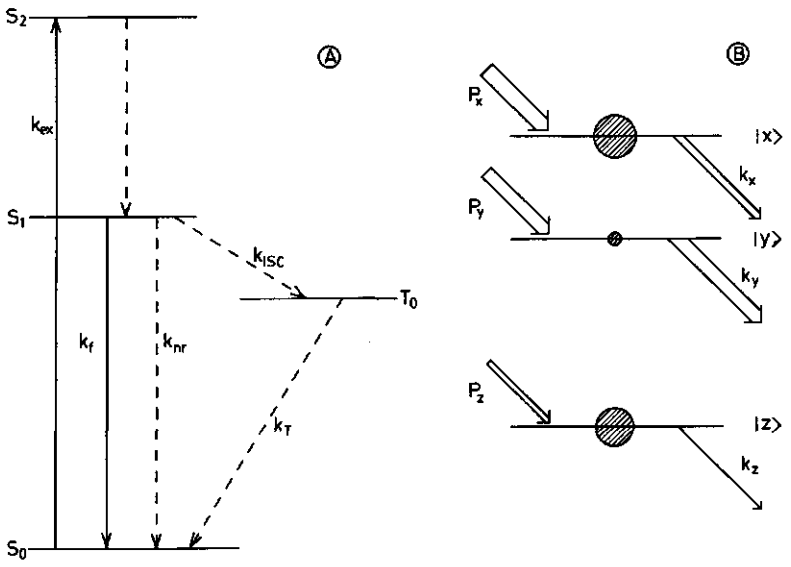

Fig. 2. A) Energy level diagram of the lowest electronic states of H_2-TPP. The symbols are explained in the text.

B) ZFS diagram and kinetic data of H_2-TPP. Separation between ZFS levels is drawn to scale. Arrows entering end leaving spin levels have widths corresponding to their relative magnitudes. Hatched circles represent relative steady state populations, the relative magnitudes are represented by the radius of the circle.

Fig. 2 represents the energy level diagram of the four lowest electronic states of free-base tetraphenylporphyrin (H_2-TPP, see fig. 3) (A) and the T_0 sublevels (B). S_0, S_1, S_2 and T_0 stand for ground state, first and second excited singlet and lowest excited triplet state respectively, k_{ex} is the rate constant for optical excitation from S_0 into S_1 or S_2 and contains among other things the excitation light intensity, k_f and k_{nr} are the radiative and non-radiative decay rate constants of $S_1 \rightarrow S_0$ decay, k_{ISC} represents the rate constant of intersystem crossing (ISC) $S_1 \rightarrow T_0$ and k_T the mean rate constant of $T_0 \rightarrow S_0$ decay. All k's are expressed in s^{-1}. For dilute solutions, providing Beer's law is valid, k_{ex} is /14,15/:

$$k_{ex} = 2300.\varepsilon.I_0/N_{AV} \qquad (1)$$

with I_0 the excitation light intensity (in number of photons.$cm^{-2}.s^{-1}$), ε the extinction coefficient (in $l.mol^{-1}.cm^{-1}$) and N_{AV} Avogadro's number.

For H_2-TPP in benzene, exciting with the 457.9 nm line of an argon-ion laser ($\simeq$ 70 mW on the sample, diameter of the laserspot $\simeq$ 1 mm), I_0 = 8.75 W.cm^{-2}, ε is $\simeq 10^{+3}$ $l.mol^{-1}.cm^{-1}$ and $k_{ex} \simeq 75\ s^{-1}$. Exciting with 592 nm light from a dye-laser, $\varepsilon = 5.3 \times 10^{+3}$ $l.mol^{-1}.cm^{-1}$ and $k_{ex} \simeq 500\ s^{-1}$.

Now we have determined the rate constant for optical excitation, the next question is: what is the steady state population of S_1 w.r.t. that of S_0 and T_0. Following the treatment in ref. 13, it can be shown that the steady state population of S_1 will always be low under our experimental conditions:

$$\frac{[S_1]}{[S_0]} = \frac{k_{ex}}{k_{ISC} + k_f + k_{nr}} \qquad (2)$$

where the concentration of molecules in the denoted electronic states is expressed in $mol.l^{-1}$. For a 10^{-4} M H_2-TPP solution under our experimental conditions, using $k_{ex} = 75\ s^{-1}$ and the values for k_f, k_{ISC} and k_{nr} as given in Table 6, $[S_1]/[S_0]$ is $\simeq 10^{-6}$, i.e. the number of molecules in S_1 can be neglected w.r.t. the populations of S_0 and T_0, as follows from:

$$\frac{[T_0]}{[S_0]} = \frac{k_{ISC}\ k_{ex}}{(k_{ISC} + k_f + k_{nr})\ k_T} \qquad (3)$$

which equals $\simeq 10^{-1}$, again using the same values as in eqn. (2). The ratio $[T_0]/[S_0]$ is the relative triplet population. It is assumed that $k_T \simeq 600\ s^{-1}$, based on the experimental results described in ref. 16. Eqn. (3) can also be written as:

$$\frac{[T_0]}{[S_0]} = \frac{k_{ex}}{k_T}\,\phi_T \qquad (4)$$

where ϕ_T is the triplet yield, defined as:

$$\phi_T = \frac{\text{number of absorbed photons leading to triplets}}{\text{total number of absorbed photons}}$$

$$= k_{ISC} / (k_f + k_{nr} + k_{ISC})$$

This results in $\phi_T = 0.82$, which is the same value as reported in ref. 17. Eqn. 4 can be used to determine ϕ_T, when for a specific experiment $[T_0]/[S_0]$, k_{ex} and k_T are well known, because $[T_0]/[S_0]$ (see Appendix 1) as well as k_T /16/ are dependent on k_{ex}.

For an FDMR experiment the most important question is: how is the fluorescence intensity related to the triplet population and kinetic constants under our experimental conditions? Again, following ref. 13, the fluorescence intensity under steady state conditions, I_f, is given by:

$$I_f = \frac{k_{ex}\, k_f}{k_{ex} + k_{ISC} + k_f + k_{nr}} ([N] - [T_0]) \qquad (5)$$

where [N] is the total concentration in $mol.l^{-1}$. For the abovementioned H_2-TPP solution the fluorescence intensity is 1.3×10^{-3} $Einstein.l^{-1}.s^{-1}$.

In an FDMR experiment the fluorescence intensity is changed by applying microwaves resonant with the frequency difference between a pair of triplet sublevels $|i\rangle$ (fig. 2B). Van der Bent et al. /14/ have derived that under continuous illumination and irradiation with resonant microwaves connecting a pair of sublevels $|i\rangle$ and $|j\rangle$ the change of fluorescence will be:

$$\Delta I_f = A(k_i - k_j)(k_i + k_j)^{-1}([N_i^0] - [N_j^0]) \qquad (6)$$

where $[N_i^0]$ is the steady state population (in $mol.l^{-1}$) of sublevel $|i\rangle$. The constant A can be defined as:

$$A = -I_f / [S_0] \qquad (7)$$

Eqn. (6) can now be written as:

$$\delta I_f = \frac{\Delta I_f}{I_f} = - \frac{1}{[S_0]} \frac{k_i - k_j}{k_i + k_j} ([N_i^0] - [N_j^0]) \qquad (8)$$

with: $[S_0] = [N] - [T_0]$

and $[N_i] = n_i\, [T_0]$

where n_i is the relative population, which can be determined from a fluorescence fading experiment /16/.

Finally, the relative change of the triplet population under continuous illumination as a result of resonant microwave irradiation can be written as:

$$\frac{[\Delta T_0]}{[T_0]} = - \delta I_f \frac{[S_0]}{[T_0]} \qquad (9)$$

For a 10^{-4} M solution of H_2-TPP under our experimental conditions with $[T_0]/[S_0] = 10^{-1}$, and the values for k_i and n_i as given in /16/ (see chapter 4, Table 3) this results for the $|x\rangle$ - $|y\rangle$ FDMR transition in $\delta I_f = 0.014$ and $[\Delta T_0]/[T_0] = -0.14$ and for the $|y\rangle$ - $|z\rangle$ transition in $\delta I_f = 0.023$ and $[\Delta T_0]/[T_0] = -0.23$. For both transitions this implies (i) an increase of the fluorescence intensity and (ii) the $|y\rangle$ - $|z\rangle$ transition has an amplitude of about 1.5 times that of the $|x\rangle$ - $|y\rangle$ transition. Both conclusions are in agreement with the experimental results /16/. For the $|x\rangle$ - $|z\rangle$ transition the calculated relative populations, including the error boundaries are to close to determine in this way the sign and amplitude of that transition.

1.4 THE FLUORESCENCE FADING METHOD.

Apart from conventional optical methods of investigating molecular triplet state kinetics, such as phosphorescence decay measurements and flash photolysis /18/ the ODMR technique yields more detailed information about the lowest triplet state properties /10,19/. On the other hand, it has been established that in fluorescence onset experiments the fluorescence intensity was fading as a result of the increasing triplet state population /10/. Using a chopped laser beam as excitation source, giving a short risetime of the light block pulses, for relatively short living triplets the kinetic data can be obtained quite easily /11-20/.

With the energy level diagram of fig. 2A, it is not necessary to include the population of the S_2-states in a kinetic model, since its lifetime is very short w.r.t. the lifetimes of S_0, S_1 and T_0. Following the treatment given in appendix 1 of this thesis, the rate equations for the relative steady state population of sublevel $|i\rangle$ result in the relation:

$$\dot{\vec{n}} = - \underline{A}.\vec{n} \qquad (10)$$

where $\dot{\vec{n}} \equiv \frac{d\vec{n}}{dt}$ and

$$\underline{\underline{A}} = \begin{pmatrix} k_{ex} & -k_f & -k_T \\ -k_{ex} & k_f + k_{ISC} & 0 \\ 0 & -k_{ISC} & k_T \end{pmatrix} \qquad (11)$$

(The kinetic constants have been defined in § 1.3.). Solving this equation, the fluorescence intensity can be shown to have the following form:

$$I_f(t) = I_f(0)\ [1 - \frac{I_f(0)-I_f(\infty)}{I_f(0)}\ \{1 - \frac{1}{\sum_i c_i}\ \sum_i\ c_i\ \exp - (k_i + \phi_T^i\ k_{ex})t\}] \qquad (12)$$

with $I_f(t) = k_f.n_2(t)$, where n_2 (mol.l^{-1}) is the population of S_1, ϕ_T defines the triplet yield, k_i represents the decay rate constant of spinlevel !i> and $c_i / \sum_i c_i$ is the relative amplitude of this decay component in the $I_f(t)$ curve. From the fluorescence fading curves at various exciting light intensities we are able to determine the decay rate constant k_i by extrapolating to zero relative triplet population (= $\phi_T.k_{ex}$).

The relative amplitude $c_i / \sum_i c_i$ in $I_f(t)$ in fact is a direct measure for the relative steady state populations n_i, as can be seen from eqn. (12) (see Appendix 1). Obviously, the decay rate constant of a particular triplet sublevel can not be determined from the fluorescence fading curve, if it does not carry any population, e.g. because ϕ_T for that level is close to zero. In this respect the fluorescence fading method is more limited than the microwave-induced fluorescence response method. On the other hand the microwave technique needs an extended instrumental set-up, whereas the FF method only uses a chopped (laser) excitation source and a light detection system. In addition, the FF method is not subject to the condition, that saturating microwaves should be applied in order to obtain the true decay rate constants of the triplet sublevels /10/ in a microwave-induced fluorescence response experiment.

It is possible to obtain, apart from the three decay rate constants, from one and the same experiment the relative steady state populations and the relative populating rates by using:

$$p_i = n_i . k_i \qquad (13)$$

where p_i is the relative populating rate.

1.5 TETRAPHENYLPORPHYRIN.

Since a long time, porphyrins have received the interest of many investigators because of the occurrence of their basic skeleton in biologically important molecules, such as the chlorophylls and hemoglobins. The earliest systematic studies of porphyrin were done by Stern and co-workers /21/ and since that time porphyrins by many others (see reviews in refs. 22-24).

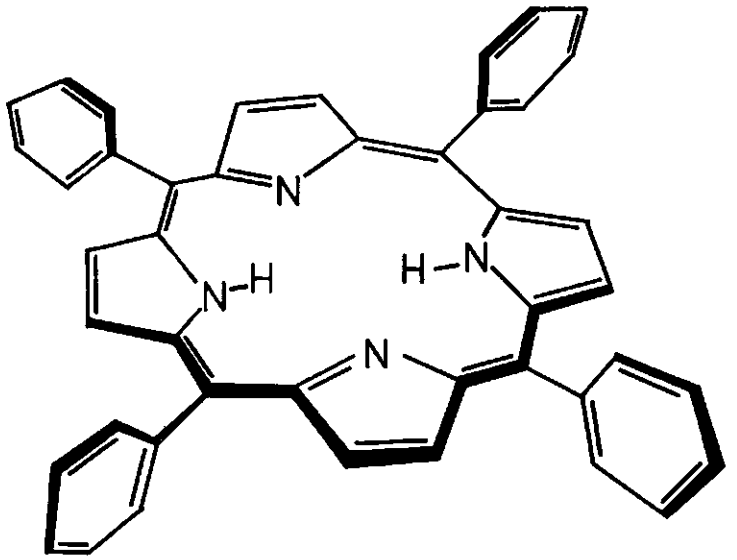

Fig. 3. α,β,γ,δ meso tetraphenylporphyrin free-base (H2-TPP). The ring protons are outside the porphyrin plane, i.e. one above and one below the molecular plane (≃ .02 nm). The phenyl rings make an angle of ≃ 60° w.r.t. the porphyrin plane /25/.

In fig. 3 the structure of the free-base meso tetraphenylporphyrin (H_2-TPP) is shown based on X-ray diffraction date /25/; the cyclic tetrapyrrole structure

is the basic skeleton for all porphyrins and related compounds. The unsubstituted skeleton is denoted 'porphin', abbreviated as P /22/, and has D_{2h} symmetry, when considered as a planar molecule. The two protons in the centre of H_2-P can be exchanged for a metal to give the metal porphin (MeP) /22,23,26/ which has D_{4h} symmetry. The hemegroups of hemoglobin and the cytochromes, for instance, have an iron atom as central ion, whereas the chlorophylls are a magnesium complex.

Spectroscopically all metal porphyrins exhibit characteristic common features in their absorption spectrum, namely a very intense band often denoted as the Soret band) between 380 and 420 nm. It is the origin B(0,0) /27/ of the second excited singlet state and has a molar extinction coefficient generally from 2 to $5x10^{+5}$ $M^{-1}.cm^{-1}$. Between 500 and 600 nm two visible bands are seen, which are separated by $\simeq$ 1250 cm^{-1}. The lower energy band is the electronic origin Q(0,0) of the lowest excited singlet state. The higher energy band includes one mode of vibrational excitation and is denoted Q(0,1), and has a molar extinction coefficient between 1.2 and $2x10^{+4}$ $M^{-1}.cm^{-1}$. The visible absorption spectrum of free-base porphyrins changes from the two-banded (D_{4h}-type) to a four-banded (D_{2h}-type) spectrum. This dramatic effect is attributed to a break-down of the D_{4h} symmetry of the porphyrin ring by the central protons /28/. Thus, Q(0,0) splits into $Q_x(0,0)$ and $Q_y(0,0)$ by about 3000 cm^{-1}. Each band has a vibronic transition $Q_x(0,1)$ and $Q_y(0,1)$ respectively. The absorption maxima of a solution of H_2-TPP in benzene are given in Table 1. Recently, Even at al. have studied the fluorescence excitation spectrum of H_2-TPP and Zn-TPP in a pulsed supersonic

TABLE 1.

Absorption maxima and extinction coefficients of H_2-TPP in benzene at roomtemperature /29/.

assignment of absorption band	λ max (nm)	ε (10^{+3} $l.mol^{-1}.cm^{-1}$)
B	419	470
Q_y (0-1)	515	18.7
Q_y (0-0)	548	8.1
Q_x (0-1)	592	5.3
Q_x (0-0)	647	3.4

expansion of helium /30/. The energies of the electronic origins for the two molecules resulting from this study are summarized in Table 2.

TABLE 2.

The origins of the electronic transitions in H_2-TPP and Zn-TPP, measured in a pulsed supersonic expansion of helium /30/.

Molecule	transition	assignment	peak energy (cm^{-1})	spectral bandwidth (cm^{-1})
H_2-TPP	$S_0 - S_{1x}$	0 - 0	15617	2
	$S_0 - S_{1y}$	0 - 0	18900	100[a]
	$S_0 - S_{2x}$	0 - 0	25114	3
Zn-TPP	$S_0 - S_1$	0 - 0	17490	1.2
	$S_0 - S_2$	0 - 0	25168	6

a) broadened by I $S_{1y} \rightarrow S_{1x}$ electronic relaxation
II appearance of low-frequency torsional motion of the phenyl groups in the S_{1y} manifold

Many of the qualitative features of the electronic structure and excited state properties of porphyrins have been succesfully interpreted in terms of Gouterman's 'four-orbital model' /31/. The model focusses on the importance of the two highest filled (HOMO) and two lowest unfilled molecular orbitals (LUMO) (see Fig. 4) in describing the nature of the low-lying excited states of porphyrins. A metal complex of the porphyrin ring has D_{4h} symmetry. The two lowest unfilled orbitals are a symmetric-degenerate e_g pair. Although the two highest filled orbitals (a_{1u} and a_{2u} in D_{4h}) are not degenerate by symmetry, it was Gouterman's postulate that they are accidentally degenerate or nearly degenerate. Later this was supported by semi-empirical CNDO/2 calculations /32/. The excited state configurations $^1[a_{1u}(\pi) \rightarrow e_g(\pi^*)]$ and $^1[a_{2u}(\pi) \rightarrow e_g(\pi^*)]$ give rise to two doubly degenerate 1_{Eu} states. Configuration interaction (CI) mixes the two excited state configurations in such a way that one observes a weak transition (Q-band), corresponding to destructive CI interference, and a strong transition (B-band), corresponding to constructive CI interference. In free-base TPP

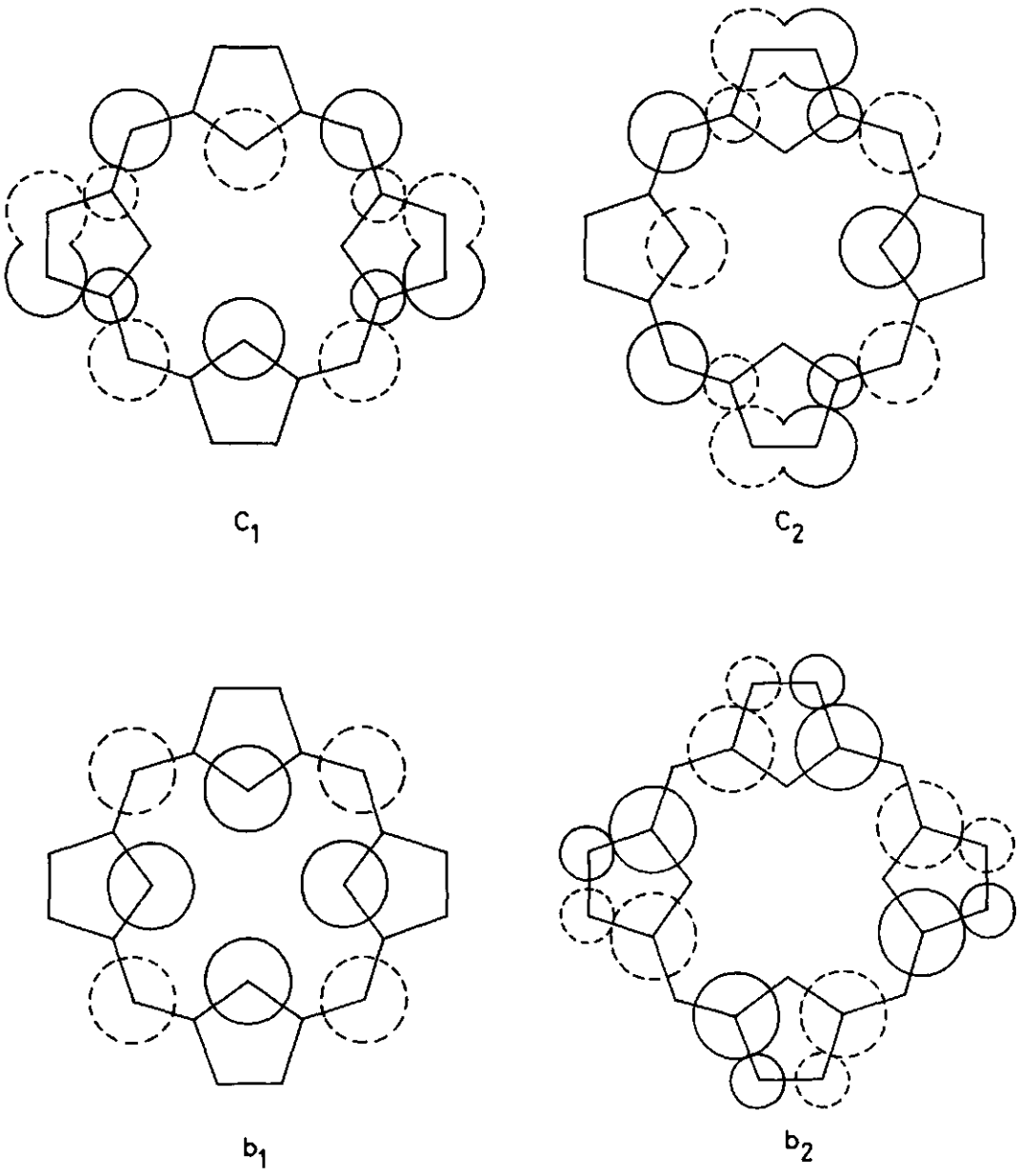

Fig. 4. The four orbitals of the Gouterman /31/ model, representing the two HOMO's and the two LUMO's of a porphyrin with D_{4h} symmetry. The atomic orbital coefficients are proportional to the circles; solid and dashed circles indicate the sign of the wave function. In D_{4h} or D_{2h} symmetry the symmetries of the four orbitals are $b_1 = a_{2u}$ or b_{1u}, $b_2 = a_{1u}$ or a_u, $c_1 = e_g$ or b_{2g} and $c_2 = e_g$ or b_{3g}, respectively.

the symmetry of the molecule is lowered from D_{4h} to D_{2h}. The D_{4h} orbitals a_{1u}, a_{2u} and $2xe_g$ correspond to a_u, b_{1u}, b_{2u} and b_{3g}, respectively, in D_{2h} symmetry. There still is a strong CI between the electron configurations of like symmetry, B_{2u} or B_{3u}, and again a strong Soret band and a weak Q-band arise. But because the lowering of symmetry, the degeneracy of both S_1 and S_2 which occurs in a metal porphyrin is removed. For the Q-band this results in two separate electronic transitions; the Q_x-band and at higher energy the Q_y-band.

So far we have only considered states which, like the ground state, have a total spin S=0, the singlet states. However, when in an excited state the unpaired electrons have their spins parallel one has a total spin S=1, which is characteristic for a triplet state. Transitions from the ground state to a triplet state are spin-forbidden and therefore not observed in the absorption spectra. Although the ordering of the lower triplet states cannot be obtained unambiguously from absorption spectra it has become evident from calculation /32/ that a number of these states are close together, slightly below the first excited singlet state. The CI which caused the splitting into the Soret and Q bands in the singlet system is absent for the triplet states in the approximation of the four orbital model. Thus from theory one expects for a diamagnetic metal porphyrin two almost degenerate triplet states, close together in energy, both have a relatively pure configuration, either $^3[a_{1u} \rightarrow e_g]$ or $^3[a_{2u} \rightarrow e_g]$ /33/. For Zn-TPP ODMR-results indicate that the lowest triplet state arises from an $a_{2u}(\pi)$ to $e_g(\pi^*)$ transition /34/.

Since the introduction of the four-orbital model, a number of theoretical calculations have appeared on porphyrins /32,35,36/ (CNDO and ab initio calculations), but H_2-TPP in considered only in ref. 32. Since the results of the ab initio calculations on H_2-P of Ohno /36/ are the same as those of Petke et al. /35/, we will compare the latter results with those from CNDO calculations of ref. 32.

Both methods show that for H_2-P (D_{2h} symmetry) the four-orbital model is correct w.r.t. the energies of the two lowest unoccupied MO's and the two highest filled MO's (HOMO1 and HOMO2, respectively). The postulate of Gouterman, that these two HOMO's are nearly degenerate is supported by these calculations but the b_{1u} level has a slightly lower energy than the a_u level. For the following two occupied MO's (HOMO3 and HOMO4) the result of both calculations are different. Petke et al. find a b_{2g} and a b_{1u} level, whereas Chantrell et al. find a b_{3g} and $a_g(\pi)$ level. In the ab initio calculations these levels are HOMO5 and HOMO6, respectively.

TABLE 3.

Singlet excited states of H_2-P: calculated energies and composition (C) in terms of excitations as calculated by Chantrell et al. /32/ and Petke et al. /35/.

State	symmetry	Chantrell et al.			Petke et al.		
		excitation[a] HOMO → LUMO	C	energy (cm^{-1})	excitation[a] HOMO → LUMO	C	energy (cm^{-1})
Q_x	B_{3u}	$a_u \rightarrow b_{3g}$ $b_{1u} \rightarrow b_{2g}$	.52 .45	14357	$a_u \rightarrow b_{3g}$ $b_{1u} \rightarrow b_{2g}$	.49 .40	17770
Q_y	B_{2u}	$a_u \rightarrow b_{2g}$ $b_{1u} \rightarrow b_{3g}$	.66 .33	16858	$a_u \rightarrow b_{2g}$ $b_{1u} \rightarrow b_{3g}$	.37 .48	15220
B_x	B_{3u}	$a_u \rightarrow b_{3g}$ $b_{1u} \rightarrow b_{2g}$ $a_g \rightarrow b_{2g}$ [b]	.32 .31 .32	26940	$a_u \rightarrow b_{3g}$ $b_{1u} \rightarrow b_{2g}$ $b_{1u} \rightarrow b_{2g}$	.31 .32 .15	25800
B_y	B_{2u}	$a_u \rightarrow b_{2g}$ $b_{1u} \rightarrow b_{3g}$	.32 .64	28796	$a_u \rightarrow b_{2g}$ $b_{1u} \rightarrow b_{3g}$ $b_{1u} \rightarrow b_{3g}$	.30 .35 .15	23260
B_z	B_{1u}				$b_{3u} \rightarrow b_{2g}$ [c]	.77	28480

a) (π,π^*) unless specified otherwise

b) (n,π^*)

c) very low intensity

Table 3 shows the calculated energies for the singlet excited states, with the symmetries, polarizations and major composition of the various states as results from both methods of calculation. Concerning the Q_x and Q_y states both methods are in agreement with the four-orbital model, only the order of Q_x and Q_y is reversed in the ab initio calculations and not in agreement with the experiment. For the Soret states the results differ from the four-orbital method,

because there is a contribution of lower occupied MO's to the composition of these states. Petke et al. even find a z-polarized transition under the Soret linewidth, although with very low intensity.

TABLE 4.

Triplet excited states of H_2-P: symmetry, calculated energies and composition (C) in terms of excitations as calculated by Chantrell et al. /32/ and Petke et al. /35/.

	Chantrell et al.				Petke et al.			
State	symm.	excitation[a] HOMO → LUMO	C	energy (cm^{-1})	symm.	excitation[a] HOMO → LUMO	C	energy (cm^{-1})
T1	B_{2u}	$a_u \rightarrow b_{2g}$ $b_{1u} \rightarrow b_{3g}$	.80 .15	8066	B_{3u}	$a_u \rightarrow b_{3g}$ $b_{1u} \rightarrow b_{2g}$	.61 .27	13350
T2	B_{3u}	$a_u \rightarrow b_{3g}$	.98	11373	B_{3u}	$a_u \rightarrow b_{3g}$ $b_{1u} \rightarrow b_{2g}$	.28 .59	14420
T3	B_{2u}	$a_u \rightarrow b_{2g}$ $b_{1u} \rightarrow b_{3g}$	.17 .81	12986	B_{2u}	$a_u \rightarrow b_{2g}$ $b_{1u} \rightarrow b_{3g}$	.49 .45	14690
T4	B_{3u}	$b_{1u} \rightarrow b_{2g}$	.98	13793	B_{2u}	$a_u \rightarrow b_{2g}$ $b_{1u} \rightarrow b_{3g}$	.42 .45	16160

a) (π,π^*)

Table 4 shows the calculated energies for the four lowest triplet states, the symmetries and the major composition. Here the results of both methods of calculation are different, only for T2 and T3 the results are in reasonable agreement. Both methods show, however, that the four lowest triplet states can be described by mixed four-orbital configurations. Analysis of triplet EPR spectra was carried out by Van Dorp et al. /37/ suggesting that a single configuration $b_{1u} \rightarrow b_{3g}$ best describes their experimental zero field splitting and proton hyperfine data. This result, together with the experimental energy of the lowest

triplet state of $\tilde{\sim}$ 13000 cm^{-1} /38/ and the symmetry $^3B_{2u}$ /37/, show that state T3 from the CNDO calculations best describes the lowest triplet state T_0 of free-base porphin.

TABLE 5.

Singlet and triplet excited states of H_2-TPP: symmetries, calculated energies and composition in terms of excitation as calculated by Chantrell et al. /32/.

State	symmetry	excitation[a] HOMO → LUMO	composition	energy (cm^{-1})
Q_x	B_{3u}	$a_u \rightarrow b_{3g}$ $b_{1u} \rightarrow b_{2g}$	.41 .57	14277
Q_x	B_{2u}	$a_u \rightarrow b_{2g}$ $b_{1u} \rightarrow b_{3g}$	.57 .42	16858
B_x	B_{3u}	$a_u \rightarrow b_{3g}$ $b_{1u} \rightarrow b_{2g}$ $b_{2u} \rightarrow b_{2g}$[b]	.44 .26 .27	26940
B_y	B_{2u}	$a_u \rightarrow b_{2g}$ $b_{1u} \rightarrow b_{3g}$	.24 .56	27828
T1	B_{2u}	$a_u \rightarrow b_{2g}$ $b_{1u} \rightarrow b_{3g}$	.76 .22	10486
T2	B_{3u}	$b_{1u} \rightarrow b_{2g}$	.98	11212
T3	B_{2u}	$a_u \rightarrow b_{2g}$ $b_{1u} \rightarrow b_{3g}$	.23 .76	12181
T4	B_{3u}	$a_u \rightarrow b_{3g}$	.98	13551

a) (π,π^*) unless specified otherwise

b) (n,π^*)

For free-base TPP the two highest occupied MO's are reversed w.r.t. the order of H_2-P, HOMO3 is the same, but HOMO4 and HOMO5 are again reversed, so HOMO4 of TPP has symmetry b_{2u}. This reversal is a consequence of the electron population of HOMO2 and 5 at the meso carbon atoms (α, β, γ and δ). The corresponding orbital in TPP should be significantly changed owing to the substituted phenyl groups at the meso positions. This destabilizes this orbital to such an extend that it will reverse position with the next higher orbital. Triplet EPR spectra /39/ demonstrate this reversal of the two highest occupied MO's /37/. The lowest unoccupied MO's are again a b_{2g} and b_{3g} level, respectively.

Table 5 summarizes the calculated energies of the singlet and triplet excited states of H_2-TPP, with the symmetries, polarizations and the major composition. The result is again, that the four-orbital model is justified for the Q and T states, but the B states have a contribution from lower occupies MO's. State T3 again agrees with the experimental energy of $\tilde{\sim}$ 11700 cm^{-1} (see Table 2 and 7), the symmetry B_{2u} and the configuration $b_{1u} \rightarrow b_{3g}$.

TABLE 6.

Deactivation of the first excited singlet state of H_2-TPP and Zn-TPP in methylcyclohexane /40/.

		compound		
		H_2-TPP	Zn-TPP	
quantum yield for fluorescence	ϕ_f	0.13	0.04	
		0.12	0.033	a)
lifetime of S_1	τ_S (ns)	13.6	2.7	
		9.7	1.56	b)
radiative decay rate constant $S_1 \rightarrow S_0$	k_f (s^{-1})	$9.6 \times 10^{+6}$	$1.7 \times 10^{+7}$	
non-radiative decay rate constant $S_1 \rightarrow S_0$	k_{nr} (s^{-1})	140	40	
rate constant for intersystem crossing $S_1 \rightarrow T_0$	k_{ISC} (s^{-1})	$4.7 \times 10^{+7}$	$3.6 \times 10^{+8}$	
quantum yield for triplet formation	ϕ_T	0.82	0.88	c)
		0.82	0.95	d)

a) from ref. 41

b) from ref. 16

c) from ref. 17

d) calculated with $k_{ISC}/(k_f+k_{nr}+k_{ISC})$

When a porphyrin molecule is excited into its Soret band, the molecule relaxes very fast ($\tilde{}$ 10^{-12} s) to its lowest excited singlet state S_1. From S_1 decay to the ground state may occur by emission of fluorescence, by radiationless processes or by intersystem crossing to the lowest triplet state. Table 6 contains the photophysical data for the deactivation of the first excited singlet state of H_2-TPP and Zn-TPP. The triplet state can decay to the ground state either by radiative (phosphorescence) or radiationless processes. The lifetime of the metastable triplet state is rather long (1 - 100 ms) because of the difference in multiplicity between the triplet and the ground state. The phosphorescence properties of H_2-TPP and Zn-TPP are collected in Table 7. When a molecule is in

TABLE 7.

Phosphorescence properties of H_2-TPP and Zn-TPP at 77 K in methylcyclohexane (A) /40/ and diethyl ether:petroleum ether: isopropyl alcohol 5:5:2 (EPIP) (B) /41/.

		Compound			
		H_2-TPP	H_2-TPP	Zn-TPP	Zn-TPP
solvent		A	B	A	B
phosph. quantum yield	ϕ_p	4×10^{-5}	6.7×10^{-5}	1.2×10^{-2}	3.6×10^{-3}
phosph. lifetime	τ_p (ms)	6	5.6	26	25.5
radiative decay rate constant $T_0 \rightarrow S_0$	k_p (s^{-1})	5.6×10^{-3}[b]	1.2×10^{-2}[a]	.48	.14[a]
wavelength of max. emission	λ_{max} (nm)	865	859	778	782
Stokes shift for phosph.	ΔE_{ST} (cm^{-1})	3900	3860	3830	3820

a) calculated from $k_p = \phi_p . \tau_p^{-1}$
b) 6.6×10^{-3} as calculated from a

its lowest triplet state it is possible to excite this molecule into higher triplet states ($T_0 \rightarrow T_n$) and in Table 8 the triplet-triplet absorption data of these molecules are given.

TABLE 8.

Triplet-triplet absorption maxima and relative extinction coefficients, ε_{rel}, of H_2-TPP and Zn-TPP in toluene /42/.

H_2-TPP		Zn-TPP		
λ (nm)	ε_{rel}	λ (nm)	ε_{rel}	ε_{abs} [a] (10^{+4} l.mol^{-1}.cm^{-1})
390 (max)	0.51	370 (min)	0.34	
405 (min)	0.40	400 (max)	0.57	3.8
430 (max)	1.00	410 (min)	0.18	
690 (max)	0.04	470 (max)	1.00	7.1
780 (max)	0.07	745 (max)	0.07	
		790 (min)	0.05	
		845 (max)	0.11	

a) from ref. 38.

1.6 SCOPE OF THIS THESIS.

Chlorophyll and related pigment molecules serve several important functions in the photosynthetic process. Antenna chlorophyll absorbs the incident light and transfers the excitation energy to photochemically active pigment-protein complexes, called reaction centres, where the initial charge separation process takes place. In the reaction centre, the harvested energy promotes an electron donor to an excited state, which then transfers an electron to the primary acceptor via one or more intermediary electron carriers. In reaction centres, isolated from photosynthetic bacteria, the primary donor appears to be a special pair of bacteriochlorophyll /44-47/. It is believed that special electronic properties resulting from the excitonic interactions within this dimer contribute to its important role in the charge separation process. Similarly, chlorophyll dimers or 'special pairs' have been proposed as electron donors in plant reaction centres /48/. Thus, it is important for devising model systems based on

photosynthetic energy conversion that we understand the effects of dimer formation and exciton interactions on the electronic properties of porphyrin complexes.

Studying the primary processes in photosynthesis, use is made of cofacial or other dimers of chlorophylls and porphyrins with a fixed geometry /49-70/, see review given in ref. 71. A second group of dimers which is widely studied, involves singly linked dimers /70,72-78/. These type of dimers are often rather flexible so that the porphyrin rings can assume a wide range of relative orientations.

Dimers derived from meso tetraphenylporphyrin (TPP) or its tolyl analog (TTP) used in this study have rotational freedom partly restricted by steric hindrance depending on the points of attachment of the covalent link to the phenyl- c.q. tolyl groups (ortho or para position) /79/.

This thesis tries to answer the following questions about the properties of covalently linked porphyrin dimers: i) what is the geometry (position of both porphyrin macrocycles w.r.t. each other) of the various dimer-configurations. With these parameters the S-S energy transfer process from a metallated part to a free base part of the dimers can be studied under well-defined conditions, possibly serving as a model for photosynthetic reaction centres, which contain chlorophyll and pheophytin at short distance. ii) Which excitonic interactions occur within these dimers, and how do these depend on their geometry. iii) Are the properties of the first excited triplet state of the dimer influenced by the the presence of a second porphyrin macrocycle at close distance from the excited porphyrin macrocycle; iv) is it possible to relate the ground state geometry of the various configurations to spectral characteristics, in particular to the ^{1}H-NMR spectrum? v) To what extent is it allowed to compare the dimer geometries derived from measurements in the liquid solution (roomtemperature) and in solid solution (low temperature)?

From optical (absorption-, fluorescence- and phosphorescence) spectra it can be concluded that the geometry of the monomers and dimers in the first excited singlet (S_1) and triplet (T_0) state is the same as in the ground state (S_0). Thus, we may use the properties of all three states to probe the geometry of the dimers. Using fluorecence decay and fluorescence spectroscopy we have measured the properties of the first excited singlet state of porphyrin-dimers in the absence and presence of energy transfer, and as a function of geometry. The lowest excited triplet state can be used to probe the interactions as a function of geometry. Because the oscillator strength of the $T_0 \rightarrow S_0$ transition is much lower than that for the $S_1 \rightarrow S_0$ transition, it can be expected, that the interac-

tions on the T_0 state can only be measured at much shorter distances than for the S_1 state. We have studied the T_0 properties via the zero field splitting parameters (with FDMR) and the kinetic constants (with fluorescence fading). Space filling models of the dimers studied show that the centre-to-centre distances of the porphyrin macrocycles are about 2 nm. This distance is far too large to allow significant interaction between the rings, e.g. in the form of T-T energy transfer. These interactions take place at much shorter distances (< 0.5 nm). The properties of the ground state are studied by NMR, ESR and the interaction between the S_0 and S_1 state by absorption spectroscopy.

Chapters 3, 4 and 5 report the results of a study of the effect of varying the geometry of the dimer on singlet-singlet energy transfer, excitonic- and spin-spin interaction, triplet state parameters and ring current effects. From EPR measurements on Cu-Cu dimers, the centre-to-centre distance can be determined. These are in good agreement with space filling model results. With fluorescence decay experiments S-S energy transfer properties in mixed zinc-free base dimers have been studied. It can be concluded, that there are large effects of the geometry on energy transfer parameters. From nuclear magnetic resonance spectra some conclusions can be drawn for the relative orientation of the porphyrin macrocycles w.r.t. each other in the dimer in various solvents. It turns out that a variation of the geometry has almost no effect on triplet state properties.

Chapter 6 contains the results of shifts and splittings of absorption bands of the dimers w.r.t. the position and bandwidth of the monomer. A method is outlined to study these shifts and splittings based on simple exciton theory. From the experimental and theoretical results the relative orientation of the porphyrin macrocycles and the angular rotational distribution around the linking chain can be determined.

Chapter 2 descibes the synthesis of the meso tetraphenylporphyrin monomers and singly linked dimers as well as a description of the ODMR-apparatus and the fluorescence fading technique. This chapter also contains a paragraph on constructional details of microwave-helices and their predicted and experimental properties.

The work collected in this thesis cannot be regarded as complete, though many properties of these types of porphyrin dimers have been revealed. Future work is necessary, using cofacial porphyrin dimers, in which the ring-ring distance is much shorter than 1 nm. The ring-ring interactions are then much greater than in the dimers used in this study and can possibly even be detected in the lowest excited triplet state. An interesting compound for this work is a biphenylene-

ylene-diporphyrin as synthesized by Chang and Abdalmuhdi /80/; this is a compound with two cofacial porphyrin macrocycles connected by a biphenylene bridge ($r \tilde{>} 0.4$ nm). Other interesting compounds are the doubly cofacial porphyrin trimer of Wasielewski et al. /68/, as well as chlorophyll-based or chlorophyll dimers as e.g. synthesized by Bucks and Boxer /70/. For photosynthesis research a third group of compounds of interest includes the porphyrin-quinone complexes, e.g. the cofacial porphyrin-quinone ($r = 1$ nm) of Lindsey and Mauzerall /81/.

For all these compounds, it can be expected that in the next few years the interactions between the macrocycles will be extensively studied helping to understand the unresolved questions on primary processes in photosynthesis.

All symbols, used throughout this thesis, have been collected in a list, preceeding chapter 1. Mathematical derivations of expresions, relevant for the fluorescence fading method are given in the appendices 1 and 2.

1.7 REFERENCES.

1. C.A. Hutchison and B.W. Mangum, J.Chem.Phys., 29 (1958) 952.
2. C.A. Hutchison and B.W. Mangum, J.Chem.Phys., 34 (1961) 908.
3. R.H. Clarke and J.M. Hayes, J.Chem.Phys., 57 (1972) 679.
4. W.G. van Dorp, T.J. Schaafsma, M. Soma and J.H. van der Waals, Chem.Phys.Lett., 21 (1973) 221.
5. R.H. Clarke and R.H. Hofeldt, J.Am.Chem.Soc., 96 (1974) 3005.
6. R.H. Clarke and R.E. Connors, Chem.Phys.lett., 33 (1975) 365.
7. H.J. den Blanken, G.P. van der Zwet and A.J. Hoff, Chem.Phys.Lett., 85 (1982) 335-338.
8. H.J. den Blanken and A.J. Hoff, Biochem.Biophys.Acta, 681 (1982) 365-374
9. R.H. Clarke, D.J. Graham, E.B. Hanlon and P. Mitra, J.Chem.Phys., 79 (1983) 1549-1550.
10. W.G. van Dorp, W.H. Schoemaker, M. Soma and J.H. van der Waals, Mol.Phys., 30 (1975) 1701-1721.
11. R. Avarmaa, Mol.Phys., 37 (1979) 441-454.
12. R. Avarmaa and T.J. Schaafsma, Chem.Phys.Lett., 71 (1980) 339-344.
13. G.H. van Brakel, Ph.D thesis, Wageningen Agricultural University, Wageningen,The Netherlands (1982).
14. S.J. van der Bent, P.A. de Jager and T.J. Schaafsma, Rev.Sci.Instrum., 47 (1976) 117-121.
15. N.J. Turro, Molecular Photochemistry, (Benjamin, New York, 1967), p. 73.

16. L. Benthem, R.B.M. Koehorst, L.H. de Graaff and T.J. Schaafsma, to be published
Chapter 4 of this thesis.
17. G.P. Gurinovich and B.M. Jagarov, in Luminescence of crystals, molecules and solutions, F. Williams (ed.), (Plenum Press, New York, 1973), p. 196.
18. S.P. McGlynn, T. Azumi and M. Kinoshita, Molecular spectroscopy of the triplet state, (Prentice Hall, Englewoods Cliffs, NJ, 1969).
19. R.H. Clarke and R.H. Hofeldt, J.Chem.Phys., 61 (1974) 4582-4587.
20. R. Avarmaa, Chem.Phys.Lett., 46 (1977) 279-282.
21. A listing of the references of A. Stern and co-workers in Ann.Phys. and Z.Phys.Chem. during the period 1932-1937 can be found as refs. 637-648 in Falk, ref. 22.
22. J.E. Falk, Porphyrins and Metalloporphyrins, (Elsevier Scientific Publ. Co., Amsterdam, 1964).
23. K.M. Smith (ed.), Porphyrins and metalloporphyrins, (Elsevier Scientific Publ. Co., Amsterdam, 1975).
24. D. Dolphin (ed.), The Porphyrins, Vol. I - VIII, (Academic Press, New York, 1978-1979).
25. S.J. Silvers and A. Tulinsky, J.Am.Chem.Soc., 89 (1967) 3331.
26. A.D. Adler, F.R. Longo, F. Kampas and J. Kim, J.Inorg.Nucl.Chem., 32 (1970) 2443-2445.
27. J.R. Platt, in Radiation biology, Vol. III, A. Hollaender (ed.), (McGraw-Hill, New York, 1956), Ch. 2.
28. M. Gouterman, J.Chem.Phys., 30 (1959) 1139.
29. G.M. Badger, R.A. Jones and R.L. Laslett, Aust.J.Chem., 17 (1964) 1028.
30. U. Even, J. Magen, J. Jortner, J. Friedman and H. Levanon, J.Chem.Phys., 77 (1982) 4374-4383.
31. M. Gouterman, J.Mol.Spectr., 6 (1961) 138-163.
32. S.J. Chantrell, C.A. McAuliffe, R.W. Munn, A.C. Pratt and R.F. Weaver, Bioinorg.Chem., 7 (1977) 283-296.
33. R.L. Ake and M. Gouterman, Theor.Chim.Acta, 15 (1969) 20-42.
34. W.R. Leenstra, M. Gouterman and A.L. Kwiram, Chem.Phys.Lett., 65 (1979) 278-280.
35. J.D. Petke, G.M. Maggiora, L.L. Shipman and R.E. Christoffersen, J.Mol.Spectr., 71 (1978) 64-84.
36. K. Ohno, in Horizons of Quantum Chemistry, K. Fukui and B. Pullman (eds.), (D. Reidel Publ. Co., Dordrecht, The Netherlands, 1980), p. 245-266.

37. W.G. van Dorp, M. Soma, J.A. Kooter and J.H. van der Waals, Mol.Phys., 28 (1974) 1551-1568.
38. M. Gouterman, in The porphyrins, Vol. IIIA, D. Dolphin (ed.), (Academic Press, New York, 1978), Ch. 1.
39. H. Levanon and A. Wolberg, Chem.Phys.Lett., 24 (1974) 96.
40. A. Harriman, J.C.S. Faraday I, 76 (1980) 1978-1985.
41. G.D. Egorova, V.N. Knyukshto, K.N. Solovev and M.P. Tsvirko, Opt.Spectrosc. (USSR), 48 (1980) 602-607.
42. L. Pekkarinen and H. Linschitz, J.Am.Chem.Soc., 82 (1960) 2407-2411.
43. A. Harriman, J.C.S. Faraday Trans. 2, 77 (1981) 1281-1291.
44. G. Feher, A.J. Hoff, R.A. Isaacson and L.C. Ackerson, Ann.N.Y.Acad.Sci., 244 (1975) 239.
45. J.R. Norris, R.A. Uphaus, H.L. Crespi and J.J. Katz, Proc.Natl.Acad.Sci. USA, 68 (1971) 625.
46. J. Fajer, M.S. Davis, D.C. Brune, L.D. Spaulding, D.C. Borg and A. Forman, in Chlorophyll-proteins, reaction centers and photosynthetic membranes, (Brookhaven Symp. Biol., 1977), p. 74.
47. J.J. Katz, J.R. Norris, L.L. Shipman, M.C. Thurnauer and M.R. Wasielewski, Ann.Rev.Biophys.Bioeng., 7 (1978) 393.
48. D. Holten and M.W. Windsor, Ann.Rev.Biophys.Bioeng., 7 (1978) 189.
49. K. Sauer, in Bioenergetics of photosynthesis, Govindjee (ed.), (Academic Press, New York, 1975), Ch. 3.
50. F.K. Fong and V.J. Koester, Biochim.Biophys.Acta, 423 (1976) 52-64.
51. V.J. Koester and F.K. Fong, J.Phys.Chem., 80 (1976) 2310-2312.
52. L.L. Shipman, T.M. Cotton, J.R. Norris and J.J. Katz, Proc.Natl.Acad.Sci. USA, 73 (1976) 1791-1794.
53. F.K. Fong, V.J. Koester and J.S. Polles, J.Am.Chem.Soc., 98 (1976) 6406.
54. M.R. Wasielewski, U.H. Smith, B.T. Cope and J.J. Katz, J.Am.Chem.Soc., 99 (1977) 4172.
55. H. Ogoshi and H. Sugimoto, Tetrahedron Lett., 2 (1977) 169.
56. C.K. Chang, M.-S. Kuo and C.-B. Wang, J.Heterocycl.Chem., 14 (1977) 943.
57. C.K. Chang, J.Heterocycl.Chem., 14 (1977) 1285.
58. M.R. Wasielewski, W.A. Svec and B.T. Cope, J.Am.Chem.Soc., 100 (1978) 1961.
59. J.P. Collman, C.M. Elliot, T.R. Halbert and B.S. Tovrog, Proc.Natl.Acad.Sci. USA, 74 (1977) 18-22.

60. N.E. Kagan, D. Mauzerall and R.B. Merrifield, J.Am.Chem.Soc., 99 (1977) 5484.
61. C.K. Chang, Adv.Chem.Ser., 173 (1979) 162-177.
62. T.L. Netzel, P. Kroger, C.K. Chang, I. Fujita and J. Fajer, Chem.Phys.Lett., 67 (1979) 223-228.
63. T.L. Netzel, M.A. Bergkamp, C.K. Chang and J. Dalton, J.Photochem., 17 (1981) 451.
64. M.A. Bergkamp, J. Dalton and T.L. Netzel, J.Am.Chem.Soc., 104 (1982) 253-259.
65. I. Fujita, T.L. Netzel, C.K. Chang and C.-B. Wang, Proc.Natl.Acad.Sci. USA, 79 (1982) 413-417.
66. T.L. Netzel, M.A. Bergkamp and C.K. Chang, J.Am.Chem.Soc., 104 (1982) 1952-1957.
67. M.A. Bergkamp, C.K. Chang and T.L. Netzel, J.Phys.Chem., 87 (1983) 4441-4446.
68. M.R. Wasielewski, M.P. Niemczyk and W.A. Svec, Tetrahedron Lett., 23 (1982) 3215-3218.
69. R.R. Durand, C.S. Bencosme, J.P. Collman and F.C. Ansom, J.Am.Chem.Soc., 105 (1983) 2710-2718.
70. R.R. Bucks and S.G. Boxer, J.Am.Chem.Soc., 104 (1982) 340-343.
71. J.S. Connolly, in Photochemical conversion and storage of solar energy, part A, J. Rabani (ed.), (The Weizmann Science Press of Israel, 1982), p. 175-204.
72. S.G. Boxer and G.L. Closs, J.Am.Chem.Soc., 98 (1976) 5406.
73. M.R. Wasielewski, M.H. Studier and J.J. Katz, Proc.Natl.Acad.Sci. USA 73 (1976) 4282-4286.
74. F.P. Schwartz, M. Gouterman, Z. Muljiani and D.H. Dolphin, Bioinorg.Chem., 2 (1972) 1-32.
75. J.A. Anton, P.A. Loach and Govindjee, Photochem.Photobiol., 28 (1978) 235-242.
76. R. Selensky. D. Holten, M.W. Windsor, J.B. Paine III, D. Dolphin, M. Gouterman and J.C. Thomas, Chem.Phys., 60 (1981) 33-46.
77. R.E. Overfield, A. Scherz, K.J. Kaufmann and M.R. Wasielewski, J.Am.Chem.Soc., 105 (1983) 5747-5752.
78. P. Krausz and C. Gianotti, J.Chim.Phys., 80 (1983) 299-303.
79. R.G. Little, J.Heterocycl.Chem., 15 (1978) 203-208.
80. C.K. Chang and I. Abdalmuhdi, Angew.Chem., 96 (1984) 154-155.
81. J.S. Lindsey and D.C. Mauzerall, J.Am.Chem.Soc., 104 (1982) 4498-4500.

Chapter 2.

EXPERIMENTAL.

2 EXPERIMENTAL.

2.1 MODEL COMPOUNDS.

Mono-functional tetra-arylporphyrins were synthesized by the mixed aldehyde approach described by Little et al. /1/.

A mixture of 3 equivalents benzaldehyde (or p-tolylaldehyde) and 1 equivalent monohydroxy benzaldehyde (on ortho or para position) is condensed with 4 equivalents pyrrole. The resulting mono-substituted porphyrin I (from o-hydroxybenzaldehyde), see Scheme 1, or II (from p-hyd roxybenzaldehyde) can be separated from the main product tetraphenyl-porphyrin (or tetratolyl porphyrin, respectively) and small amounts of poly-substituted tetra-aryl porphyrins by adsorption chromatography on silica gel (Merck Kieselgel 60) and/or aluminiumoxide (Woelm Pharma N-Super I).

Two tetra-aryl porphyrins were linked by the method of Little /2/. The synthetic route is illustrated in Scheme 1, where the synthesis of the porphyrin dimer o,p-C_3-$(TTP)_2$, IV (R = $-CH_3$), is shown.

The reaction of an excess of dibromopropane with o-hydroxyporphyrin I in DMF in the presence of K_2CO_3, gives the 3-bromopropoxy derivative III. The latter compound is easily separated from the starting material by adsorptionchromatography, since it is relatively non-polar. The porphyrin dimer IV is formed in almost quantitative yield by the reaction of III with an equimolar amount of p-hydroxyporphyrin II. Unreacted II, being relatively polar, can be easily separated from the mixture by adsorption chromatography on silica gel with chloroform as eluent. The compounds III and IV were separated by gel permeation chromatography using styrene-divinylbenzene copolymer beads (Biorad Laboratories, Biobeads SX2, 200-400 mesh with toluene).

Metals may be inserted into the free base porphyrin by standard procedures /3,4/. Mixed metallo-free base porphyrin dimers were synthesized by inserting a metal-ion into either of the porphyrin monomers before coupling. In the ortho-para mixed dimer the metal ion is always in the centre of the porphyrin macro-

Scheme 1

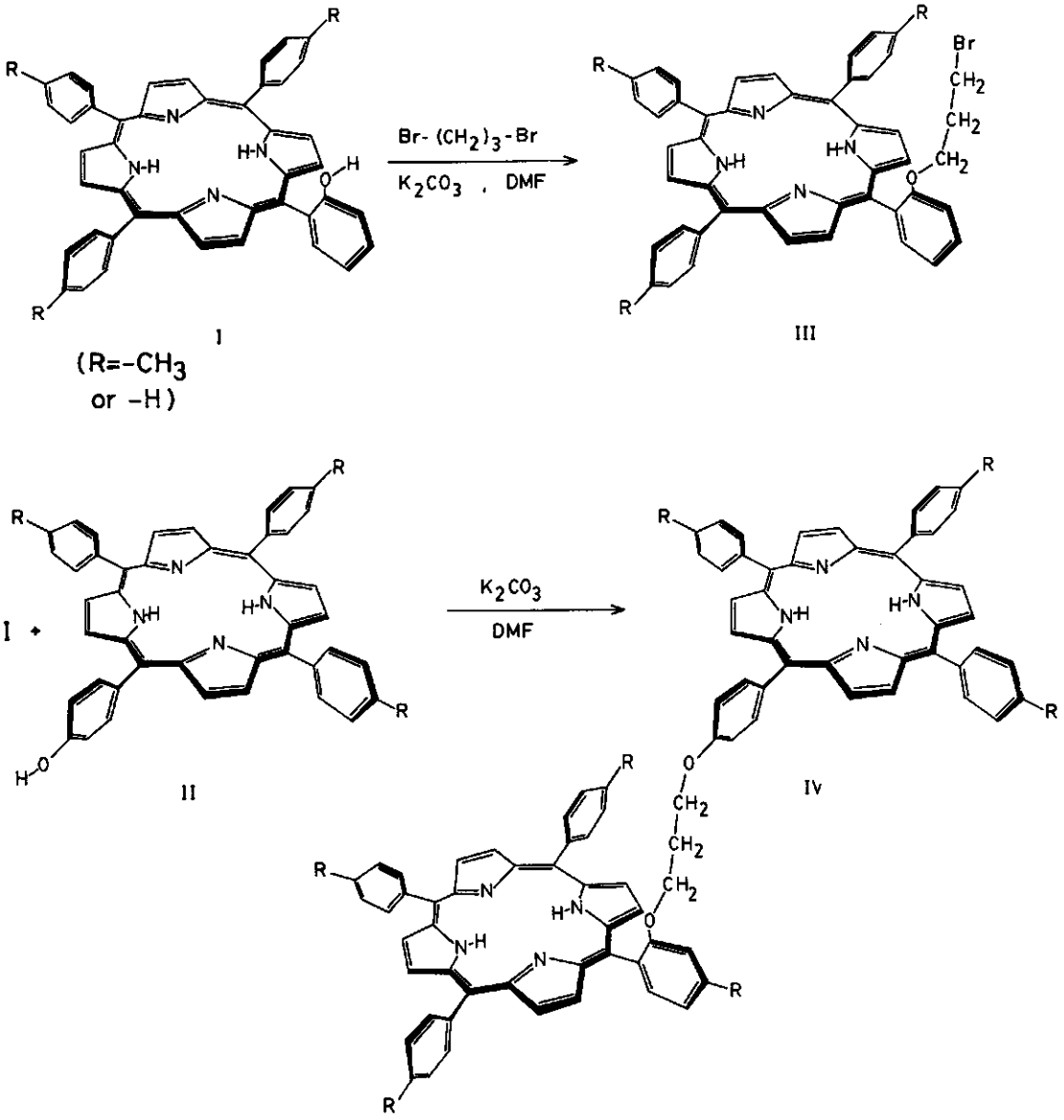
R
N-H
H-N
N
O
H
Br- (CH2)3-Br
K2CO3 , DMF
Br
CH2
CH2
CH2
I
(R=-CH3
or -H)
III
III +
K2CO3
DMF
II
IV

cycle with the linking chain at the ortho position. Doubly metallated porphyrin dimers were synthesized from the corresponding metallo-porphyrin monomers or by metallating both porphyrin macrocycles of a double free base porphyrin dimer.

All compounds produce a single spot by thin layer chromatography (silica gel-plates from Merck, Kieselgel 60 and toluene).

Using absorption-, fluorescence-emission and fluorescence-excitation spectroscopy the presence of a metal atom in one or both porphyrin macrocycles can be detected. Table 1 shows the absorption band maxima of all compounds. A typical fluorescence emission spectrum is shown in fig. 9 of chapter 4 and a typical fluorescence-excitation spectrum in fig. 1.

TABLE 1.

Absorption band maxima of 10^{-7} - 10^{-6} M solutions in toluene at roomtemperature. Bandwidth: 1 nm.

Compound	λ max				
	B	Q_{IV}	Q_{III}	Q_{II}	Q_{I}
TPP	417.7	513.2	547.5	590.1	646.4
TTP	419.6	515.3	550.3	592.7	650.1
ZnTPP	421.6		548.5	587.7	
ZnTTP	423.9		550.1	590.3	
p,p-C_3-(TTP)$_2$	421.0	515.8	551.3	592.8	648.8
o,p-C_3-(TTP)$_2$	420.5	515.5	550.6	592.4	648.1
o,o-C_3-(TTP)$_2$	419.5	514.8	549.3	591.8	647.5
p,p-C_3-(ZnTTP)$_2$	424.2		550.0	589.7	
o,p-C_3-(ZnTTP)$_2$	424.3		549.9	589.1	
o,o-C_3-(ZnTPP)$_2$	420.1		548.9	587.9	
p,p-C_3-(TTP-ZnTTP)	422.9	515.4	550.5	591.1	649.3
o,p-C_3-(TTP-ZnTTP)	423.7	514.8	549.8	590.3	647.6
o,o-C_3-(TTP-ZnTTP)	419.4	514.9	549.6	590.1	647.9
p,p-C_{10}-(TTP-ZnTTP)	422.0	514.4	549.4	590.0	650.9

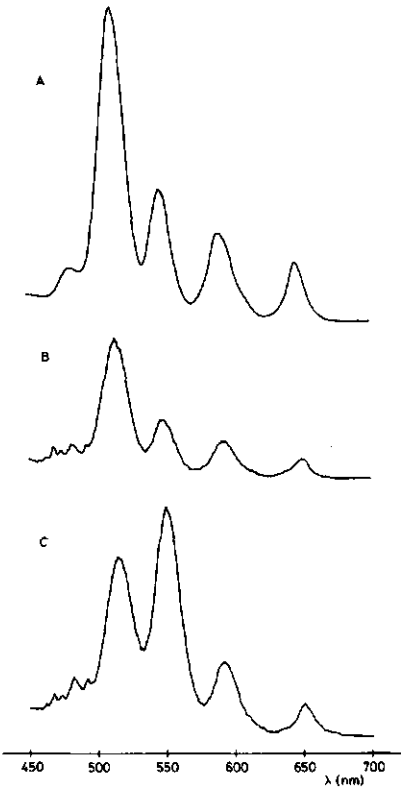

Fig. 1. Absorption spectrum of H_2-TPP (A); fluorescence-excitation spectra of a mixture of H_2-TPP and Zn-TPP (1:1) (B) and of the p,p-C_3-(TPP-ZnTPP) dimer (C). The fluorescence-excitation spectra are detected at 720 nm, where we only have a H_2-TPP fluorescence band. The fluorescence-excitation spectrum of the mixture corresponds to the absorption spectrum of H_2-TPP, whereas in the dimer the relative intensities of the bands at 550 and 590 nm are changed due to energy transfer from the zinc to the free-base part of the dimer. This fluorescence-excitation spectrum is a superposition of the H_2-TPP and Zn-TPP absorption spectra (see Table 1).

The NMR spectra of the porphyrins prepared in this study clearly indicate the structure of the compound, especially the position of the phenylring at which the linking chain is coupled. For a detailed NMR study of these porphyrins we refer to chapter 5 of this thesis /5/.

0.5 mm, outer tube 7.5 mm inner diameter and a wall thickness of 0.25 mm. The inner and outer conductor were kept separated by Delrin spacers. The inner tube ended in a 0.7 mm ∅ stainless steel rod. The helix was made of 0.5 mm ∅ silver or tinned copper wire and silver soldered to the outer tube (fig. 4) and sur-

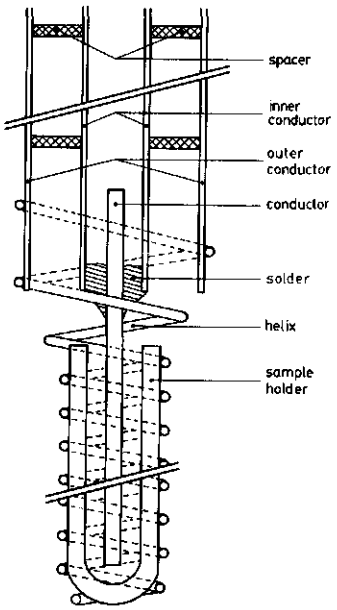

Fig. 4. The microwave helix, used in the spectrometer of fig. 2. For details see text.

rounded the quartz sample holder, made from Suprasil I (Schott) quartz tube of 4 mm outer diameter, .75 mm wall thickness and 25 mm length. The sample holder was closed at one side. The last turn of the helix was used to keep the sample holder in position.

Care was taken to ensure that the resonance lines were traversed in a time longer than the longest lifetime of the triplet sublevels in order to avoid asymmetric distortion and displacement of the resonance lineshapes. In our ODMR experiments, carried out at 4.2 K, we normally used a sweep rate of 1 second, so the resonances (FWHM 75 MHz) were traversed in 75/1300 second $\simeq$ 58 ms, whereas the longest lifetime of the triplets which we studied was about 30 ms (see § 4.3.3). For the ODMR experiments at 1.4 K a normal sweep rate of 7-10 seconds was used. We chose our experimental conditions always in such a way, however, that the lineshape had the least deviation from being symmetrical.

Moreover it was checked by sweeping at a lower rate that no displacement of the resonance position occurred as a result of a too high sweep rate.

For calibrating the resonance frequencies in the experimentally recorded spectrum we used a Systron-Donner model 1017 frequency counter + 1292 A transfer oscillator. In the second channel of the signal averager we recorded the marker of the microwave sweep generator on top of the peaks in the recorded spectrum. Switching to the 'cw marker mode' the marker frequency could be measured and thus by interpolation the frequency of our peaks. The reproducibility of the calibration system of the microwave frequency was better than +/- 3 MHz.

The ODMR spectrometer shown in fig. 2 has also be used for non-zero magnetic field ODMR, by placing the cryostat between the poles of a modified Alpha 4" (Systron Donner, model 4500) electromagnet. With a Heinzinger EA 565-10 power supply we reach a maximum magnetic field at the position of the sample of 0.12 T, and a long-term continuous magnetic field of 0.11 T. The excitation beam may enter the cryostat via a hole in the magnet yoke and polefaces, or perpendicular to this direction.

2.2.2 Design of the coaxial line and the microwave helix.

A simple device for coupling microwave radiation to the sample in ODMR is the helix. The helix acts as a microwave delay line. In an infinite helical arrangement of conductor (sheath helix) the electromagnetic wave propagates along the helical axis with a reduced speed, given by $v=c/2\pi na$, where n is the number of turns per unit length and a the radius of the helix, i.e. reduced w.r.t. the phase velocity, which equals the speed of light (c). Therefore the helix is called a slow-wave structure. The distance between the adjacent repeating field patterns, the so-called guided wavelength, is shorter than in free space. Since the energy stored in one wavelength is the same, the compression of wavelength enhances the maximum magnetic field (B_1) attainable with a given power as given by $\lambda=\lambda_0/2\pi na$. The most important feature of the helix is its broadband response compatible with the ODMR requirement of a wide frequency coverage.

Usually a helix is constructed via the procedure described by Chan /9/ winding two wires of the same diameter around a metal rod of the same diameter as the sample holder (bifilar winding). After the winding is complete, one of the wires is unwound while keeping the other from being distorted. The pitch of a helix constructed in this way is twice the diameter of the wire of which the helix is made. For experiments with perpendicular viewing (through the helix)

a trifilar construction can be used, and the pitch here is three times the wire diameter. With this approach the compression factor, defined approximately by $2\pi a/p$, where a and p are the radius and the pitch of the helix respectively, is smaller, so the microwave magnetic field density is less than in a bifilarly wound helix. For more details, see refs. 10 and 11.

Conventionally the helix is attached to the inner conductor of the coaxial line, the outer conductor being grounded. This design causes an impedance jump at the transition from the coaxial transmission line (about 50Ω and output impedance of the microwave generator $\tilde{\sim}$ 50Ω) to the helix. A mismatch of helix and coaxial line and 50 Ω cable causes loss of power due to reflections. Therefore have we constructed an extended coaxial line helix according to fig. 4, which has a reduced impedance jump, w.r.t. that of a normal helix.

The characteristic impedance of a low-loss coaxial line is /12,13/:

$$Z_0 = 60\sqrt{\frac{\mu_r}{\varepsilon_r}}\ln\frac{b}{a} \qquad (1)$$

with Z_0 the characteristic impedance, μ_r the relative permeability (=1 for almost all conductors), ε_r the relative dielectric constant (=1 for vacuum), b the inner radius of the outer conductor and a the outer radius of the inner conductor. Unless the frequency is specified at which the dielectric constant is valid, the so-called static value (= the limiting value at low frequencies) of the dielectric constant is given and the frequency dependence is neglected, because we only want a rough indication. For our coaxial line made from two tubes with 2a = 3 mm and 2b = 7.5 mm and liquid helium as the separating medium (ε_r(liquid) = 1.05, ε_r(gas) = 1.00 at microwave frequencies), the characteristic impedance turns out to be $\tilde{\sim}$ 53 Ω.

For the helix we used the design of fig. 4. The inner conductor of the coaxial line ended in a stainless steel rod of 0.7 mm Ø and was silver soldered with a smooth transition between the 3 mm Ø inner conductor of the coaxial line to the 0.7 mm Ø steel rod of the helix construction. To the outer conductor a helix was tin soldered, which was wound with a smooth transition from the 8 mm Ø of the conductor to the 4 mm Ø of the sample holder (see fig. 4) and was made of silver or tinned copper wire with a diameter of 0.5 mm. The helix itself was wound via the trifilar approach, so the pitch is 1.5 mm and the compression factor $\tilde{\sim}$ 8.4.

The sample holder was made from uncoated Suprasil quartz tube ($\varepsilon_r \tilde{\sim} 4$ at microwave frequencies) with an outer diameter of 4 mm and an inner diameter of

2.5 mm. The samples were frozen solutions of organic solvents (mostly benzene and toluene). In the solid phase ε_r is determined only by the polarizability of the molecule in the liquid phase, if the solution is frozen in without an electric field. A frozen solution of organic solvents can therefore be regarded as the liquid phase of a non-polar molecule, thus neglecting the dipole moment if present, at very high freqencies. As a mean value for ε_r we took $\varepsilon_r = 2.3$. The relative dielectric constant for sample and holder can then be calculated according to the ratio sample-holder and is $\simeq 3.5$ resulting in $Z_0 \simeq 50\Omega$ according to eqn. 1. This figure is a rough indication because eqn. 1 determines the characteristic impedance of a coaxial transmission line. The helix in our construction is not a normal conductor as defined in coaxial transmission line theory, and the helix is not terminated. But we can say that both our coaxial line and the helix match to the microwave generator impedance and the impedance of the RG 58 cable in order to have the losses of power as low as possible.

Since coaxial transmission lines have two conductors, they are capable of carrying the principal TEM (transverse electromagnetic mode) /12/ implying that neither the electric nor the magnetic field has components in the direction of propagation. Both electric and magnetic fields can only be perpendicular to each other. Consequently, there exists a unique pattern for the electric and magnetic fields in a coaxial structure. This is shown in fig. 5A.

As the electric field is only present between two conductors in the principal mode it has to be radial. The magnetic field is perpendicular to the electric field and the field lines are pointing from one conductor to the other. On the longitudinal cross-sectional part of fig. 5A, the electric field intensity distribution is periodical according to the wavelength. The magnetic field intensity is out-of-phase with the electric field.

As the propagation frequency increases, the wavelength decreases. Beyond the limit where the cross-sectional dimensions of the coaxial line are comparable with the wavelength, higher order modes will be able to propagate besides the principal mode, and cause field losses. For these modes, the coaxial line acts as a high-pass filter, and a given line will carry energy in one of the higher order modes only if excited above the critical (cut-off) frequency for the given mode. The approximate cut-off wavelength for the first higher order mode is:

$$\lambda_c = \pi \, (a + b) \, \sqrt{\varepsilon_r} \qquad (2)$$

This formula is accurate up to about 8%. For our coaxial line (2a = 3 mm, 2b = 7.5 mm and $\varepsilon_r = 1.05$) $\lambda_c(TE_{11}) = 3.38$ cm and the cut-off frequency is $\simeq 9$ GHz.

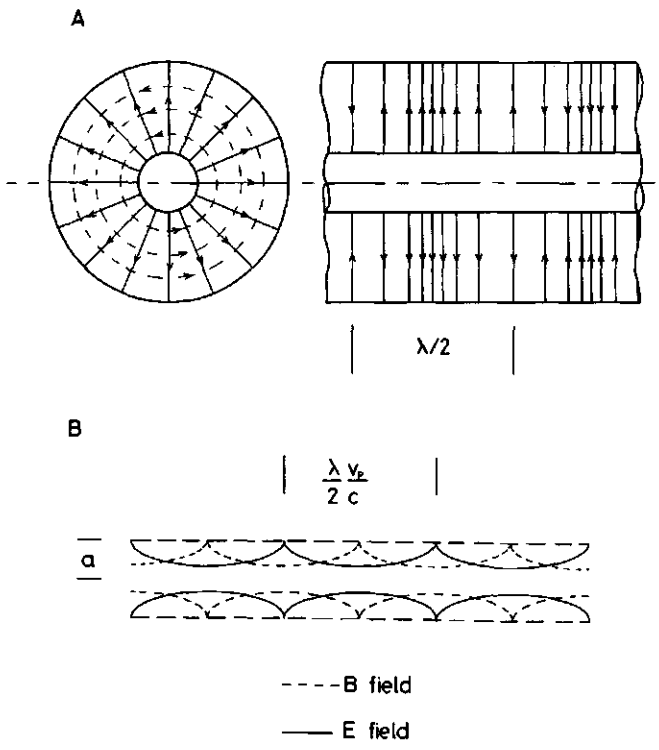

Fig. 5. Field distribution for the principal mode (TEM) in a coaxial line (A and the field distribution in a sheath helix (B), v_p is the propagating velocity of the electro-magnetic fields. The dotted lines are the electric and the solid lines the magnetic field lines.

In the coaxial line shown in fig. 4 we have only the TEM mode up to $\tilde{}$ 8 GHz.

A mathematical solution has been made on a model 'sheath' helix, which is a thin cylinder with infinite conductivity in the direction parallel to the wires and zero conductivity perpendicular to this direction /10/. The field distribution for such an idealized helix is shown in fig. 5B. Note that half of the microwave power is inside the helix; furthermore the magnetic field contains both longitudinal and transverse components, even in the lowest mode. Field patterns for a real life helix constructed of finite size wires are necessarily more complicated. For an extended theoretical description the reader is refered to the article of Webb /10/. For an open-ended helix, microwaves reflect at the end, creating a standing wave with a maximum amplitude at one quarter of a compressed

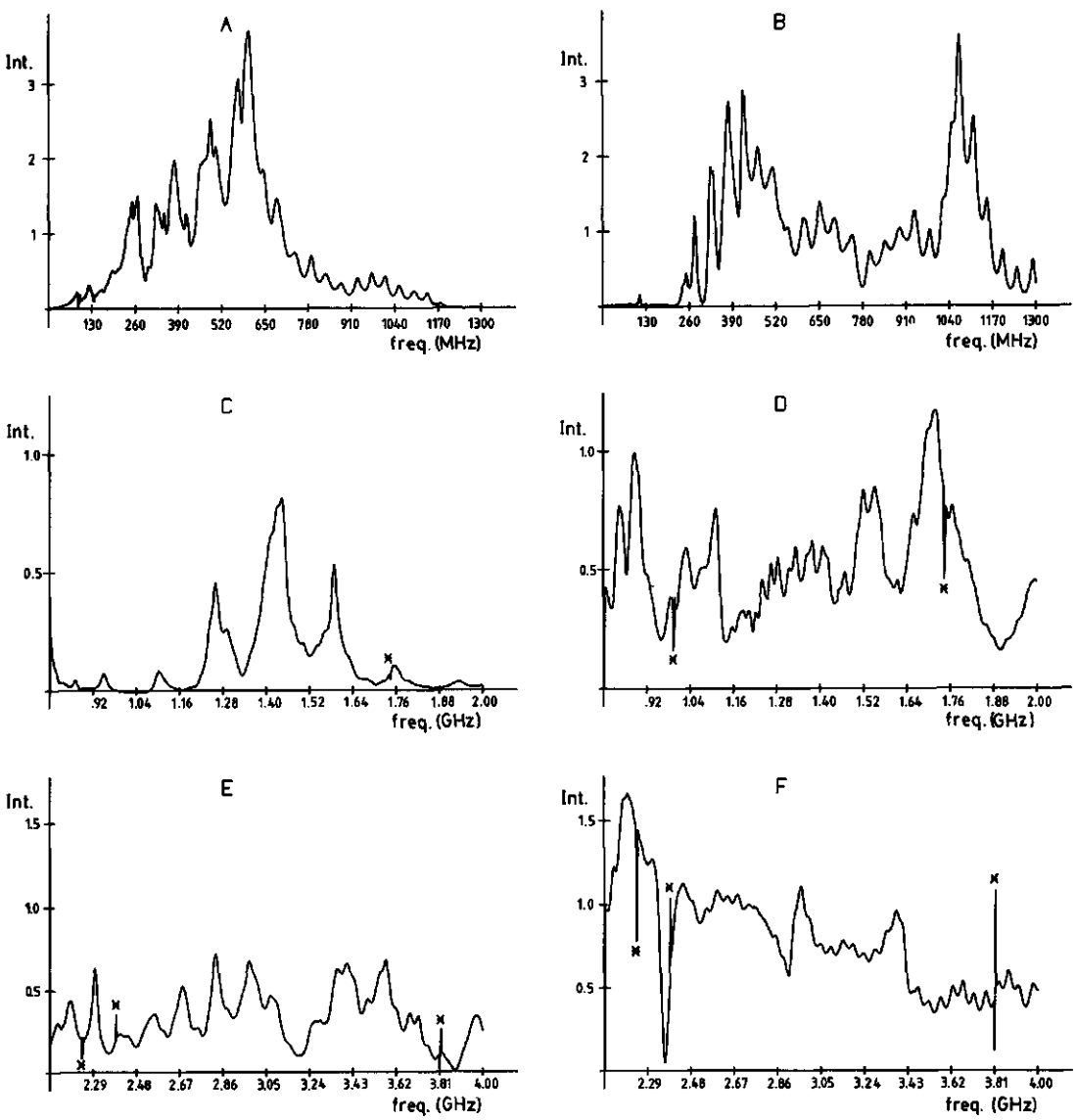

Fig. 6. Power-vs-frequency curves for two types of microwave helices, a conventional bifilarly wound helix (A, C and E) and the our extended coaxial helix (B, D and F), described in the text. All curves are corrected for antenna response. An asterix indicates a marker signal from the microwave sweep generator. Note the different y-axis scales (in arb. units) in the various frequency ranges.

wavelength from the open end. For our helix construction with a compression factor of 8.4 and a frequency range 400 - 4000 MHz, the maximum field lies inside the helix between 2.2 and 0.2 cm from its end.

We have determined the frequency dependency of the microwave power inside this type of helix and a conventional bifilarly wound helix, that is used in our 4.2 K spectrometer. This has been investigated using a short ($<< \lambda$) antenna and a crystal detector (Hewlett-Packard, model 423A (neg)). The recorded frequency response curves were corrected for the antenna response; corrected curves are given in fig. 6 for the various frequency ranges. The error in the intensity of the detected signal is rather large (a factor 2), and they do not yield the microwave power as detected by the sample in an ODMR experiment, because we measured in free space instead of in the sample with a typical value of ε_r of $\simeq$ 3.5. Therefore the different frequency response curves should be considered as qualitative. For one and the same frequency range the response curves of the two types of helices may be compared, however for the conventional helix the response curve is very sensitive to the position of the antenna in the helix, in contrast with the behaviour of the other type of helix, which turns out to be almost independent of the antenna position. The response curves given in fig. 6 are taken at the position were we normally place our sample. Especially in the high frequency ranges (1-4 GHz) the average power inside the extended coaxial line helix is 2 - 3 times higher than in the conventional type and is more continuous over the full frequency range.

2.3 THE FLUORESCENCE FADING METHOD.

The ODMR spectrometer as shown in fig. 2 can also be used for triplet state kinetic measurements by microwave induced changes in the fluorescence intensity via the microwave pulse method, described by van Dorp et al. /14/, or via the 'equilibrium method' given by Clarke and Hofeldt /15/. The set-up necessary for these experiments is described by Searle et al. /7/ for our 4.2 K ODMR spectrometer and the same equipment can be used on the ODMR spectrometer of fig. 2.

Triplet state kinetic parameters were also determined via the fluorescence fading technique /16,17/. For this type of experiments no microwave source is required usually. The response of the fluorescence intensity of the sample to a light block pulse was measured and averaged over many cycles in order to obtain a good signal-to-noise ratio. Light block pulses were generated via a laboratory built chopper blade driven by a function generator and an amplifier. In order to

obtain very fast rate constants ($k \simeq 10^{+4}\ s^{-1}$) positive 100 mm focal length lenses were used to focus the laser beam at the chopper blade. With our chopper blade with two holes and a light-on/light-off period of 1:2 and a distance of the laserspot to the turning point of the chopper blade of 100 mm the rise time of the light block pulse is 1% of the light-on period. For H_2-TPP solutions we used light-on periods of $\simeq$ 50 ms (driving frequency of the chopper $\simeq$ 3.3 Hz) and the rise time of the light block pulse is $\simeq$ 0.5 ms. The fluorescence signal was synchronously recorded on the signal averager (PAR model 4203) triggered on the rising flank of the light block pulse via a beamsplitter and a battery powered photodiode (EG & G, type DT 25).

As with ODMR kinetics the fluorescence fading method is highly sensitive to distortion due to coherent noise, especially for samples with a very low triplet yield. This means that the whole set-up must be mechanically as rigid as possible, because vibrations may give rise to changes in the fluorescence intensity of the same order as due to triplet formation. Therefore special attention was given to the fixation of the sample holder w.r.t. the light beam, and avoiding transmission of mechanical vibrations of the chopper to other parts of the spectrometer. The chopper was therefore suspended by steel wires to the laboratory ceiling.

In order to have a good signal-to-noise ratio most curves were obtained by averaging the signal over 10,000 to 50,000 light block pulses depending on the triplet concentration and covering a time period of 15 - 60 minutes. We took care the light-on period is long enough for reaching the steady-state situation, determining the baseline. Obtaining a reliable baseline is indispensible for the exponential fit procedure. Also the light-off period must be long enough for the system to return to the groundstate. Because the anode impedance and the capacitance (100 $pF.m^{-1}$) of the coaxial cable form a RC-filter which influences the detected fluorescence intensity we used a 100 kΩ anode impedance and a coaxial cable as short as possible (1.5 m).

Multi-exponential fits to digitally recorded experimental fluorescence fading curves were determined using a weighted least squares approximation method /18/.

The rate constants are dependent on the excitation light intensity /19/ and the true rate constants are found by extrapolating the calculated kinetic parameters to zero light intensity.

2.4 MEASUREMENTS OF FLUORESCENCE LIFETIMES.

Fluorescence lifetimes were measured with the apparatus described in /20/, except that the electro-optic modulator was used in the double-pass configuration /21/. The samples were solutions in benzene, benzene/1% pyridine and toluene with a concentration of 10^{-4} - 5 x 10^{-4} M and were measured at room temperature.

The apparatus consists of a mode-locked argon-ion laser (Coherent Radiation, CR18 UV) pumping a dye laser (Coherent Radiation, model CR 590) with extended cavity to match the cavity length of the two lasers. For decreasing the repetition rate of the exciting pulses from 76.160 MHz to 297.5 kHz an electro-optic modulator was used /21/. The detection was perpendicular to the excitation direction. For wavelength selection two 0.25 m monochromators (Jarrel-Ash, model 82-410, bandwidth 10 nm) were used in tandem. The photomultiplier detecting the emission photons was a Philips PM2254 (S20 cathode), placed in a thermo-electric cooled housing (Products for Research, model TE104 RF with vacuum window optics). For the registration of the fluorescence decays we used time-resolved single photon counting; data were collected in a Laben 8001 multichannel analyzer (MCA). The digital output of the MCA was recorded on a cassette tape recorder (Racal Digideck) for storage. The data were analyzed on a DEC-10 computer.

2.5 EPR SPECTRA.

EPR spectra were recorded on an X-band Varian E-6 spectrometer. The samples were carefully placed in the centre of a rectangular cavity (Varian E-213). The modulation frequency was 100 kHz, the modulation amplitude 0.8 - 1.6 mT (centre of the sample) and the microwave power 5 - 30 mW.

Low temperature spectra were obtained via a liquid nitrogen flow cryostat (Varian E-257) or a modified Oxford Instruments ESR-9 (ESR-6) flow cryostat.

Triplet EPR spectra were obtained by irradiation of the sample with a 900 W Xe-lamp (Osram) filtered via a saturated $CuSO_4$ solution and a UV cut-off filter (Schott GG395).

2.6 REFERENCES.

1. R.G. Little, J.A. Anton, P.A. Loach and J.A. Ibers, J.Heterocycl.Chem., 12 (1975) 343-349.
2. R.G. Little, J.Heterocycl.Chem., 15 (1978) 203-208.
3. A.D. Adler, F.R. Longo, F. Kampas and J. Kim, J.Inorg.Nucl.Chem., 32 (1970) 2443-2445.
4. K.M. Smith (ed.), Porphyrins and Metalloporphyrins, (Elsevier Scientific Publ. Co., Amsterdam, The Netherlands, 1975).
5. L. Benthem, R.B.M. Koehorst and T.J. Schaafsma, to be published Chapter 5 of this thesis.
6. S.J. van der Bent, P.A. de Jager and T.J. Schaafsma, Rev.Sci.Instrum., 47 (1976) 117-121.
7. G.F.W. Searle, A. van Hoek and T.J. Schaafsma, in Picosecond Chemistry and Biology, T.A.M. Doust and M.W. West (eds.), (Science Reviews Ltd., Northwood, England, 1983), p. 35-67.
8. G.H. van Brakel, Ph.D Thesis, Wageningen Agricultural University, The Netherlands (1982).
9. I.Y. Chan, in Triplet State ODMR Spectroscopy, R.H. Clarke (ed.), (Wiley Interscience, New York, 1982), p 1-24.
10. R.H. Webb, Rev.Sci.Instrum., 33 (1962) 732-737.
11. M.R. Pearlman and R.H. Webb, Rev.Sci.Instrum., 38 (1967) 1264-1267.
12. T. Moreno, Microwave Transmission Design Data, (Dover publications, New York, 1958), Ch. 4.
13. S.F. Adam, Microwave Theory and Applications, (Prentice-hall, Englewood Cliffs, 1969), Ch. 2.
14. W.G. van Dorp, W.H. Schoemaker, M. Soma and J.H. van der Waals, Mol.Phys., 30 (1975) 1701-1721.
15. R.H. Clarke and R.H. Hofeldt, J.Chem.Phys., 61 (1974) 4582-4587.
16. R. Avarmaa, Chem.Phys.Lett., 46 (1977) 279-282.
17. R. Avarmaa, Mol.Phys., 37 (1979) 441-454.
18. S.W. Provencher, J.Chem.Phys., 64 (1976) 2772-2777.
19. L. Benthem, R.B.M. Koehorst, L.H. de Graaff and T.J. Schaafsma, to be submitted Chapter 4 of this thesis.

20. A. van Hoek, J. Vervoort and A.J.W.G. Visser, J.Biochem.Biophys.Meth., 7 (1983) 243-254.

21. A. van Hoek and A.J.W.G. Visser, Rev.Sci.Instrum., 52 (1981) 1199-1205.

Chapter 3.

FLUORESCENCE RESPONSE TO TRIPLET STATE POPULATIONS.

3 FLUORESCENCE RESPONSE TO TRIPLET STATE POPULATIONS IN PORPHYRINS.

3.1 INTRODUCTION.

Molecular triplet state kinetics can be investigated by conventional optical methods such as phosphorescence decay measurements and by magnetic resonance and its optical detection (ODMR). The ODMR-technique, especially fluorescence detected magnetic resonance (FDMR), has yielded much detailed information about the properties of the lowest triplet states.

Triplet state kinetics can be conveniently determined by measuring the time-dependence of the low temperature fluorescence intensity response to a step-wise increase of the excitation light intensity /1/.

In this paper we would like to answer the following questions, which are important for future studies on in vivo systems:

1. Which effect has a change of solvent on triplet state kinetics?
2. Is there a dependence of the kinetic constants on the fluorescence detection wavelength?
3. Which effect has the presence of the heavy zinc-atom and a change of geometry on the triplet state properties of mixed, covalent porphyrin dimers?

3.2 EXPERIMENTAL.

As an excitation source we have made use of an intensity stabilized argon-ion laser (230 mW, 457 nm line). The ratio of triplet- to singlet populations under steady state conditions was always kept < 10% by using neutral density filters.

Fluorescence was monitored employing a surface-excitation configuration; the imaging system simultaneously focussed the laser beam on the sample. Laser excitation light was square wave modulated by a chopper, whereas the time-dependence of the fluorescence was summed over about $5 \times 10^{+4}$ light pulses. The edges of the excitation light pulses were sharpened by forming an intermediate focus of the laser beam in the plane of the chopper disk, resulting in a resolution better than 1 percent within the 40-60 ms. period.

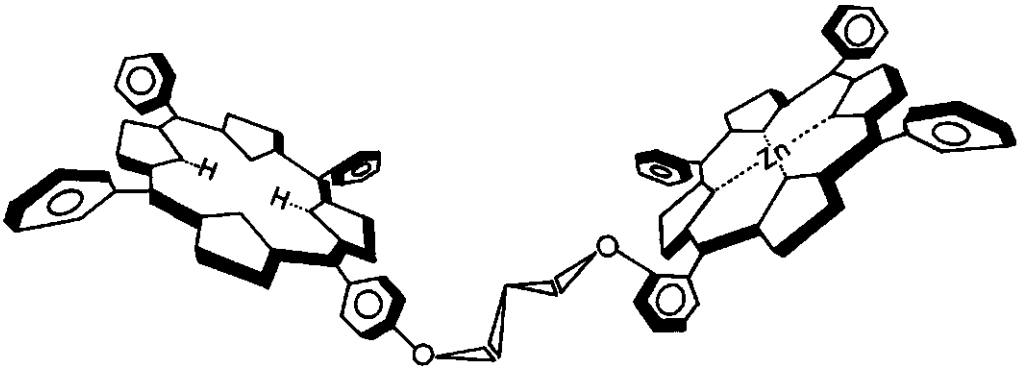

Fig. 1. A mono-bridged dimer with ortho-para bound porphyrins.

The samples were polycrystalline solid solutions of 10^{-5} - 5 x 10^{-5} M of free base tetraphenylporphyrin (H_2-TPP), Zn-TPP and their mixed dimers in benzene with 1 percent pyridine added. All compounds were purified by chromatography and purity was checked by TLC. The mixed dimers (fig. 1) were synthesized as described in the literature /5/. The samples were rapidly frozen by immersion in liquid helium (4.2 K) or in liquid nitrogen (77 K).

Multi-exponential fits to digitally recorded experimental fluorescence fading curves were determined using a weighted least squares approximation method /2/.

3.3 RESULTS.

For all compounds the time dependent fluorescence intensity is found to consist of at least two exponential terms at 4.2 K and even at 77 K. For H_2-TPP it has been shown that triplet spin polarization exists to temperatures up to 100 K /3/. Triplet state properties (ZFS values, kinetics) obtained from fluorescence response kinetics and FDMR at 4.2 K and 77 K have been summarized in Tables 1 and 3 for H_2-TPP, Zn-TPP and the dimers, as well as some decay rate constants obtained by other methods.

TABLE 1

Decay rate constants of the triplet spinlevels of free base-TPP at various temperatures.

Solvent	T (K)	k_x (s^{-1})	k_y (s^{-1})	k_z (s^{-1})
benzene(a)	4.2	198 ± 50	567 ± 140	62 ± 15
MTHF(b)	4.2	184 ± 55	606 ± 225	68 ± 24
n-octane(c)	2	168 ± 40	692 ± 50	50 ± 10
benzene(a)	77	330 ± 100	627 ± 225	91 ± 30
n-octane(d)	100	300 ± 100	600 ± 200	150 ± 50

(a) rate constants a weighted average of six experiments
(b) rate constants from two experiments
(c) from /5/
(d) from /4/

TABLE 3

Zero field splitting (ZFS) parameters D and E (in units 10^{-4} cm^{-1}) and triplet state decay rate constants of various mixed, covalent dimers and monomers. Solvent: benzene/1% pyridine; T = 4.2 K.

Compound	D[a]	E[a]	k_x (s^{-1})	k_y (s^{-1})	k_z (s^{-1})
H_2-TPP (A)	377	81	198 ± 50	567 ± 140	62 ± 15
Zn-TPP (B)	308	96	49 ± 2		143 ± 6
pp-AB	361	81	88 ± 50	443 ± 35	----[b]
op-AB	376	81	142 ± 9	438 ± 40	13 ± 3
oo-AB	378	81	142 ± 10	477 ± 40	29 ± 6

a. error about 1%
b. not quoted in view of large error

Decay rate constants as a function of the fluorescence detection wavelength are summarized in Table 2.

TABLE 2

Decay rate constants of the triplet spinlevels of H_2-TPP in solid benzene as a function of detection fluorescence wavelength.
(T = 4.2 K; detection bandwidth 10 nm)[a]

λ (nm)	k_x (s^{-1})	k_y (s^{-1})	k_z (s^{-1})
644	262	1120	69
648	202	603	59
653[b]	198	567	62
658	203	603	42
662	232	1350	47

a. rate constants from two experimental runs, error for all data 25%
b. fluorescence maximum

3.4 DISCUSSION.

The fluorescence detection of triplet state kinetics appears to be an effective tool to measure the three decay rate constants of the triplet sublevels /1/. Immediately following a stepwise increase of the exciting light, the fluorescence intensity can be shown to have the following form:

$$I_f(t) = I_f(0)[1 - \frac{I_f(0)-I_f(\infty)}{I_f(0)} \{1 - \frac{1}{\sum_i c_i} \Sigma_i c_i \exp - (k_i + \phi_T^i k_{ex})t\}] \quad (1)$$

where k_i represents the decay rate constant of spinlevel i of the lowest triplet state and $c_i / \sum_i c_i$ is the relative amplitude of this decay in the $I_f(t)$ curve. This method is useful for non-phosphorescing samples. Furthermore it is possible to obtain all three decay rate constants by a single experiment. Besides, for severly broadened FDMR transitions it is not always possible to obtain triplet state kinetic constants from microwave pulse experiments under steady state illuminations.

Apart from the three decay rate constants it is possible to obtain from one and the same experiment all three steady state populations and the populating rates. These can be calculated from the relative amplitudes of the relevant

exponential terms by:

$$P_i = n_i . k_i \qquad (2)$$

P_i = populating rate.
n_i = relative steady state population = $c_i / \sum c_i$, where i refers to the spinlevel. From the six experiments on H_2-TPP in benzene (Table 1), we derive the values of n_i as a weighted average to be $n_x = 0.46$, $n_y = 0.14$ and $n_z = 0.40$ (error $\simeq$ 25%). Together with the decay rate constants from Table 1 we can now calculate the populating rates, which are $P_x = 0.47$, $P_y = 0.40$ and $P_z = 0.13$ (estimated error $\simeq$ 25%). The populations are in agreement with the sign of the D-E and 2E transitions in our FDMR experiments: for both transitions we find a fluorescence increase, as predicted.

From the experiments on H_2-TPP in various solvents at 2 and 4.2 K as stated in Table 1 we can conclude that there is not a significant solvent effect on the decay rate constants. At 77-100 K the rate constants are systematically larger than at 2-4 K, but again there is no significant difference for the two solvents studied. The observed increase is probably due to thermally excited vibrational modes.

We have also determined the decay rate constants as a function of the detection fluorescence wavelength; the results are summarized in Table 2. It is clear that especially k_y is rather sensitive to the detection wavelength, whereas k_x and k_z are much less dependent on λ. We must therefore conclude that it is generallly necessary to specify the detection wavelength and the fluorescence maximum when quoting triplet state kinetics obtained by this method as well as by the FDMR technique. Probably the same holds for posphorescence detection of triplets.

From fig. 2A it can be concluded that, when we monitor the fluorescence of a 1:1 mixture of H_2-TPP and Zn-TPP exciting with 421 nm light, the fluorescence of H_2-TPP (dotted curve) is observed, whereas excitation at 431 nm yields the Zn-TPP fluorescence (solid line). Fig. 2B represents the fluorescence spectrum of a mixed dimer excited with 421 nm light; 431 nm excitation yields an identical spectrum, ascribed to the fluorescence of the H_2-TPP, as is observed from fig. 2A. In view with the fact that the absorption spectra of the dimer and the mixture are almost the same we conclude that there is an intramolecular energy transfer of the singlet-singlet type from the Zn-TPP part of the dimer to the H_2-TPP part. This is consistent with the results of Table 3. Comparing the ZFS values and the decay rate constants of the various mixed dimers, these look

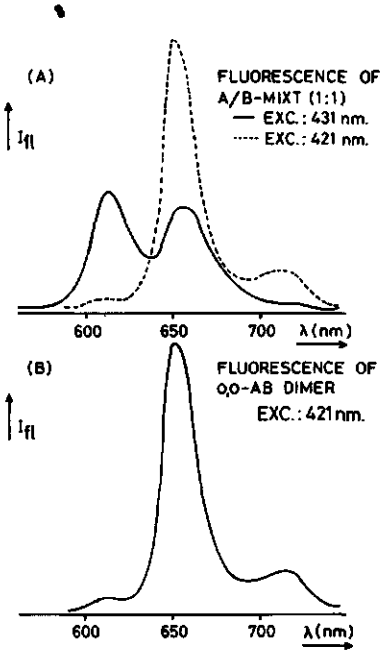

Fig. 2. Fluorescence spectrum of a mixture of H_2-TPP and Zn-TPP (a) and the ortho-ortho bound mixed dimer (b). The samples are irradiated with 421 nm light (dotted curve) and 431 nm light (solid curve). In (b) only the 431 nm spectrum is shown; the 421 nm spectrum is identical.

almost the same to those of H_2-TPP and not to those of Zn-TPP or an intermediate of both sets of values. From Table 3, we can conclude that the ZFS values and the decay rate constants are insensitive to the presence of the heavy zinc-atom and in addition to the geometry of the dimer. This is not surprising in view of the absence of a resonant perturbation in the mixed dimers.

3.5 REFERENCES.

1. R. Avarmaa, Mol.Phys., 37 (1979) 441-454 and references 2-4 and 6 therein.
2. S.W. Provencher, J.Chem.Phys., 64 (1976) 2772-2777.
3. H. Levanon and S. Vega, J.Chem.Phys., 61 (1974) 2265-2274.
4. R.H. Clarke and R.E. Connors, J.Chem.Phys., 62 (1975) 1600-1601.
5. R.G. Little, J.Heterocycl.Chem.,15 (1978) 203-208.

3.6 ACKNOWLEDGEMENT.

This investigation was supported by the Netherlands Foundation for Chemical Research (S.O.N.), with financial aid from the Netherlands Organization for the Advancement of Pure Research (Z.W.O.).

This chapter is published in the proceedings of the XV EUCMOS conference, organized in Norwich (1981) by L. Benthem, R.B.M. Koehorst and T.J. Schaafsma, J.Mol.Struct., 79 (1982) 455-460.

Chapter 4.

ENERGY TRANSFER AND GEOMETRY OF COVALENTLY LINKED PORPHYRIN DIMERS.

Submitted to Chemical Physics.

4 ENERGY TRANSFER AND GEOMETRY OF COVALENTLY LINKED PORPHYRIN DIMERS.

L. Benthem, R.B.M. Koehorst, L.H. de Graaff and T.J. Schaafsma

Department of Molecular Physics, Agricultural University,
De Dreijen 11, 6703 BC Wageningen, The Netherlands.

4.1 INTRODUCTION.

Since the early work of Schwarz et al. /1/ on energy transfer in covalently linked porphyrin dimers a large number of studies have been devoted to this subject /2-14/. For a review see ref. 15.

In this paper we report a study of the effect of varying the geometry of such dimers on singlet-singlet energy transfer, excitonic- and spin-spin interaction and triplet state parameters in particular for meso-tetraphenylporphyrin (TPP) dimers, linked by a single chain, attached to various positions of the phenyl-groups of each porphyrin (see fig. 1).

Calculations of excitonic interactions accounting for spectral shifts /16-18/ have been applied to interacting porphyrins both in solution and in the solid state /6,19/. This paper makes use of a similar treatment, taking into account the presence of proton tautomers in porphyrin monomers and dimers /20-22/. By comparing experimental and predicted spectral shifts, the conformational distribution of the dimer in solid solution can be obtained.

A straightforward method to study the conformation of porphyrin dimers in solid solution makes use of the spin-spin interaction between two paramagnetic ions, inserted into each of the porphyrin moieties. The average distance between the centres of both porphyrin rings can be calculated from the observed broadening or splitting in the solid state EPR spectra of paramagnetic dimers. It is advantageous to chose Cu^{2+} as the paramagnetic ion, since Cu-porphyrins have been widely studied by EPR both as monomers /3,23-28/ and as aggregation dimers /29-31/.

Short-range interactions between the porphyrin macrocycles in a covalent dimer can also be detected by studying the properties of the triplet state: e.g.,

any proces in which the triplet spin is delocalized over both porphyrin moieties is predicted to result in a decrease of the zero field splitting parameters, which directly proportional to the average value $\langle r^{-3} \rangle$, where r is the distance between both triplet spins. Also the triplet kinetics can be used as a means to probe interactions between both monomeric units.

The triplet state of porphyrins can be conveniently studied by optical detection of magnetic resonance (ODMR) /32-35/. The kinetic constants of the spin-levels of the lowest triplet state of TPP can be determined by the microwave-induced changes of the fluorescence /36-38/ or by analyzing the response of the fluorescence intensity to a step-wise increase of the exciting light, using the so-called fluorescence fading (FF) method /39-41/.

Whereas the triplet states of both macrocycles in a porphyrin dimer can be considered to be isolated from each other, since this excitonic interaction is predicted to be small, due to the small S_0-T_0 oscillator strength and T-T energy transfer is unlikely to occur, singlet-singlet energy tranfer does occur in covalently linked metal porphyrins /1,2/, containing two different metal ions or consisting of a mixed metallo-free base porphyrin. The rate of singlet energy transfer in porphyrin dimers depends on the centre-to-centre distance and their relative orientation /1,2,42/. We have analyzed S-S energy transfer between the zinc(II) and the free-base moiety in porphyrin dimers, following previously published methods /1,2/ as well as by measuring fluorescence kinetics /43/.

In this study we used the term monomer for a free base TPP unit and the term macrocycle or monomeric unit for a TPP unit in the dimer.

The goal of these investigations is to elucidate the influence of the relative orientation of the macrocycles in porphyrin dimers on shifts in the optical absorption spectra, on S-S energy transfer, EPR spectra and triplet state kinetic constants.

4.2 EXPERIMENTAL.

Free-base meso α,β,γ,δ-tetraphenylporphyrin (H_2-TPP) dimers (fig. 1) were synthesized according to ref. 44, and purified by adsorption chromatography on silicagel (Merck, Kieselgel 60) with chloroform as an eluent, and gel permeation chromatography (Biorad Laboratories, Biobeads SX2 with toluene). The purity was checked by TLC on silica gel plates (Merck, Kieselgel 60) with toluene.

Metals were inserted into the free-base porphyrin by standard procedures /45/. Mixed metallo-free base porphyrin dimers may be synthesized by inserting

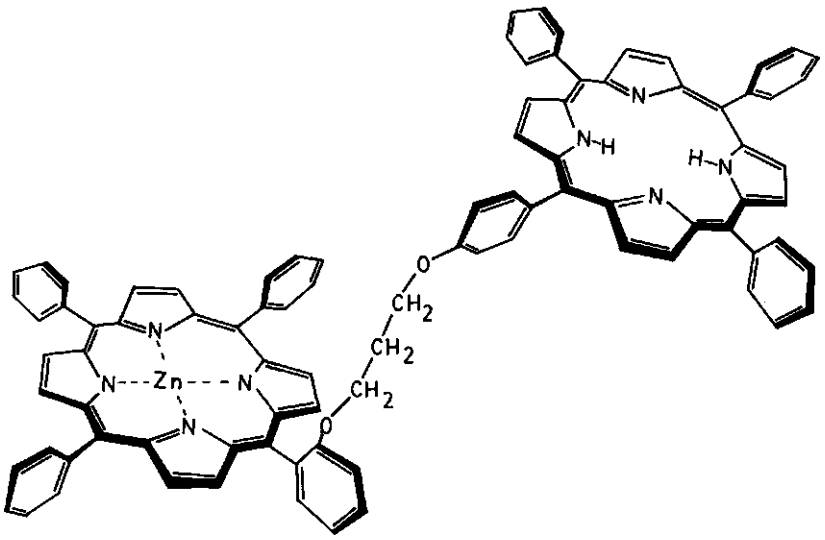

Fig. 1 A singly linked mixed dimer with ortho-para bound porphyrins.

a metal-ion into either of the porphyrin monomers. In the ortho-para mixed dimer the metal ion is always in the porphyrin macrocycle with the linking chain at the ortho position. Metallated porphyrin dimers were synthesized from the corresponding metallo-porphyrin monomers or by metallating both porphyrin macrocycles of a free-base porphyrin dimer. All solvents (PA grade) were used without further purification.

By taking fluorescence spectra at various concentrations, both at room temperature and at 77 K in toluene, we studied the possible formation of intermolecular aggregation of TPP monomers and -dimers. Up to a concentration of 10^{-3} M we saw no evidence of dimerization or aggregation. This in sharp contrast to the aggregation behaviour of other types of porphyrins, where aggregation occurs at concentrations well below 10^{-3} M. The lower tendency to aggregation for TPP is most likely due to steric hindrance of the phenylgroups.

Absorption spectra of 10^{-7} - 10^{-6} M in hexane/toluene (3:1) solutions were taken on a Kontron Uvikon 810 spectrophotometer. Fluorescence spectra and fluorescence detected magnetic resonance (FDMR) spectra at 4.2 K were recorded as decribed previously /46/. For FDMR we employed a 1000 W Osram high-pressure Xe-lamp or a Coherent Radiation CR-4 argon-ion laser as excitation source, a RCA C31034 A photomultiplier tube, and an EG&G PAR model 4203 signal averager for

detecting. Fluorescence fading traces were determined as described in ref. 41. For FDMR and FF the samples consisted of poly-crystalline solid solutions of 10^{-5} - 10^{-4} M in benzene containing 1% pyridine. Fluorescence lifetimes were measured at roomtemperature by exciting 10^{-5} - $5x10^{-5}$ M solutions in benzene/ 1% pyridine with $\tilde{}$ 4.5 ps (theoretical limiting value) dye-laser pulses and analyzing the time-resolved single photon counting decay curves /47/.

EPR spectra of CuTPP monomers and -dimers and of the mixed (Cu-TPP)(H_2-TPP) dimers were recorded at T = 125 K in hexane/toluene (2:1) and in MTHF on a Varian E-6 spectrometer interfaced to a Digital MINC-11 minicomputer. We employed solutions of 10^{-4} - $5x10^{-4}$ M. in order to obtain sufficient signal-to-noise ratios. This concentration is still sufficiently low to prevent the formation of aggregation dimers; up to a concentration of 10^{-3} M we observed no line broadening due to intermolecular dipole-dipole interactions, in agreement with ref. 48.

4.3 RESULTS.

4.3.1 Absorption spectra of free-base dimers.

B(0,0) (Soret)bands of H_2-TPP dimers in hexane/toluene (3:1) all exhibit a redshift w.r.t. the corresponding monomer band. The magnitude of this shift depends on the dimer configuration (see Table 1). As a reference we used the H_2-TPP monomer corresponding to the dimer with -O-(TPP) replaced by -Br in the same configuration. From this Table we note that the B(0,0) shift of the para-para (p,p) linked dimer is 1.5 (± .25) nm, whereas the ortho-para (o,p) and the ortho-ortho (o,o) linked dimers have shifts of $\tilde{}$ 1.0 (± .25) nm. The B(0,0) band of the o,p dimer is $\tilde{}$ 75 % broader than that of the other two configurations. In order to determine shoulders or split absorption bands we have also recorded 2^{nd} derivative absorption spectra. From these spectra it is evident that the o,p dimer Soret absorption band is split with $\Delta E \tilde{}$ 110 cm^{-1}, whereas the p,p and o,o dimer absorption bands are only shifted.

We have also synthesized a p,p linked dimer with a $-(CH_2)_{10}-$ instead of a $-(CH_2)_3-$ bridge. For this compound no shift was observed.

TABLE 1

Peak positions $\tilde{\nu}_B$ of the Soret absorption bands of free base tetraphenyl porphyrin monomers and various dimers[a] in hexane/toluene (3:1) at room temperature.

Configuration/ chain lenght[b]	$\tilde{\upsilon}_B$ (monomer) $(cm^{-1})^c$	$\tilde{\upsilon}_B$ (dimer) $(cm^{-1})^c$	shift $(cm^{-1})^c$
para-para / $(CH_2)_3$	24004	23918	86
ortho-para / $(CH_2)_3$	24021	23969	52[d]
		24079e	-58
ortho-ortho / $(CH_2)_3$	24038	23975	63
para-para / $(CH_2)_{10}$	24004	24004	0

a) Monomers have the same linking chain, with -O-(TPP) replaced by -Br, in the same configuration as in the dimers.

b) For structure, see fig. 1.

c) Errors: peakposition ± 7 cm^{-1}; shift ± 14 cm^{-1}

d) Broadened absorptionband.

e) Shoulder.

4.3.2 EPR of Cu-Cu dimers.

Dipolar interactions between paramagnetic ions, resulting in broadening of EPR transitions depend on the interionic distance r as $\langle r^{-3} \rangle$ /49/. Therefore we replaced the two protons in both H_2-TPP macrocycles by Cu^{2+} ions. As a reference we used (Cu-TPP)-(H_2-TPP) dimers with the same configuration.

EPR spectra of a number of dimers are shown in fig. 2. For p,p-$(Cu\text{-}TPP)_2$ all superhyperfine lines are broadened, quite noticably in the region 3300 -3400 G.

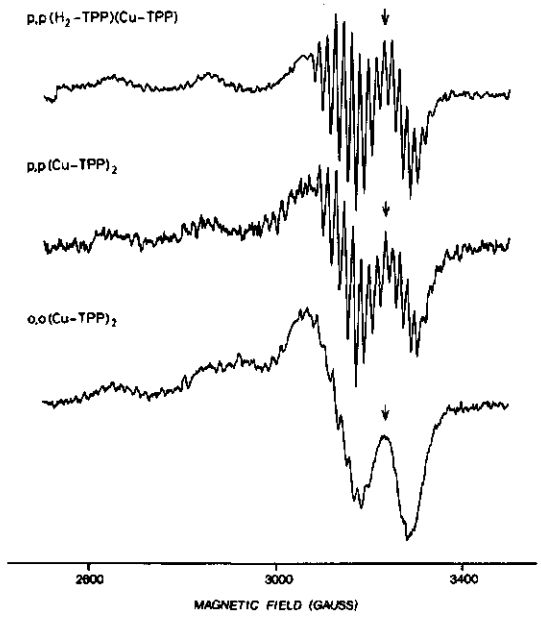

Fig. 2 EPR spectra of p,p-(H_2-TPP)(Cu-TPP) (upper), p,p-(Cu-TPP)$_2$ (middle) and o,o-(Cu-TPP)$_2$ (lower spectrum) in toluene at 125 K. The superhyperfine line used for determination of the linewidth is marked with an arrow. Note, that in the o,o dimer in toluene the linewidth cannot be determined, because the superhyperfine structure has almost disappeared. For the other solvents, the linewidth could be determined (see Table 2).

In the o,o-(Cu-TPP)$_2$ in toluene the linewidth of each individual superhyperfine component has so much increased that the perpendicular transition has no structure any more. For a detailed EPR study of Cu-TPP see ref. 50. To obtain the net broadening, due to spin-spin interaction between the Cu^{2+} ions in a particular dimer, the derivative peak-to-peak width was determined, using a specific line in the perpendicular region, marked with an arrow in fig. 2, followed by subtraction of the linewidth of the corresponding superhyperfine component in the spectrum of the (CuTPP)(H_2TPP) dimer. From the experimental broadening we have calculated (see Discussion) the average Cu-Cu distance in the various dimers, and thus the centre-to-centre distance between both porphyrin macrocycles in the various configurations (Table 2). There is a definite effect of solvent polarity on the centre-to-centre distance between both rings (compare entries A and B in Table 2).

TABLE 2

First derivative peak-to-peak EPR linewidths $(CuTPP)_2$ and (CuTPP)(H_2TPP) dimers; spin-spin broadening and distances in $(CuTPP)_2$ dimers; solvent: toluene/hexane (1:2) (A) and MTHF (B); T = 125 K.

Configuration	ΔH_{pp} (Cu-H_2)[a] (G)		ΔH_{pp} (Cu-Cu) (G)		δH_{pp} (G)		r^b (nm)		r^c (nm)	
	A	B	A	B	A	B	A	B		
para-para	8.3	-[d]	9.2	-[d]	0.9	-	2.7	-	2.7	
ortho-para	8.0	6.1	9.7	7.5	1.7	1.5	2.2	2.2	1.9	
ortho-ortho	8.0	6.4	10.0	10.5	2.0	4.1	2.1	1.7	1.7	exo
									0.9	endo

a) Reference dimers have the same configuration as the corresponding CuTPP dimer.

b) Estimated error, resulting from error in determining peak-to-peak linewidth (± 0.1 G): ± 0.1 nm.

c) From space filling models.

d) Not quoted in view of large error and broadening.

4.3.3 Fluorescence detected magnetic resonance (FDMR) and fluorescence fading.

FDMR spectra of H_2-TPP and the p,p-(H_2-TPP)-(Zn-TPP) dimer are presented in fig. 3. For most solvents the shape of the monomer and the dimer spectra are very similar: the dimer peak positions are only slighted shifted w.r.t. those of the corresponding monomers. In acetone, we observe a site-structure (Fig. 3) (see Discussion). In general the spectra contain three transitions at 2E.c, (D-E).c and (D+E).c Hz, where D and E are the zero field splitting parameters

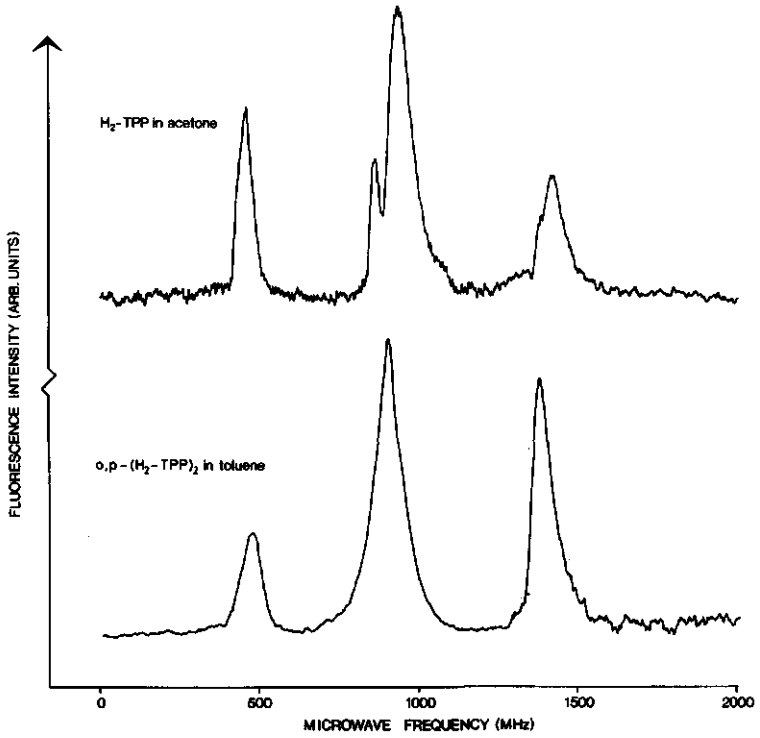

Fig. 3 Fluorescence detected ODMR spectra of H_2-TPP in acetone and o,p-$(H_2$-TPP$)_2$ in toluene at 4.2 K. The spectra are taken in two parts, from 0-1200 MHz and from 800-2000 MHz resulting in different signal-to-noise ratios in these regions.

/49/ in cm^{-1} and c is the speed of light in $cm.s^{-1}$. The 2E transition is observed for the free-base compounds, but not for the corresponding Zn-compounds. Table 3 collects the D and E values for all monomers and dimers studied by FDMR.

We have also measured the response of the fluorescence intensity to a stepwise increase of the excitation light intensity, the so-called fluorescence fading curves /41/. These curves can be described by two exponentials for the zinc monomer and dimers and three exponentials for the free-base monomer and all dimers containing the free-base, and represent the decay rate constants k_i of the triplet spinlevels, when determined at $T \leq 4.2$ K. Since at low excitation rate all k_i's are proportional to the fractional triplet population n_T/N /51,52/ (where n_T is the number of triplet molecules, and N the total number of molecul-

TABLE 3

Zero field splitting (ZFS) parameters D and E (in units 10^{-4} cm^{-1}), decay rate constants and relative populations of the spin levels of the lowest triplet state of the H_2-TPP and Zn-TPP monomers and their covalently bound dimers.

Solvent: benzene/1% pyridine; T = 4.2 K.

Method	FDMR		FF					
Compound	D[a]	E[a]	k_x (s^{-1})	n_x[b]	k_y (s^{-1})	n_y[b]	k_z (s^{-1})	n_z[b]
H_2-TPP (A)	377	81	180 ± 15	.44	480 ± 50	.14	46 ± 8	.42
Zn-TPP (B)	308	96	145 ± 10	.15	145 ± 10	.15	48 ± 5	.70
pp-AA	381	83	196 ± 40	.40	508 ± 60	.10	46 ± 12	.50
op-AA	384	84	226 ± 15	.46	535 ± 60	.18	51 ± 13	.36
oo-AA	385	83	161 ± 16	.76	462 ± 35	.24	[c]	[c]
pp-AB	371	81	168 ± 20	.53	[c]	[c]	62 ± 15	.42
op-AB	376	81	158 ± 30	.56	610 ± 60	.15	47 ± 9	.29
oo-AB	378	81	201 ± 25	.45	560 ± 45	.17	58 ± 6	.38
pp-BB	305	98	151 ± 11	.15	151 ± 11	.15	56 ± 4	.70
op-BB	307	97	149 ± 17	.13	149 ± 17	.13	59 ± 5	.74
oo-BB	308	98	136 ± 8	.15	136 ± 8	.15	51 ± 4	.70

a) Error $\tilde{\sim}$ 1%.

b) Error $\tilde{\sim}$ 20%.

c) Not quoted in view of large error.

es), the true values of k_i have been determined by extrapolating to zero triplet population (see Fig. 4 and Table 3).

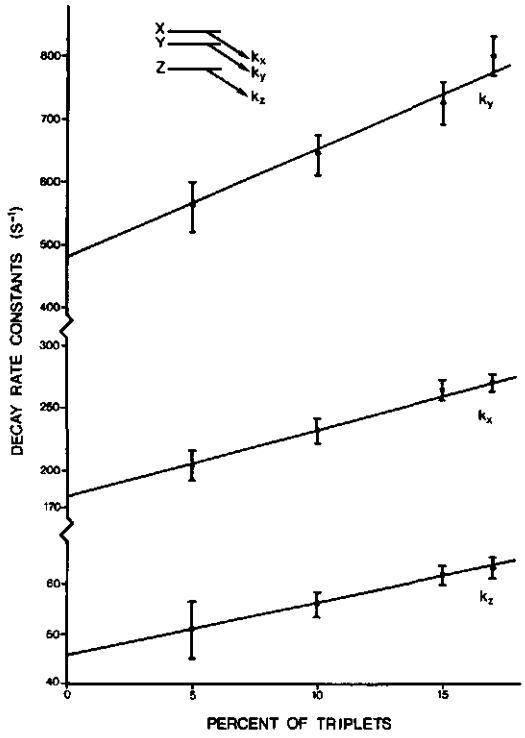

Fig. 4 Dependence on the triplet percentage $n_{T_0}/(n_{T_0} + n_{S_0})$ of the decay rate constants of the sublevels of the lowest triplet state in H_2-TPP. Note the different vertical scale for the various decay rate constants. Inset: the relative position of the three triplet sublevels.

4.3.4 Lifetime measurements.

Table 4 summarizes the fluorescence lifetimes (τ_i) and the relative amplitudes (f_i) of the various TPP monomers and dimers. For the H_2-TPP monomer and -dimers we find a single lifetime of about 10 ns, whereas for the Zn-containing monomer and dimers, $(ZnTPP)_2$ and $(ZnTPP)(H_2TPP)$, two or three different lifetimes are found.

In the mixed dimers S-S energy transfer from the zinc to the free-base part of the dimer can be detected by monitoring the fluorescence decay of the Zn-TPP emission or by monitoring the increase of the a H_2-TPP emission after excitation in a Zn-TPP absorption band.

TABLE 4

Fluorescence lifetimes (τ_i) and relative amplitudes (f_i)[a] of monomeric free base and zinc TPP and their homo- and heterodimers.

Solvent: benzene/1% pyridine; detection bandwidth: 4 nm.
Error in τ_i and f_i ± 4%.

Compound	detection wavelength (nm)	τ_1 (ns)	f_1	τ_2 (ns)	f_2	τ_3 (ns)	f_3
H_2-TPP (A)	717	9.72	1.00				
Zn-TPP (B)	613	1.56	.89	1.18	.11		
pp-AA	717	9.32	1.00				
op-AA	717	9.84	1.00				
oo-AA	717	9.91	1.00				
pp-BB	613	1.42	.85	.51	.15		
op-BB	613	1.52	.83	.49	.17		
oo-BB	613	1.91	.57	.97	.43		
pp-AB	717	9.64	.84	3.53	.16		
op-AB	717	10.76	.76	3.69	.24		
oo-AB	717	10.59	.50	7.54	.50		
pp-AB	613	.264	.93	1.59	.05	9.51	.02
op-AB	613	.295	.71	1.43	.24	9.15	.05
oo-AB	613	.206	.85	1.27	.06	8.68	.09

a) The entries in the columns with headings τ_1, f_1 through τ_3, f_3 have been arranged in order of decreasing amplitude.

4.4 DISCUSSION.

4.4.1 Absorption spectra.

In order to interpret the shift of the Soret absorption band of dimers vs. monomers the orientation of the H-H axis in H_2-TPP needs to be defined w.r.t. the molecular axis system. Following Platt /53/, the out-of-plane axis is

denoted by z, whereas x and y represent both in-plane axes (x// H-H). Whereas the Q-bands are split into Q_x and Q_y components about 3000 cm^{-1} apart, the splitting of the Soret band remains unresolved at room temperature /54-56/. In fact, calculations indicate /57/ that the Soret band contains a number of strongly mixed x- and y- polarized transitions. Because of the ground state N-H tautomerism in H_2-TPP /21,22/ there are two H-H orientations, w.r.t. the molecular frame of reference, assumed to occur with equal probability. Since rotation of the H-H axis in the H_2-TPP unit results in an interchange of x and y polarizations, the interaction between the transition moments of both H_2-TPP units has been calculated, assuming that the transition moments in both units have equal probability to be oriented along the x or y direction (see fig. 5).

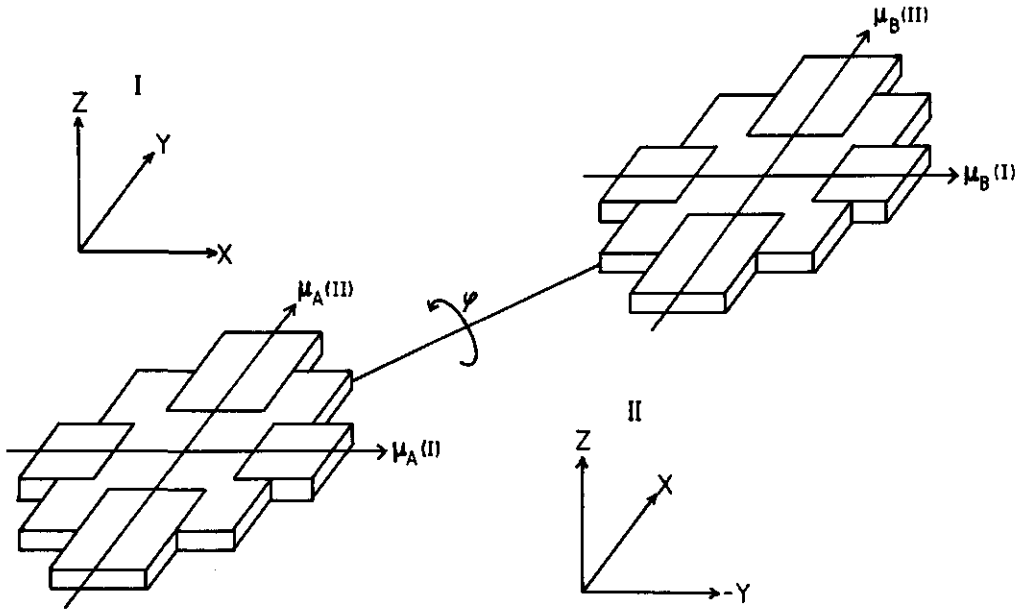

Fig. 5 A schematic representation of p,p-(H_2-TPP)$_2$ with the two possible relative orientations of the transition dipole moments (I or II). The directions μ_A and μ_B are independent of each other for both porphyrin macrocycles. The x-axis is defined as parallel to the H-H axis. Note that the pyrole rings are represented by squares.

The excited state energies of TPP dimers can be calculated w.r.t. those of the

monomer from Eqn. (1), representing the energy shift caused by an interaction between the transition dipole moments $\vec{M}_1$ and $\vec{M}_2$ on the porphyrin moieties 1 and 2, separated by a centre-to-centre distance r:

$$\Delta E = \frac{\vec{M}_1 . \vec{M}_2}{r^3} - 3 \frac{(\vec{M}_1 . \vec{r})(\vec{M}_2 . \vec{r})}{r^5} \qquad (1)$$

The interaction V (exciton splitting) is defined by $V = 2\,|\Delta E|$.

In the p,p-TPP dimer, shown in fig. 5, rotation is possible around the linking chain over an angle ϕ. We have used a single rotation angle, because other possible rotations of one porphyrin ring w.r.t. the other are highly sterically hindered as can be concluded from space filling models, and because of the use of apolar solvents, in which the dimers have an unfolded conformation (see Table 2). Due to the presence of two H-H tautomers in each of the macrocycles and the relative phase of the transition dipole moments, $\vec{M}_1$ and $\vec{M}_2$ are mutually oriented in four different ways. Since for p,p dimers $\vec{M}_1$ and $\vec{M}_2$ make an angle of 45° with the linking axis, the number of different orientations of $\vec{M}_1$ w.r.t. $\vec{M}_2$, which has to be considered over the full 2π rotation of $\vec{M}_2$ w.r.t. $\vec{M}_1$, reduces to two for this dimer.

In an accompagnying paper /58/ we have calculated the excited state energies and their probability distribution as they depend on the relative orientation on both porphyrin rings in the dimers. Here, we will only summarize the results.

For the p,p dimers we find the following results for the energy shifts:

$$\Delta E_1 = - \Delta E_2 = (M^2/r^3)(\tfrac{1}{2} \cos \phi - 1) \qquad (2)$$

where $M = |M_1| = |M_2|$ and $\Delta E_{1,2}$ represent both abovementioned relative orientations of $\vec{M}_1$ and $\vec{M}_2$, and ϕ is the rotation angle for rotation around the chain axis ($-\pi < \phi < \pi$). The corresponding transition probabilities P_i are proportional to M^2, and are given by:

$$P_1 \; (:) \; M^2 \; (3 + \cos \phi) \qquad (3a)$$

$$P_2 \; (:) \; M^2 \; (1 - \cos \phi) \qquad (3b)$$

For our calculations, we assume that all angles ϕ have equal probability of occurence. This results in two absorption profiles, one of which is redshifted

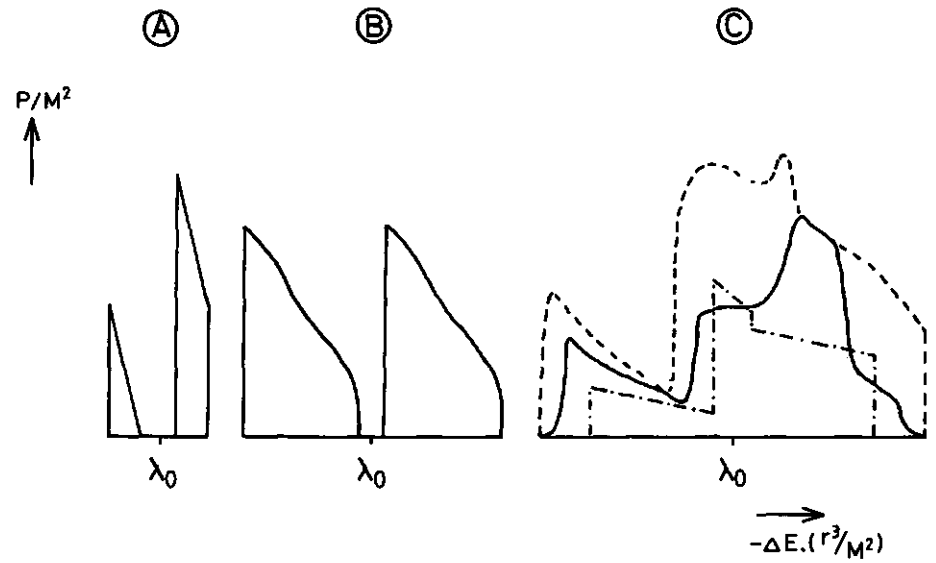

Fig. 6 Calculated energy shifts of the Soret absorption band for the p,p (A), the o,p (B) and the o,o linked dimer (C). The shift is dependent on the angle of rotation round the linking axis, which is in (A) and (B) from $-\pi$ to π. In (C) we have calculated three possibilities: $-1/3\pi < \phi < 1/3\ \pi$ (dashed line), $-1/6\pi < \phi < 1/6\pi$ (solid line) and $\phi = 0$, but with a rotation of one porphyrin macrocycle w.r.t. the other ($-\pi < \psi < \pi$). See fig. 7 for an explanation of ϕ and ψ.

($\Delta E_1 < 0$) and a second one blueshifted ($\Delta E_2 > 0$) w.r.t. the monomeric absorption, taken as a reference. Since $P_1 > P_2$, the redshifted component has higher amplitude than the blueshifted component (see fig. 6A). From this figure, we may also conclude that, if a band splitting occurs (e.g. for $\phi = \pi/2$), the redshifted part of this band has equal or higher amplitude as compared to the blueshifted component.

Similarly, expressions for the energy shifts and the transition probabilities can be derived for the o,p and o,o dimers. For the o,p dimer the result is a red- and a blueshifted absorption band with equal probabilities, as shown in fig. 6B. The o,o dimer is more difficult to analyze, due to the presence of steric hindrance, preventing a ϕ-rotation over the full 2π range. The conclusion of our calculation, however, is again a red- and a blueshifted absorption band. For the o,o compound, we have calculated three possibilities: first a rotation

around the linking chain corresponding to $-\pi/3 < \phi < \pi/3$, second for $-\pi/6 < \phi < \pi/6$, both with $\psi = 0$ and third no rotation around the linking axis ($\phi = 0$), but a rotation of one porphyrin ring w.r.t. the other ($-\pi < \psi < \pi$). The intensity ratio of these bands strongly depends on the accessible range of ϕ and ψ (see fig. 6C).

In each of the abovementioned cases we find a redshifted as well as a blueshifted transition. The solvent polarity largely controls the average relative orientation of both porphyrin macrocycles and their angular distribution, and thus the shape of the absorption band. The width of the dimer absorption band or a possible splitting w.r.t. that of the monomer is determined by the angular constraints for the relative rotation of the porphyrin rings (ϕ, ψ).

The experimental data are summarized in Table 1. For the p,p dimer we find a 86 cm^{-1} redshift, no splitting, and a linewidth which is $\tilde{}$ 5 % larger than that for the monomer. This implies an almost stretched geometry, and either a ϕ-distribution over the full 2π range, or a preferential orientation with $\phi \tilde{} \pi/2$ (see fig. 7A). Experimentally the predicted blueshifted component cannot be resolved. For the o,p dimer the experiment yields a net average redshift, a splitting of 110 cm^{-1}, and a linewidth $\tilde{}$ 75 % larger than that of the monomer. This can be accounted for by a conformation shown in fig. 7B. The results for the o,p dimer can be explained by assuming an angular distribution for ϕ over the full 2π range. The spectrum of the o,o dimer is more difficult to interpret. Experimentally we observe a 63 cm^{-1} redshift, no splitting, and the same linewidth as for the monomer, very similar to the situation for the p,p compound. The exo-conformation ($\phi = 0$), shown in fig. 7C, does yield a small net redshift, if the two porphyrin macrocycles are coplanar ($\psi = 0$). The small linewidth indicates a very narrow angular distribution. This finding is confirmed by space filling models. Thus, by comparing calculated and experimental spectra, we may conclude that the o,o compound predominantly occurs in the exo-conformation, and furthermore, that both porphyrin rings are severely sterically hindered w.r.t. their relative rotation. These results are in agreement with NMR results /59/.

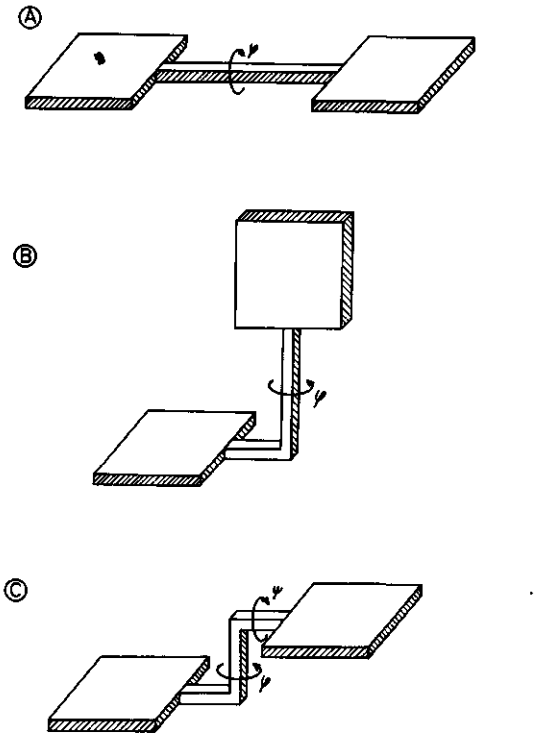

Fig. 7 Calculated conformations for the various dimers: p,p (A), o,p (B) and o,o-$(H_2\text{-TPP})_2$ as determined from the observed shift of the Soret absorptionband. ϕ and ψ are the rotation angles used in our calculations. For the p,p and o,p dimer a full ϕ-rotation over 2π radians is possible. The o,o dimer has an almost fixed geometry.

4.4.2 EPR measurements.

The second moment of the EPR linewidth of $(Cu\text{-TPP})_2$ dimers, can be related to the Cu - Cu distance r by the Van Vleck equation /49/, which is (in SI units):

$$\overline{(\Delta\upsilon)^2} = \frac{3}{16}\left(\frac{\mu_0}{4\pi}\right)^2\left(\frac{\gamma}{2\pi}\right)^2 h^2\, S(S+1)\,\frac{(1 - 3\cos^2\theta)^2}{r^6} \qquad (4)$$

with: $(\Delta\upsilon)^2$ mean square width (in Hz)

μ_0 magnetic permeability of vacuum ($H.m^{-1}$)

γ magnetogyric ratio = $\gamma_e\ g_e$, with

g_e g-factor for free electron

γ_e magnetogyric ratio of the free electron

h Planck's constant

S spin angular momentum of the electron

Θ angle between r and the magnetic field direction

It is found that each of the resolved components of the EPR spectra in fig. 2 has a Gaussian lineshape, due to unresolved hyperfinestructure. Then, Eqn. (4) yields:

$$r = 1.23\ (\delta H_{pp})^{1/3} \qquad (5)$$

with r = distance between the spins in nm

$\delta H_{pp} = \Delta H_{pp}(d) - \Delta H_{pp}(m)$, where $\Delta H_{pp}(d)$ and $\Delta H_{pp}(m)$ represent the peak-to-peak widths (in mT) of the resolved hyperfine components in the first derivative EPR spectra of dimers and monomers respectively.

From the observed linewidths and Eqn. (5) the average distance between the two Cu-atoms and thus the centre-to-centre distance between the two porphyrin macrocycles can be calculated for the various configurations (see Table 2).

From CPK-type space filling models we can estimate the distance between the rings and compare them with those from EPR linewidths. The results have been included in Table 2. As is clear from this Table, the agreement between the values from EPR linewidths and space filling models is excellent for the p,p dimer but less satisfactory for the o,p dimer. The values for the o,o dimer can only be reconciled if this compound occurs predominantly in the exo-conformation, as is corroborated by ^{1}H-NMR measurements (see Chapter 5) and from our absorption data (see § 4.4.1)/58,59/.

As expected, the distances obtained from EPR linewidths are solvent-dependent: the o,o dimer spectrum in MTHF yields r = 1.7 ± 0.2 nm, in very good agreement with the value from the space filling model. This effect is expected, since the apolar porphyrin rings are forced together in a polar environment. This causes their distance to be more in agreement with those of a space filling model, where the distance between both rings is minimal. For the o,p dimer sol-

vent polarity has no effect on the ring-ring distance, probably because of steric effects of the phenylrings of both macrocycles, hindering the folding of the porphyrin rings; only a rotation around the linking axis is possible (see § 4.4.1).

4.4.3 Properties of the triplet state.

All three decay rate constants of the triplet sublevels of a non-phosphorescent compound can be measured from the fluorescence response, $I_f(t)$, to a stepwise increase of the exciting light intensity in a single experiment /39,40/. The response function is given by (see Appendix 1):

$$I_f(t) = I_f(0)\ [1 - \frac{I_f(0) - I_f(\infty)}{I_f(0)}\ \{\ 1 - \frac{1}{\sum_i c_i}\ \sum_i c_i\ \exp - (k_i + \phi_T^i\ k_{ex})t\}] \qquad (6)$$

k_i represents the decay rate constant of spinlevel $|i\rangle$ of the lowest triplet state and $c_i / \sum_i c_i$ represents the relative amplitude of this decay in the $I_f(t)$ curve. It can be shown, that $c_i / \sum_i c_i$ represents the relative steady state population of $|i\rangle$. (see Appendix 1).

From the values of k_i and n_i for each spinlevel $|i\rangle$ the relative populating rates p_i follows from:

$$p_i = n_i . k_i \qquad (7)$$

The fluorescence fading (FF) method offers some obvious advantages over microwave induced delayed fluorescence methods /51,60/, since for severely broadened FDMR transitions the fluorescence response to microwave pulses or -steps may be too weak to detect under steady state illumination. Furthermore, the method does not suffer from the effects of microwave undersaturation /61, 62/.

From the results, collected in Table 3, it is evident that for the homodimers substitution of a second porphyrin ring to the TPP monomer in various configurations has limited effects on the kinetic constants of the lowest triplet state. Only the D-value is slightly increasing from the p,p via the o,p to the o,o dimer. The E-value is not influenced by substitution. Comparing the ZFS values and the kinetic constants of the heterodimers, these look almost the same to those of H_2-TPP and not to those of Zn-TPP or an intermediate of both sets of

values. From Table 3 it is shown, especially in the free base dimers that there is in some cases an increase of the decay rate constants. In the homodimers a triplet excitation hopping from one porphyrin macrocycle to the other conceivably could contribute to the observed triplet decay rate constant. As is shown in appendix 2, this does not result in a shortening of the lifetime of the triplet sublevels, however, and the monomer values are predicted to be found. The reason for the variation in the decay rate constants is currently unknown. The shortening of the free base dimer triplet kinetics may be due to a symmetry perturbation of a free base by its neighbour, affecting vibrational modes of the central protons involved in the radiationless decay. The contribution of these modes to the radiationless triplet decay has been demonstrated by the effect of substituting the central protons by deuterons on the triplet decay kinetics of H_2TPP monomers /63/. We note that for $(ZnTPP)_2$ and (ZnTPP-H_2TPP) dimers the perturbing porphyrin (ZnTPP) has higher symmetry than the free base dimer.

For the mixed dimers no excitation hopping is possible, but only energy transfer from the metal porphyrin to the free base part. It is expected and found that the decay kinetics of the mixed dimers represent those of the free base part, uncontaminated by energy transfer kinetics, either of the T-T or S-S type.

Recording FDMR spectra of free base TPP in most solvents result in spectra with the normal 2E, (D-E) and (D+E) transition without any additional structure. Only in acetone the (D-E) and (D+E) transitions are split (see fig. 2). This can be the result of i) N-H tautomerism or ii) a site effect. For H_2P in an n-octane host /65/, evidence has been obtained that both tautomers have slightly different ZFS parameters, due to two distinguishable orientations of the H-H axis in a low-symmetry environment.

Very recently Gueckel et al. /64/ published an ODMR study of cofacial porphyrin dimers with relatively short centre-to-centre distances ($\tilde{<}$ 1 nm) between both macrocycles. These authors are using an exciton model in the weak coupling limit to study structural and dynamical features of their compounds: the interaction between the two macrocycles must be small compared to the zero field splitting ($2J < D, E$). However, from their experiments it can be concluded, that the interactions in their compounds cannot be described by the weak coupling limit, since the redshift of the phosphorescence spectrum of the dimers w.r.t. that of the monomer is in the order of a few hundred cm^{-1}, whereas the zero field splitting term $D \tilde{<} 0.0350\ cm^{-1}$. Also comparing the D-value of the dimer w.r.t. that of the monomer demonstrates that the weak coupling is not valid. Probably, mixing of low lying charge transfer states has to be taken into account.

4.4.4 Energy transfer kinetics.

In Table 4 the fluorescence lifetimes and the relative amplitudes of the various monomers and dimers are presented. For ZnTPP we find two lifetimes instead of one. This is due to the presence of nonligated and monoligated ZnTPP /66,67/; the 1.56 ns component is assigned to ZnTPP monoligated with pyridine and the 1.18 ns component to the nonligated species. In the free base dimers we have the same lifetime as for the free base monomer, because energy transfer is endothermic (see fig. 8 I). In the zinc dimers, we have a different situation: either one or both of the ZnTPP units may be ligated or non-ligated in the dimers. Because of the large equilibrium constant for ligation with pyridine ($K \simeq 6000$ at 20 °C /66/), the presence of doubly non-ligated dimers can be neglected. For the doubly ligated dimers the same holds as for the free base dimers; the energy transfer is, again, endothermic, so the same lifetime as for the monomer is found. In dimers where one unit is ligated energy transfer is possible from the non-ligated unit to the ligated part (see fig. 8 II_a), but not from the ligated to the non-ligated unit (fig. 8 II_b). This results in a shortening of the fluorescence lifetime of the non-ligated ZnTPP fluorescence from 1.18 ns to values below 1 ns, whereas the fluorescence lifetime of the ligated ZnTPP is only weakly affected. From Table 4 it can also be concluded that for the o,o-C_3-$(ZnTPP)_2$ dimer the ratio ligated/non-ligated is much lower than for the other configurations and the monomer. This can be ascribed to steric hindrance of the ligation position by the other TPP macrocycle.

For the mixed dimers energy transfer from a ligated, as well as from a non-ligated ZnTPP- to the H_2TPP part of the dimer is possible, as is shown in fig. 8 III. Detecting the fluorescence intensity of the ZnTPP part in a fluorescence lifetime experiment, we find three lifetimes: i) a very short component (200 - 300 ps), ascribed to the unligated ZnTPP fluorescence lifetime shortened by the rate for energy transfer to the H_2TPP part, ii) the ZnTPP.L lifetime ($\simeq$ 1.5 ns) and iii) with a low amplitude the free base lifetime ($\simeq$ 9.5 ns). This last component is found, because at 613 nm already a very small part of the 0-0 fluorescence band of H_2TPP, which has a maximum at $\simeq$ 650 nm, can be detected. As is evident from a comparison of the overlap integrals for the ZnTPP fluorescence and the H_2TPP absorption (fig. 8 III), the energy transfer between non-ligated ZnTPP to H_2TPP is predicted to be faster, than between the ligated form of ZnTPP to the free base part. However, the ratio of both overlap integrals cannot completely account for the observation of an almost unchanged 1.5 ns component in the decay of the mixed dimers (Table 4). It is conceivable that the ratio of the

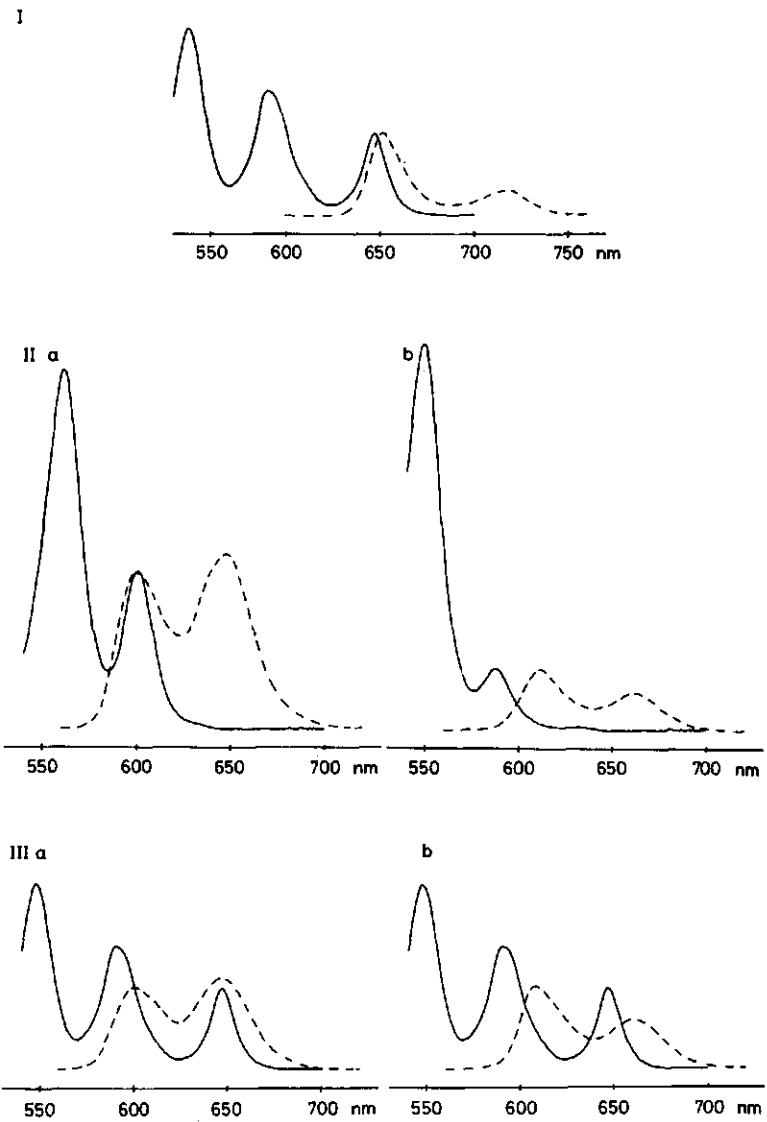

Fig. 8 Absorption (solid curve) and fluorescence (dashed curve) spectra of H_2TPP and ZnTPP (ligated and non-ligated with pyridine).

I absorption and fluorescence spectra of H_2TPP

II a) fluorescence spectrum of non-ligated ZnTPP and absorption spectrum of ZnTPP, ligated with pyridine

b) fluorescence spectrum of ZnTPP, ligated with pyridine and absorption spectrum of non-ligated ZnTPP

III a) absorption spectrum of H_2TPP and fluorescence spectrum of non-ligated ZnTPP

b) absorption spectrum of H_2TPP and fluorescence spectrum of ZnTPP, ligated with pyridine

fluorescence yields for the ligated and non-ligated ZnTPP parts of the mixed dimers differs significantly from the same ratio for the ligated and non-ligated monomers.

It is striking, that the amplitude of the fluorescence decay ascribed to the non-ligated (ZnTPP-H_2TPP) dimer for all three mixed dimers is considerably larger than the amplitude of the ligated ZnTPP in the same dimer (see table 4). We note that for the ZnTPP homo-dimers (in particular for the o,o-C_3-$(TPP)_2$ dimer) the amplitude of the non-ligated species is higher than for the correponding species of the monomers. This is to be expected in view of the more limited accessibility of the ZnTPP moiety in a dimer, as compared to the monomer. Therefore, the high amplitude of the non-ligated ZnTPP species in mixed dimers is probably due to a change of the equilibrium constant for Zn ligation in the dimers w.r.t. the monomers.

The fluorescence intensity of the free base part is biexponential. We find the H_2TPP monomer lifetime as can be expected, and a shorter component of 3 - 7 ns. The origin of this last component is unclear, and may be due to an artifact arising from our method of analysis.

From fig. 9A and 9B it is evident that singlet-singlet energy transfer occurs from the Zn-TPP part to the H_2-TPP part of a mixed dimer. In fig. 9A the fluorescence spectra of a (1:1) mixture in toluene of H2-TPP and ZnTPP are presented, whereas fig. 9B shows the fluorescence spectrum of o,o-C_3-(H_2TPP-ZnTPP). In either case, no ligated ZnTPP is present in the solution. This spectrum is identical to the H_2TPP fluorescence spectrum, even when excited in the ZnTPP absorption band. The quantum efficiency for energy transfer (ϕ_{ET}) can be calculated from the intensities of the ZnTPP fluorescence at 613 nm and the free-base fluorescence at 650 nm of the dimer as compared to a mixture (1:1) of the H_2-TPP and Zn-TPP monomers, when exciting with 431 nm light. Then, ϕ_{ET} is /2/:

$$\phi_{ET} = 1 - \frac{I^d\ (Zn)}{I^m\ (Zn)} \cdot \frac{I^m\ (H_2))}{I^d\ (H_2)} \qquad (8)$$

where d stands for dimer and m for monomer in the mixture. For the various dimers ϕ_{ET} is given in Table 5.

The most probable mechanism for the observed energy transfer is the dipole-dipole interaction /68/. Using the Förster equation the rate constant for energy transfer (k_{ET}) can be calculated using /69/:

$$k_{ET} = \frac{k_f\ \ \phi_{ET}}{\phi_f\ (1-\phi_{ET})} \qquad (9a)$$

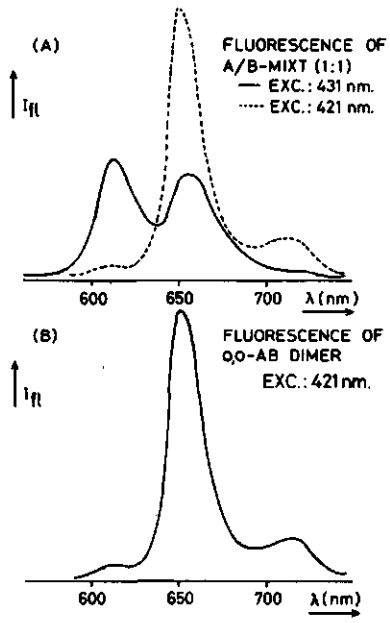

Fig. 9 Fluorescence spectra in toluene of a (1:1) mixture of H_2-TPP and Zn-TPP (A) and the o,o linked mixed dimer (B). In (A) are the samples irradiated with 421 nm light (dotted curve) and 431 nm light (solid curve). In (B) only the 421 nm spectrum is shown; the 431 nm spectrum is identical.

where ϕ_f is the donor fluorescence quantum yield in the absence of energy transfer and k_f is the intrinsic rate constant for donor fluorescence; ϕ_f is $\simeq$ 0.04 /70/ and k_f was calculated to be $3.2 \times 10^{+07}$ s^{-1} from our experimental lifetime and quantum yield. Using these values for substitution in Eqn. (9a) k_{ET} was determined for the mixed dimers in their various configurations (see Table 5).

From the lifetime of the dimer w.r.t. the monomer k_{ET} can also be calculated. Assuming that the Zn-TPP part of the dimer has the same lifetime in the absence of energy transfer as the Zn-TPP monomer, k_{ET} follows from:

$$k_{ET} = k_d - k_m \qquad (9b)$$

with $k_d = (\tau_d)^{-1}$ and $k_m = (\tau_m)^{-1}$, τ_d and τ_m are the fluorescence lifetimes of the dimer and monomer, respectively. Eqn. (9b) is equal to eqn. (9a) but more convenient to use for the fluorecence lifetimes. Using the values from Table 4

TABLE 5

Fluorescence lifetime (τ), quantum efficiency for energy transfer (ϕ_{ET}) and rate constant for energy transfer (k_{ET}) of non-ligated ZnTPP to H_2TPP in mixed (H_2-TPP)(Zn-TPP) dimers. ϕ_{ET} was calculated from eqn. (8).

Solvent: benzene/1% pyridine; room temperature.

Configuration	ϕ_{ET}	$k_{ET}(I)^a$ ($.10^{+9}$ s^{-1})	$k_{ET}(II)^a$ ($.10^{+9}$ s^{-1})	$\tau(I)^a$ (ps)	$\tau(II)^a$ (ps)
para-para	.83 ± .02	3.9 ± .3	3.0 ± .3	207 ± 20	264 ± 5
ortho-para	.81 ± .02	3.4 ± .2	2.6 ± .2	232 ± 20	295 ± 9
ortho-ortho	.86 ± .02	4.9 ± .3	4.1 ± .2	171 ± 17	206 ± 13

a) I refers to a calculation from the emission spectrum and
II as calculated from time-resolved fluorescence spectroscopy.

k_{ET} was determined as given in Table 5. Both sets of values are in good agreement.

The lifetime of the donor in the presence of energy transfer (τ_d) can be calculated from the transfer efficiency and the lifetime of the monomer (τ_m) from /71/:

$$\tau_d = (1 - \phi_{ET}).\tau_m \qquad (9c)$$

which is, again, a rearranged form of Eqn. (9a). Using the values for ϕ_{ET} as calculated from Eqn. (8) and the value τ_m = 1.18 ns, the lifetimes of the zinc fluorescence for the various dimers are as given in Table 5. These values are in rather good agreement with the values from our timeresolved fluorescence measurements. It is expected that the lifetime would decrease from p,p, via o,p to the o,o dimer, as a result of decreasing ring-ring distance. Table 5 shows, however, that the o,p dimer has the longest lifetime. This is due to the always perpendicular position of both porphyrin macrocycles, resulting in a less fa-

vourable mutual orientation of the transition dipole moments as compared to the other compounds. Also the energy transfer efficiencies as given in Table 5 show this trend: the o,p dimer has a lower ϕ_{ET} than would be expected from the other two values, taking only into account the distance effect.

The donor-acceptor distance r can be calculated from the Förster equation /72/:

$$r = (2.999 \times 10^{13} \frac{\kappa^2}{n} \frac{\Omega}{k_{ET}})^{1/6} \qquad (r \text{ in nm}) \qquad (10)$$

where n is the refractive index of the medium, Ω is the overlap integral for donor fluorescence and acceptor absorption and κ is the orientation factor for the donor and acceptor and is given by:

$$\kappa^2 = [\vec{U}_D.\vec{U}_A - 3(\vec{U}_D.\vec{r})(\vec{U}_A.\vec{r})] \qquad (11)$$

with $\vec{U}_D$ and $\vec{U}_A$ are the unit vectors in the direction of the transition dipole moments of donor and acceptor respectively. We calculated the overlap integral with the help of a series expansion /72/ and using the following experimental values for the positions of the donor and acceptor absorption maxima ν_D = 18182 and ν_A = 15456 cm^{-1}. The Stokes shift of the donor Δ_D = -1869 cm^{-1}. Then, Ω is .172 $Debye^4.cm$. The value of κ can be calculated from the conformation as defined via the absorption shifts, and are as tabulated in Table 6. The distances r are then for the dimers as given in this Table. All values are in reasonable agreement with the distances from the EPR measurements and the values as determined with space filling models.

TABLE 6

Squared orientation factor and calculated centre-to-centre distance r from the energy transfer measurements in comparison with the distances from EPR measurements and from space filling models.

Configuration	κ^2	r (nm)	r^a (nm)	r^b (nm)	
para-para	0.47	2.8 ± .3	2.7 ± .2	2.75	
ortho-para	0.10	2.2 ± .5	2.2 ± .2	1.9	
ortho-ortho	0.04	1.8 ± .2	2.1 ± .2	1.7	exo

a) from EPR measurements

b) from space filling models

4.5 CONCLUSIONS.

The preferred conformations and their distribution for monolinked porphyrin dimers as they follow from the application of widely different spectroscopic techniques are in good mutual agreement. Attaching the linking chain to various positions of the phenylrings of both TPP monomers results in predictable changes of the average centre-to centre distance between the rings, and therefore of parameters which depend on this distance as well as on the relative orientation of both rings. Dimers of this type are an attractive tool to study the effects of geometry on the weak interaction between singlet states. The triplet states of the dimers are largely localized on the monomer units, however, due to the much weaker triplet excitonic interaction. Interactions of that type are expected to be observable by magnetic resonance techniques for much shorter distances between both rings (< 0.5 nm). This is only conceivable if both rings are approximately cofacial.

4.6 ACKNOWLEDGEMENT.

This investigation was supported by the Netherlands Foundation for Chemical Research (S.O.N.) with financial aid from the Netherlands Organization for the Advancement of Pure Research (Z.W.O.).

We would like to thank Mr. A. van Hoek for his help with the time-resolved experiments.

4.7 REFERENCES.

1. F.P. Schwartz, M. Gouterman, Z. Muljiani and D.H. Dolphin, Bioinorg.Chem., 2 (1972) 1-32.
2. J.A. Anton, P.A. Loach and Govindjee, Photochem.Photobiol., 28 (1978) 235-242.
3. C.K. Chang, Adv.Chem.Ser., 173 (1979) 162-177.
4. T.L. Netzel, P. Kroger, C.K. Chang, I. Fujita and J. Fajer, Chem.Phys.Lett., 67 (1979) 223-228.
5. J.P. Collman, F.C. Ansom, S. Bencosme, A. Chong, T. Collins, P. Denesevich, E. Evitt, T. Geiger, J.A. Ibers, G. Jameson, Y. Konai, C. Koval, K. Meier, P. Oakley, R. Petttman, E. Schmittou and J. Sessler, proc. IUPAC Symp.Org.Synth., 3rd, 1980, (1981) 29-45.
6. R. Selensky, D. Holten, M.W. Windsor, J.B. Paine III, D. Dolphin, M. Gouterman and J.C. Thomas, Chem.Phys., 60 (1981) 33-46.
7. R.R. Bucks and S.G. Boxer, J.Am.Chem.Soc., 104 (1982) 340-343.
8. I. Fujita, T.L. Netzel, C.K. Chang and C.B. Wang, Proc.Natl.Acad.Sci. USA, 79 (1982) 413-417.
9. T.L. Netzel, M.A. Bergkamp and C.K. Chang, J.Am.Chem.Soc., 104 (1982) 1952-1957.
10. M.R. Wasielewski, M.P. Niemczyk and W.A. Svec, Tetrahedron Lett., 23 (1982) 3215-3218.
11. J.P. Collman, F.C. Ansom, C.E. Barnes, C.S. Bencosme, T. Geiger, E.R. Evitt, R.P. Kreh, K. Meier and R.B. Pettman, J.Am.Chem.Soc., 105 (1983) 2694-2699.
12. J.P. Collman, C.S. Bencosme, R.R. Durand jr, R.P. Kreh and F.C. Ansom, J.Am.Chem.Soc., 105 (1983) 2699-2703.
13. J.P. Collman, C.S. Bencosme, C.E. Barnes and B.D. Miller, J.Am.Chem.Soc., 105 (1983) 2704-2710.

14. P. Krausz and C. Giannotti, J.Chim.Phys.Phys.-Chim.Biol., 80 (1983) 293-303.
15. D. Dolphin, J. Hiom and J.B. Paine III, Heterocycl., 16 (1981) 417-447
and references therein.
16. V.J. Koester and F.K. Fong, J.Phys.Chem., 80 (1976) 2310-2312.
17. L.L. Shipman and J.J. Katz, J.Phys.Chem., 81 (1977) 577-581.
18. M. Kasha, H.R. Rawls and M. Ashraf El-Bayoumi, in Molecular spectroscopy VII
(IUPAC, Butterworths, London, 1965), p. 371-392
M. Kasha, in Spectroscopy of the excited state, B. Di Bartolo (ed.),
(Plenum Press, New York, 1976), p. 337-363
and references therein.
19. M. Gouterman, D. Holten and E. Lieberman, Chem.Phys., 25 (1977) 139-153.
20. C.B. Storm and Y. Teklu, J.Am.Chem.Soc., 94 (1972) 1745-1747.
21. P. Stilbs and M.E. Moseley, J.C.S. Faraday II, 76 (1980) 729-731.
22. H.-H. Limbach and J. Henning, J.Chem.Phys., 71 (1979) 3120-3124.
23. J.M. Assour and S.E. Harrison, Phys.Rev. A, 136 (1964) 1368-1373.
24. J.M. Assour, J.Chem.Phys., 43 (1965) 2477-2489.
25. W.E. Blumberg and J. Peisach, J.Biol.Chem., 240 (1965) 870-876.
26. A. MacGragh, C.B. Storm and W.S. Koski, J.Am.Chem.Soc., 87 (1965) 1470-1476.
27. J.F. Boas, J.R. Pilbrow and T.D. Smith, J.Chem.Soc. (A), (1969) 721-723.
28. C.M. Guzy, J.B. Raynor and M.C.R. Symons, J.Chem.Soc. (A),
(1969) 2299-2303.
29. S. Konishi, M. Hoshino and M. Imamura, Chem.Phys.Lett., 86 (1982) 228-230.
30. S. Konishi, M. Hoshino and M. Imamura, J.Phys.Chem., 86 (1982) 4888-4892.
31. S. Konishi, M. Hoshino and M. Imamura, Chem.Phys.Lett., 94 (1983) 267-269.
32. I.Y. Chan, W.G. van Dorp, T.J. Schaafsma and J.H. van der Waals,
Mol.Phys., 22 (1971) 741-751.
33. I.Y. Chan, W.G. van Dorp, T.J. Schaafsma and J.H. van der Waals,
Mol.Phys., 22 (1971) 753-760.
34. A.L. Kwiram, Ann.Rev.Biophys.Bioeng., 11 (1982) 223-249
and references therein.
35. R.H. Clarke (ed.), Triplet state ODMR spectroscopy, (Wiley Interscience,
New York, 1982).
36. H. Levanon and S. Vega, J.Chem.Phys., 61 (1974) 2265-2274.
37. R.H. Clarke and R.E. Connors, J.Chem.Phys., 62 (1975) 1600-1601.
38. W.R. Leenstra, M. Gouterman and A.L. Kwiram, Chem.Phys.Lett.,
65 (1979) 278-280.
39. R. Avarmaa, Mol.Phys., 37 (1979) 441-454
and references 2-4 and 6 therein.

40. G.H. van Brakel, Ph.D Thesis, Wageningen Agricultural University, Wageningen, The Netherlands, (1982).
41. L. Benthem, R.B.M. Koehorst and T.J. Schaafsma, J.Mol.Struct., 79 (1982) 455-460
Chapter 3 of this thesis.
42. N.J. Turro, Modern molecular photochemistry, (The Benjamin/Cummings Publ. Co., Menlo Park, 1978), Ch. 9.
43. J.N. Demas, Excited state lifetime measurements, (Academic Press, New York, 1983), Ch. 2 and 9.
44. R.G. Little, J.Heterocycl.Chem., 15 (1978) 203-208.
45. A.D. Adler, F.R. Longo, F. Kampas and J. Kim, J.Inorg.Nucl.Chem., 32 (1970) 2443-2445.
46. S.J. van der Bent, A. de Jager and T.J. Schaafsma, Rev.Sci.Instrum., 47 (1976) 117-121.
47. A. van Hoek, J. Vervoort and A.J.W.G. Visser, J.Biochem.Biophys.Meth., 7 (1983) 243-254.
48. P.D.W. Boyd and T.D. Smith, J.Chem.Phys., 56 (1972) 1253-1263.
49. A. Carrington and A.D. McLachlan, Introduction to magnetic resonance, (Harper and Row, New York, 1969).
50. P.T. Manoharan and M.T. Rogers, in Electron spin resonance of metal complexes, Teh Fu Yen (ed.), (Adam Hilger Ltd., London, 1969), p. 143-173.
51. R.H. Clarke and R.H. Hofeldt, J.Chem.Phys., 61 (1974) 4582-4587.
52. R.H. Clarke and R.E. Connors, Chem.Phys.Lett., 33 (1975) 365-368.
53. J.R. Platt, in Radiation biology, Vol. III, A. Hollaender (ed.), (McGraw-Hill, New York, 1956), Ch. 2.
54. G.D. Dorough, J.R. Miller and F.M. Huennekens, J.Am.Chem.Soc., 73 (1951) 4315-4320.
55. M. Gouterman, J.Mol.Spectr., 6 (1961) 138-163.
56. C. Rimington. S.F. Manson and O. Kennard, Spectrochim. Acta, 12 (1958) 65.
57. J.D. Petke, G.M. Maggiora, L.L. Shipman and R.E. Christoffersen, J.Mol.Spectr., 71 (1978) 64-84.
58. R.B.M. Koehorst, L. Benthem, J. Kielstra and T.J. Schaafsma, to be published
Chapter 6 of this thesis.
59. L. Benthem, R.B.M. Koehorst and T.J. Schaafsma, to be published
Chapter 5 of this thesis.

60. W.G. van Dorp, W.H. Schoemaker, M. Soma and J.H. van der Waals, Mol.Phys., 30 (19/5) 1701-1721.
61. A.J. Hoff, in Triplet state ODMR spectroscopy, R.H. Clarke (ed.), (Wiley Interscience, New York, 1982), p. 367-425.
62. A.J. Hoff and B. Cornelissen, Mol.Phys., 45 (1982) 413-525.
63. A.M. Ponte Goncalves and R.P. Burgner, J.Chem.Phys., 65 (1976) 1221-1222.
64. F. Gueckel, D. Schweitzer, J.P. Collman, S. Bencosme, E. Evitt and J. Sessler, Chem.Phys., 86 (1984) 161-172.
65. W.G. van Dorp, T.J. Schaafsma, M. Soma and J.H. van der Waals, Chem.Phys.Lett., 21 (1973) 221-225.
66. J.R. Miller and G.D. Dorough, J.Am.Chem.Soc., 74 (1952) 3977-3981.
67. E.F. Caldin and J.P. Field, J.C.S. Faraday I, 78 (1982) 1923-1935.
68. Th. Förster, Ann.Phys., 2 (1948) 55-75.
69. R.H. Conrad and L. Brand, Biochemistry, 7 (1968) 777-787.
70. A. Harriman, J.C.S. Faraday I, 76 (1980) 1978-1985.
71. J.R. Lacowicz, Principles of fluorescence spectroscopy, (Plenum Press, New York, 1983), Ch. 10.
72. L.L. Shipman and D.L. Housman, Photochem.Photobiol., 29 (1979) 1163-1167.

Chapter 5.

AN NMR-STUDY OF THE CONFORMATION OF COVALENTLY LINKED PORPHYRIN DIMERS.

Submitted tot Organic Magnetic Resonance

5 AN NMR-STUDY OF THE CONFORMATION OF COVALENTLY LINKED PORPHYRIN DIMERS.

L. Benthem, R.B.M. Koehorst and T.J. Schaafsma

Department of Molecular Physics, Agricultural University,
De Dreijen 11, 6703 BC Wageningen, The Netherlands.

5.1 INTRODUCTION.

The interactions between porphyrins and related tetrapyrrolic macrocycles play many varied and important biological functions. In photosynthesis the harvesting and transport of photons by antenna molecules, such as chlorophyll a, depends on the close proximity of these molecules. The final destination of the photons are the 'special pairs' (P700, or P870 in bacteria /1-4/), which are two macrocyclic tetrapyrroles serving as electron donors of photosynthesis. These photochemically derived electrons, like those generated chemically during respiration are conducted through the cell by a series of heme proteins, the cytochromes, where once again the proximity and interaction of the porphyrin rings allow for the facile electron flow.

While in none of the above systems the tetrapyrrolic macrocycles are covalently linked, their proximity and relative orientations are of critical importance for their function. In nature this spacing is in general achieved by orientation in membranes. As yet the biorganic chemist is not sufficiently skilled to mimic these membranes. Instead the relative orientation of dimeric porphyrins have been controlled by linking them covalently. Cofacial or other dimers of chlorophyll and porphyrins with a fixed geometry are used /5-26/, see review in ref. 27, as well as singly linked dimers /26,28-34/, where the ring-ring interactions are more flexible than in the fixed-conformation dimers. However, these singly linked dimers are often rather flexible so that the porphyrin rings can asume a wide range of relative orientations.

Dimers derived from meso tetraphenylporphyrin (TPP) or its tolyl analog (TTP) used in this study have rotational freedom partly restricted by steric considerations and the position of the covalent link /35-38/. For these dimers, changing

the polarity of the solvent influences the folding or unfolding of the two porphyrin rings w.r.t. each other /37/. Thus, spin-spin interaction between two paramagnetic ions, inserted into each of the porphyrin moieties and the energy transfer processes in mixed metal-free base dimers are expected and found to be affected by solvent polarity. Also the excitonic interaction between the two monomeric units changes as a result of the solvent polarity /38/.

NMR has been previously applied to porphyrin monomers /39-44/. It is the purpose of this chapter to establish by NMR the dimer conformation in the ground state as well as the effects of solvent polarity on these configurations.

5.2 EXPERIMENTAL.

Free-base meso α,β,γ,δ-tetraphenylporphyrin (TPP) or tetratolylporphyrin (TTP) monomers p-C_3-TTP (1) and o-C_3-TPP (2) and the dimers p,p-C_3-(TTP)2 (3), o,p-C_3-(TTP)2 (4) and o,o-C_3-(TPP)2 (5) (see fig. 1) were synthesized according

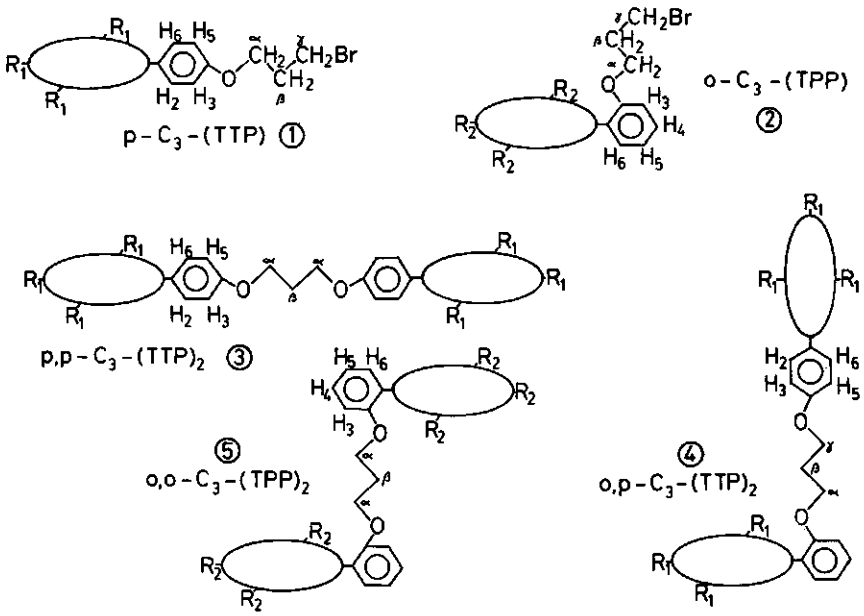

Fig. 1 Schematic representation of all porphyrin compounds used in this study, with R_1 = tolyl and R_2 = phenyl. The ellipses shown in the structural formulea represent the tetrapyrrole ring system. -C_3- represents the five atom bridge: -O-CH_2-CH_2-CH_2-O-.

to Little /35/, and purified by adsorption chromatography on silica gel (Merck, Kieselgel 60) with chloroform as an eluent and gel permeation chromatography (Biorad Laboratories, Biobeads SX2 with toluene). Sample homogeneity was checked by thin layer chromatography (TLC) on silica gel plates (Merck, Kieselgel 60) using toluene as the eluent.

^{1}H-NMR spectra were recorded on a Bruker CXP 300 and a Bruker WM 250 NMR spectrometer. Sample concentration was $\simeq 10^{-3}$ M for the monomers and $\simeq 5.10^{-4}$ M for the dimers, both in deuterochloroform (CDCl3, Merck Uvasol) and the temperature was 28 °C. In the case of the monomers 100 scans were sufficient for well resolved spectra. For the dimers about 500 scans were needed to obtain the same signal-to-noise ratio in the spectra. As the internal standard tetramethylsilane (TMS) was used.

5.3 RESULTS.

The ^{1}H-NMR spectrum of the ortho substituted tetraarylporphyrin monomer (2) have been published by Little /35/. The data obtained in this study for the dimers can be compared with those for the monomers, since they have been measured under the same conditions. In Table 1 the chemical shifts and ring current shifts, due to the substitution of a porphyrin macrocycle, of the various methylene protons are summarized. The upfield or downfield shifts result from the presence of the porphyrin moieties. In Table 2 the chemical shifts and ring current shifts of the protons of the tolyl- c.q. phenylgroups at which the linking chain is attached are given. In figs. 2 and 3 the aromatic regions of the spectra are shown. Because of the complexity of the spectrum of 4 only the upfield shifts of the protons of the para-substituted phenyl-ring are shown (fig. 2C).

5.4 DISCUSSION.

Constructing spacefilling models of the dimeric tetra-arylporphyrins it turned out to be unfavourable to have folded conformations, both in the p,p (3) as in the o,o linked dimer (5), because of considerable steric hindrance /37/. In 3 the two porphyrin rings can have different orientations w.r.t. each other resulting from rotation around the linking axis. In 5 conformational changes between the two porphyrin rings w.r.t. each other are unlikely because the bulky phenyl rings hinder rotation around the linking axis. Here the two rings have

TABLE 1.

Chemical shifts (Δ) and ring current shifts (Δδ) of methylene protons in porphyrin monomers (1,2) and dimers (3-5). (internal standard: TMS; solvent: $CDCl_3$).

Compound	chem. shift (Δ) in ppm [a]			Δδ in ppm [b]		
	α	β	γ	α	β	γ
-O-$(CH_2)_3$-Br 6	3.4 [c]	2.0 [c]	3.5 [c]			
p-C_3-TTP 1	4.4	2.5	3.8	1.0	0.5	0.3
o-C_3-TPP 2	4.1	1.5	2.3	0.7	-0.5	-1.2
-O-$(CH2)_3$-O- 7	3.4 [c]	2.0 [c]	3.4 [c]			
p,p-C_3-$(TTP)_2$ 3	4.7	2.8	4.7	1.3	0.8	1.3
o,p-C_3-$(TTP)_2$ 4	4.2	- [d]	- [d]	0.8	- [e]	- [e]
o,o-C_3-$(TPP)_2$ 5	2.8	0.6	2.8	-0.6	-1.4	-0.6

a) α, β, γ refer to protons in the aliphatic chain (see fig.1)
b) calculated from the difference between Δ's for α, β and γ methylene protons of monomers 1, 2 and reference 6 or dimers 3-5 and reference 7, respectively.
c) theoretical values; these compounds are used as a reference for calculating the ring current shift resulting from a tetraphenyl- c.q. tetratolylporphyrin substitution at the ether-group.
d) signal hidden under resonances from some aliphatic impurities.
e) not determined.

nearly parallel positions with a distance and angle between the centre-to-centre axis and linking axis determined by the length of the aliphatic chain. In 4 the least sterically hindered conformation is that, which contains one of the porphyrin rings perpendicular to the other ring (see fig. 1). The distance and angle between the centre-to-centre axis and the linking axis again are determined by the length of the aliphatic chain. In this case rotation around the linking axis leads to different orientations of the rings w.r.t. each other, which have different spectral characteristics, compared to those for 3 and 5 /38/.

To account for changes in absorption spectra of the dimers /37,38/ w.r.t. those of the monomers using calculations based on the abovementioned simplified

TABLE 2.

Chemical shifts (Δ) and ring current shifts (Δδ) of the protons of the phenyl group, at which the linking chain is attached. Internal standard: TMS; solvent: $CDCl_3$.

Compound	Chem. shift (Δ) in ppm					Δδ in ppm					notes
	H_2	H_3	H_4	H_5	H_6	H_2	H_3	H_4	H_5	H_6	a
p-C_3-TTP 1	8.1	7.2		7.2	8.1						
o-C_3-TPP 2		7.4	7.8	7.4	8.2						
p,p-C_3-$(TTP)_2$ 3	8.2	7.4		7.4	8.2	0.1	0.2		0.2	0.1	b
o,p-C_3-$(T^{mn})_2$ 4	6.9	5.8		5.8	6.9	-1.2	-1.4		-1.4	-1.2	c,d
o,o-C_3-$(TPP)_2$ 5		6.0	6.7	7.0	7.8		-1.4	-1.1	-0.4	-0.4	e

a) H_2-H_6 refer to protons as denoted in fig. 1.
b) Δδ = Δ(3) - Δ(1)
c) Δδ = Δ(4) - Δ(1)
d) resonances of the protons of the phenylgroup, at which the linking chain is at the para-position. The resonances of the phenylgroup with the ortho substitution are hidden under impurity-resonances.
e) Δδ = Δ(5) - Δ(2)

models, we measured ^{1}H-NMR spectra of monomers and dimers. Abraham et al./44/ measured the proton NMR spectrum of the protonated form of TPP in deuterotrifluoroacetic acid: N-H -2.07 ppm, β-H 8.85, phenylprotons: ortho 8.59, meta and para 8.08 ppm. For the N-H and β-protons there is a large difference with the chemical shifts of unsubstituted porphyrin: N-H -4.40 and β-H 9.92 ppm. They conclude that the phenyl substituents affect these resonances through direct ring-current effects of the benzene rings and by altering the ring-current of the porphyrin macrocycle. The contribution of the ring-current of the benzene ring is about 0.45 ppm for each of these shifts. The remaining shifts correspond to an 18% decrease in the ring current of the porphyrin ring and is due to non-planarity of the macrocycle caused by repulsions between the phenyl-groups and the β-H atoms. The unusually low position of the phenyl resonances can be ascribed to the ring current effect of the porphyrin ring. Since this study was

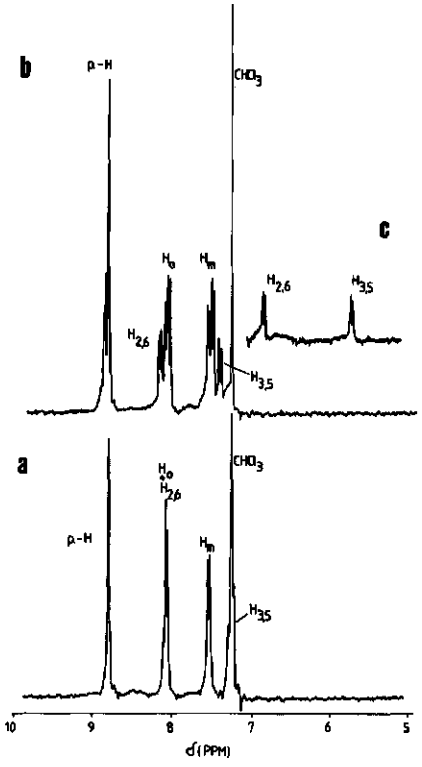

Fig. 2 300 MHz ^{1}H-NMR spectra of p-C3-TTP (A), p,p-C_3-$(TTP)_2$ (B) and o,p-C_3-$(TTP)_2$ (C, only phenyl proton resonances shown). p-H stands for the β-pyrrole protons, H_o and H_m for the ortho and meta protons of the tolyl rings and H_2 - H_6 refer to protons of the phenyl rings onto which the aliphatic chain is substituted (see fig. 1). The ppm scale is the same for all three spectra.

carried out a number of articles have appeared with ring-current calculations for porphyrins and chlorins /45-47/, chlorophyll derivatives /48/, the heme ring /49/, chlorophyll dimers /50/ and porphyrin and chlorophyll aggregates /51/. The ring current model for porphyrins has been fully documented elsewhere /45-48/. Summarizing, the various ring current loops in the porphyrin macrocycle (4 pyr-

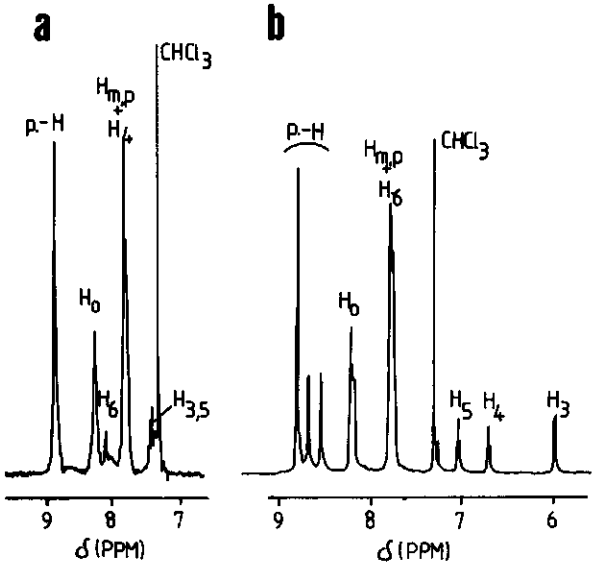

Fig. 3 300 MHz ^{1}H-NMR spectrum of o-C_3-TPP (A) and 250 MHz ^{1}H-NMR spectrum of o,o-C_3-$(TPP)_2$ (B). p-H stands for the β-pyrrole protons, H_o, H_m and H_p for, the ortho, meta and para phenyl protons, respectively, and H_3 - H_6 refer to protons of the phenyl ring onto which the aliphatic chain is attached (see fig. 1). Note the difference in horizontal scales for the spectra (A) and (B).

role rings and 4 hexagons, see fig. 4) are replaced by their equivalent dipoles,

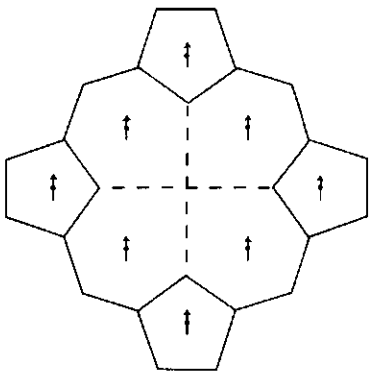

and the total ring current shift at any point R(r,θ) is obtained as the sum of the contributions of the equivalent dipoles, using the standard dipole-dipole equation, yielding /47/:

$$\Delta\delta_R^0 = \sum_{i=1,8} \mu_{Hi}\ f(iR) + \sum_{i=1,8} \mu_{Pi}\ f(iR) \qquad (1)$$

where f(iR) is a function depending on the coordinates of R, and μ_H (hexagon) and μ_P (pyrrole), both expressed in nm^3, are the values for the equivalent dipoles; i labels the polygons of the porphyrin macrocycle used in calculating the equivalent dipoles.

The shifts, due to the four phenyl rings in H_2-TPP are simply added to this summation, again using the equivalent dipole approximation of the phenyl ring current effect /45/:

$$\Delta\delta_R^1 = 27.6 \times 10^{-3} \sum_{i=1,4} (1 - 3\cos^2\theta_{PH}^i)/r_{iR}^3 \qquad (2)$$

with θ_{PH} the angle between r and the z-axis, and r_{iR} denotes the distance of proton R to the centre of the phenylring. The TPP ring current shift is thus the sum of these contributions:

$$\Delta\delta_R = \Delta\delta_R^0 + \Delta\delta_R^1 \qquad (3)$$

The calculation of the ring current shift at any point is therefore given by eqns. (1), (2) and (3) in terms of geometrical factors and the values of μ_H and μ_P (23×10^{-3} and 20×10^{-3} nm^3, respectively).

Instead of making detailed calculations of the ring current shifts of the bridge-protons, using the coordinates of each nucleus w.r.t. the porphyrin- and phenylrings, we compare the experimental ring current shifts in the various dimers with those calculated from the structures of fig. 1 and the monomer data from Table 1, and taking into account, whether a particular bridge proton has α, β or γ position to either of the porphyrin rings. For example, the ring current shifts of the α-proton of 3 (Table 1) has been calculated by summing the shifts of the α and γ protons in the corresponding monomer. The same procedure has been followed for all other calculated bridge protons (Table 4). For the tolyl- or phenyl protons of one porphyrin ring we took one ring current shift of 3 as a standard (Table 4), and with the positions of the various protons w.r.t. the other porphyrin macrocycle, as determined from space filling models (Table 3), we calculated the shifts of the remaining protons. For these calculations we con-

TABLE 3.

Position of the various protons w.r.t. the second porphyrin macrocycle, as determined from space filling models. The constant A = $(1 - 3\cos^2\theta)$, r is given in arbitrary units. The protons are labeled as in fig. 1.

Compound	p,p-C_3-$(TTP)_2$ 3		o,p-C_3-$(TTP)_2$ 4				o,o-C_3-$(TPP)_2$ 5	
proton	r	A	r	A I[a]	r	A II	r	A
α	9.5	0.9	7.0	-0.2	7.0	-0.2	7.0	-0.2
β	12.0	0.9	7.0	-0.8	7.0	-0.8	7.0	-0.8
γ	13.5	0.9	7.5	-1.0	7.5	-1.0	7.5	-1.0
H_2	16.5	0.9	9.5	-1.6	10.0	-1.5		
H_3	13.5	0.9	8.0	-1.3	8.5	-1.2	8.0	-1.3
H_4							9.5	-1.6
H_5	13.5	0.9	11.0	-0.9	8.5	-1.2	12.0	-1.3
H_6	16.5	0.9	12.0	-1.1	10.0	-1.5	12.0	-1.1

a) I: plane of phenyl group coincident with the plane containing both porphyrin-centres and the O-$(CH_2)_3$-O chain (fig. 1).
II: plane of phenylgroup perpendicular to the plane for I by a 90° rotation around the axis of the O-$(CH_2)_3$-O chain.

sidered the other macrocycle to represent a single ring current, and neglected the contribution of the unsubstituted phenyl- (tolyl) groups to the net ring current shifts ($\Delta\delta < 0.01$ ppm). Eqn. (3) can be written as:

$$\Delta\delta = C\ (1 - 3\cos^2\theta)/r^3 \qquad (4)$$

The results are summarized in Table 4. Because θ can only be approximately determined, the error in Δδ is ≃ 0.1 ppm.

It must be noted, that for the porphyrin dimers we have two conformations, a folded and an open structure, between which there exists an exchange at a time-scale faster than that of the NMR experiment. The ratio folded/open is depending

TABLE 4.

Experimental and calculated ring current shifts (Δδ) for the protons labeled in fig. 1. The entry 'ref' in the table indicates that the experimental value is used as standard for calculating the ring current shifts of the remaining nuclei. The shifts of the bridge methylene protons are calculated as given in the Discussion.

compound	p,p-C_3-(TTP)$_2$ 3		o,p-C_3-(TTP)$_2$ 4				o,o-C_3-(TPP)$_2$ 5	
proton	Δδ exp	Δδ calc	Δδ exp	Δδ calc[a] I	II	AV	Δδ exp	Δδ calc
α	1.3	1.3	0.8	1.0			-0.6	-0.5
β	0.8	1.0	-1.4	-1.0			-	0
γ	1.3	1.3	-0.6	-0.5			-	-0.2
H_2	0.1	ref	-1.2	-1.1	-1.0	-0.9		
H_3	0.2	0.2	-1.4	-1.4	-1.2	-1.1	-1.4	-1.4
H_4							-1.1	-1.0
H_5	0.2	0.2	-1.4	-0.4	-1.2	-1.1	-0.4	-0.4
H_6	0.1	ref	-1.2	-0.4	-1.0	-0.9	-0.4	-0.4

a) I and II refer to phenyl orientations, as given in Table 3;
AV = average value of Δδ for H_2/H_6, and H_3/H_5, respectively, resulting from full 2π rotation around the axis of the O-$(CH_2)_3$-O chain.

on the solvent polarity /38/, but always very small.

From our ^{1}H-NMR results we can conclude, that for the p-C_3-TTP monomer (1) the -O-$(CH_2)_3$-Br tail is unfolded, because the ring current shift of the β and γ methylene protons can be calculated, using the data from Table 3, to be 0.5 and 0.3 ppm, in agreement with the experiment, taking the ring current shift of the α-proton as a standard. In a folded conformation the angle Θ and distance r would have different values, yielding different ring current shifts. In dimer 3 we have calculated the ring current contribution to the chemical shift of the bridge protons as given above, by summing the ring current shifts of both porphyrin macrocycles as determined from the monomer, and taking into account the

position of the bridge protons w.r.t. the porphyrin rings. For the phenylprotons we have calculted the ring current contribution using the Θ and r values from Table 3, with one ring current shift as a standard. The agreement between experimental and calculated value is excellent, clearly indicating an unfolded conformation of 3. The observed splitting in the resonances of the aromatic tolyl protons (see fig. 2B) results from the inequivalence of the four inner tolyl- and the two outer tolylgroups (see fig. 1).

For dimer 4 we have calculated ring current shifts for the protons of the para-substituted phenylproup for two possible orientations; i) where the plane of the phenylgroup is coincident with the plane containing both porphyrin centres and the O-$(CH_2)_3$-O chain and ii) where the plane of the phenylgroup is perpendicular to the plane defined for i) by a 90° rotation around the axis of the O-$(CH_2)_3$-O chain. The equal shifts for the protons 2 and 6, as well as those of 3 and 5, may arise from a) a preferential orientation as described by situation ii), or b) a fast rotation of the para-substituted phenylring. By comparing experimental and calculated shifts, using orientation ii), and the average of both (see Table 4), and taking into account the error of $\tilde{}$ 0.1 ppm, we cannot conclud e which case is the correct one. From other experiments it folows that the para-substituted phenylgroup has a large rotational freedom /37/.

Because of a large distance of the unsubstituted tolylgroups to the second porphyrin ring in 4, their ring current contribution to the chemical shift can be neglected. The agreement between the calculated and experimental ring current shifts is, as can be seen from Table 4, again, excellent.

For dimer 5 we conclude, that an endo (cofacial) conformation is highly unlikely. If this dimer would have the endo-form, the ring current shift for the unsubstituted phenyl groups would be of the same magnitude as for H_3 - H_6. For the endo-conformation we also predict a large ring current contribution for the unsubstituted phenylgroup, due to the fact that $\theta \tilde{}$ 0 and the ring-ring distance is 0.9 nm /37/. In view of the absence of this large ring current shift ($\Delta\delta \tilde{}$ 1.5 ppm), we conclude that dimer 5 has an exo (unfolded) conformation. From the ring current shifts of the bridge protons, the conclusion endo or exo conformation cannot be made, because both situations would yield about the same ring current contribution. The agreement between the calculated and experimental values, where we have taken the same C value (eqn. 4) as for the p,p dimer, to calculate the ring current shifts of the phenyl protons, is gratifying.

Because of the low solubility of the porphyrin dimers in most common solvents the effect of solvent polarity (dielectric constant) on the ground state conformation is not easy to investigate. It is interesting to note that addition of

a small amount of hexadeuterated DMSO (DMSO-d_6) to a solution of 3 in $CDCl_3$ slightly increased the splitting of the resonances of the aromatic tolylprotons. This indicates, that folding of the dimer is favoured in polar solvents.

5.5 CONCLUSIONS.

Comparing ^{1}H-NMR results with the predictions from space filling models yield the average conformation of the ground state of the various porphyrin dimers used in this study. The conformation of the dimers can be described by an equilibrium between folded and open structures. Both the structure and the solvent polarity affect the average orientation of the porphyrin macrocycles w.r.t. each other. These data are in excellent agreement with other experimental results /37,38/.

5.6 ACKOWLEDGEMENT.

We thank Mr. B. van Veldhuizen for his help with the ^{1}H-NMR spectra, and dr. G.F.W. Searle for helpful discussions.

This investigation was partly supported by the Netherlands Foundation for Chemical Research (S.O.N.) with financial aid from the Netherlands Organization for the Advancement of Pure Research (Z.W.O.).

5.7 REFERENCES.

1. G. Feher, A.J. Hoff, R.A. Isaacson and L.C. Ackerson, Ann.N.Y.Acad.Sci., 244 (1975) 239.
2. J.R. Norris, R.A. Uphaus, H.L. Crespi and J.J. Katz, Proc.Natl.Acad.Sci. USA, 68 (1971) 625.
3. J. Fajer, M.S. Davis, D.C. Brune, L.D. Spaulding, D.C. Borg and A. Forman, in Chlorophyll-proteins, reaction centers and photosynthetic membranes, (Brookhaven Symp. Biol., 1977), p. 74.
4. J.J. Katz, J.R. Norris, L.L. Shipman, M.C. Thurnauer and M.R. Wasielewski, Ann.Rev.Biophys.Bioeng., 7 (1978) 393.
5. K. Sauer, in Bioenergetics of photosynthesis, Govindjee (ed.), (Academic Press, New York, 1975), Ch. 3.

6. F.K. Fong and V.J. Koester, Biochim.Biophys.Acta, 423 (1976) 52-64.
7. V.J. Koester and F.K. Fong, J.Phys.Chem., 80 (1976) 2310-2312.
8. L.L. Shipman, T.M. Cotton, J.R. Norris and J.J. Katz, Proc.Natl.Acad.Sci. USA, 73 (1976) 1791-1794.
9. F.K. Fong, V.J. Koester and J.S. Polles, J.Am.Chem.Soc., 98 (1976) 6406.
10. M.R. Wasielewski, U.H. Smith, B.T. Cope and J.J. Katz, J.Am.Chem.Soc., 99 (1977) 4172.
11. H. Ogoshi and H. Sugimoto, Tetrahedron Lett., 2 (1977) 169.
12. C.K. Chang, M.-S. Kuo and C.-B. Wang, J.Heterocycl.Chem., 14 (1977) 943.
13. C.K. Chang, J.Heterocycl.Chem., 14 (1977) 1285.
14. M.R. Wasielewski, W.A. Svec and B.T. Cope, J.Am.Chem.Soc., 100 (1978) 1961.
15. J.P. Collman, C.M. Elliot, T.R. Halbert and B.S. Tovrog, Proc.Natl.Acad.Sci. USA, 74 (1977) 18-22.
16. N.E. Kagan, D. Mauzerall and R.B. Merrifield, J.Am.Chem.Soc., 99 (1977) 5484.
17. C.K. Chang, Adv.Chem.Ser., 173 (1979) 162-177.
18. T.L. Netzel, P. Kroger, C.K. Chang, I. Fujita and J. Fajer, Chem.Phys.Lett., 67 (1979) 223-228.
19. T.L. Netzel, M.A. Bergkamp, C.K. Chang and J. Dalton, J.Photochem., 17 (1981) 451.
20. M.A. Bergkamp, J. Dalton and T.L. Netzel, J.Am.Chem.Soc., 104 (1982) 253-259.
21. I. Fujita, T.L. Netzel, C.K. Chang and C.-B. Wang, Proc.Natl.Acad.Sci. USA, 79 (1982) 413-417.
22. T.L. Netzel, M.A. Bergkamp and C.K. Chang, J.Am.Chem.Soc., 104 (1982) 1952-1957.
23. M.A. Bergkamp, C.K. Chang and T.L. Netzel, J.Phys.Chem., 87 (1983) 4441-4446.
24. M.R. Wasielewski, M.P. Niemczyk and W.A. Svec, Tetrahedron Lett., 23 (1982) 3215-3218.
25. R.R. Durand, C.S. Bencosme, J.P. Collman and F.C. Ansom, J.Am.Chem.Soc., 105 (1983) 2710-2718.
26. R.R. Bucks and S.G. Boxer, J.Am.Chem.Soc., 104 (1982) 340-343.
27. J.S. Connolly, in Photochemical conversion and storage of solar energy, part A, J. Rabani (ed.), (The Weizmann Science Press of Israel, 1982), p. 175-204.

28. S.G. Boxer and G.L. Closs, J.Am.Chem.Soc., 98 (1976) 5406.
29. M.R. Wasielewski, M.H. Studier and J.J. Katz, Proc.Natl.Acad.Sci. USA 73 (1976) 4282-4286.
30. F.P. Schwartz, M. Gouterman, Z. Muljiani and D.H. Dolphin, Bioinorg.Chem., 2 (1972) 1-32.
31. J.A. Anton, P.A. Loach and Govindjee, Photochem.Photobiol., 28 (1978) 235-242.
32. R. Selensky. D. Holten, M.W. Windsor, J.B. Paine III, D. Dolphin, M. Gouterman and J.C. Thomas, Chem.Phys., 60 (1981) 33-46.
33. R.E. Overfield, A. Scherz, K.J. Kaufmann and M.R. Wasielewski, J.Am.Chem.Soc., 105 (1983) 5747-5752.
34. P. Krausz and C. Gianotti, J.Chim.Phys., 80 (1983) 299-303.
35. R.G. Little, J.Heterocycl.Chem., 15 (1978) 203-208.
36. P. Maillard, S. Gaspard, P. Krausz and C. Gianotti, J.Organomet.Chem., 212 (1981) 185-191.
37. L. Benthem, R.B.M. Koehorst, L.H. de Graaff and T.J. Schaafsma, to be published
Chapter 4 of this thesis.
38. R.B.M. Koehorst, L. Benthem, J. Kielstra and T.J. Schaafsma, to be published
Chapter 6 of this thesis
39. D.V. Behere and S. Mitra, Ind.J.Chem., 21A (1982) 966-969.
40. T.R. Janson and J.J. Katz, in The porphyrins, Vol. IV C, D. Dolphin (ed.), (Academic Press, New York, 1979), Ch. 1.
41. R.J. Abraham, A.H. Jackson, G.W. Kenner and D. Warburton, J.Chem.Soc., (1963) 853-862.
42. H. Scheer and J.J. Katz, in Porphyrins and Metalloporphyrins, K.M. Smith (ed.), (Elsevier Publ. Co., Amsterdam, 1975), p. 433.
43. H.J. Jakobsen, P.D. Ellis, R.R. Inners and C.F. Jensen, J.Am.Chem.Soc., 104 (1982) 7442-7452.
44. F.A. Walker, V.L. Balke and G.A. McDermott, Inorg.Chem., 21 (1982) 3342-3348.
45. R.J. Abraham, S.C.M. Fell and K.M. Smith, Org.Magn.Res., 9 (1977) 367-373.
46. R.J. Abraham, G.R. Bedford. D. McNeillie and B. Wright, Org.Mag.Res., 14 (1980) 418-425.
47. K.M. Smith, D.A. Goff, R.J. Abraham and J.E. Plant, Org.Mag.Res., 21 (1983) 505-511.

48. R.J. Abraham, K.M. Smith, D.A. Goff and J.-J. Lai,
J.Am.Chem.Soc., 104 (1982) 4332-4337.
49. R.J. Abraham, J.Magn.Res., 43 (1981) 491-494.
50. R.P.H. Kooyman and T.J. Schaafsma, J.Am.Chem.Soc., 106 (1984) 551-557.
51. R.J. Abraham and K.M. Smith, J.Am.Chem.Soc., 105 (1983) 5734-5741.

Chapter 6.

EXCITONIC INTERACTIONS IN COVALENTLY LINKED PORPHYRIN DIMERS.

Submitted to Chemical Physics

6 EXCITONIC INTERACTIONS IN COVALENTLY LINKED PORPHYRIN DIMERS.

R.B.M. Koehorst, L. Benthem, J. Kielstra and T.J. Schaafsma

Department of Molecular Physics, Agricultural University,
De Dreijen 11, 6703 BC Wageningen, The Netherlands.

6.1 INTRODUCTION.

In photosynthesis, the different functions of chlorophyll (i.e. the antenna and reaction centre functions) are closely connected to different chlorophyll microenvironments, or, more specifically, to chlorophyll-chlorophyll and chlorophyll-protein interactions; for a review see ref. 1. To understand primary events in photosynthesis, it is useful to study the electronic properties of cofacial and other dimers of chlorophyll and porphyrins with a fixed geometry /2-24/. A second group of widely studied dimeric porphyrins are the singly linked porphyrin dimers, in which the porphyrin rings have a large intramolecular freedom. However, in most of these dimers, the interactions cover a relatively broad range because the ring systems can assume many orientations w.r.t. each other /22,24-31/. The conformations of these dimers requires a more detailed description in order to interpret their spectral characteristics. Sudhindra and Fuhrhop /32/ have reported the results of quantum mechanical calculations of the intermolecular interactions in the ground state of porphin 'dimers' at short and long distance.

We have studied dimers derived from meso tetratolylporphyrin (TTP) and meso-porphyrin IX dimethylester (meso IX) (see fig. 1), having rotational freedom partly restricted by steric effects and the position of the covalent link /33-39/.

This paper presents the results of a theoretical and experimental investigation of the excitonic interactions affecting the B(0,0) (Soret) absorption bands of the abovementioned dimers. General theories of excitonic interactions /40-46/ have been previously applied to both chlorophyll aggregates and porphyrin dimers /1,3,8,9,29,47-53/. Using these approaches, in particular that of Kasha /40,41/

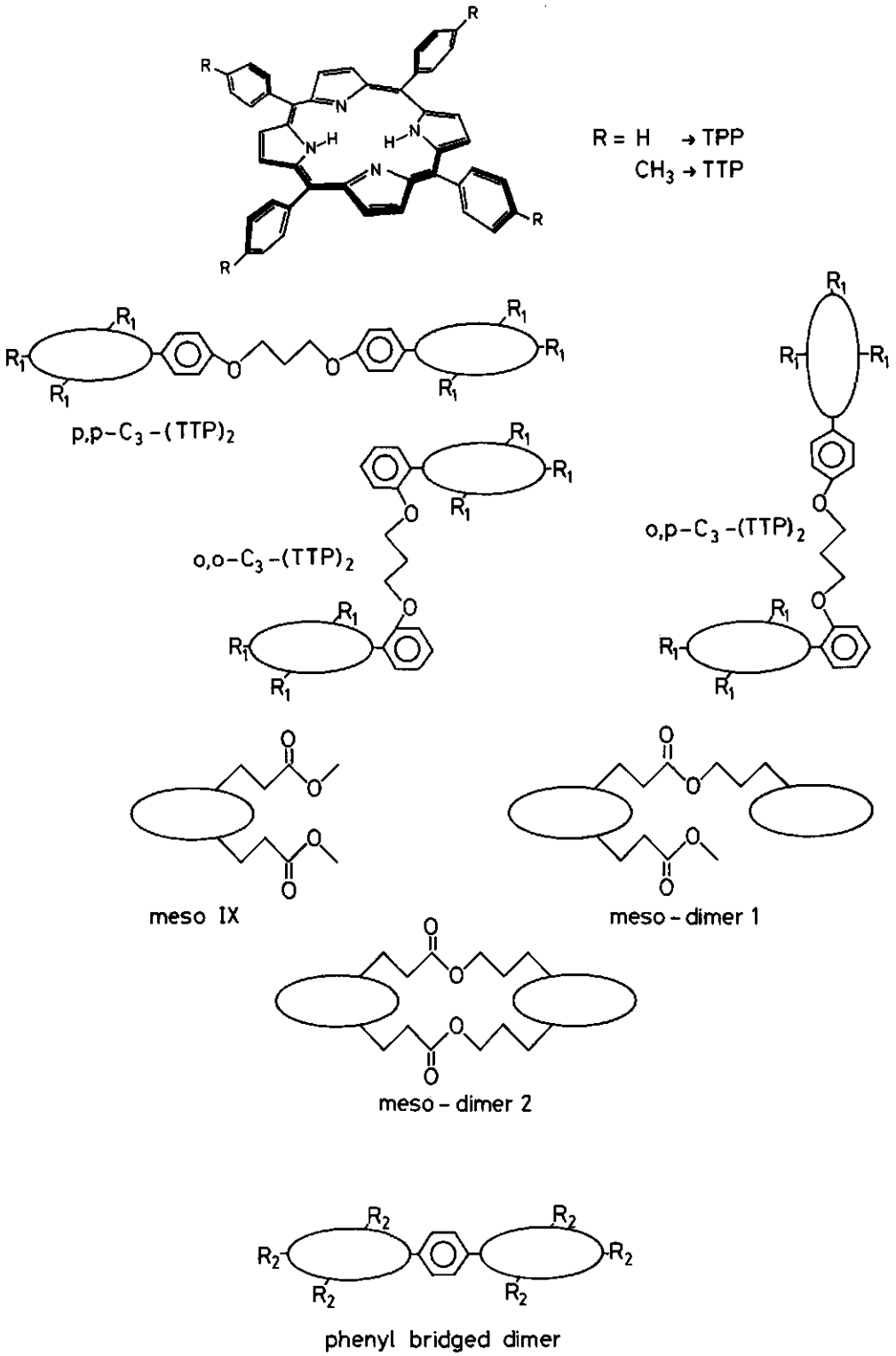

Fig. 1 Sructures of the porphyrin compounds (schematic) used in this investigation. R_1 = tolyl, R_2 = phenyl. The ellipses represent the tetrapyrrole ring system.
$-C_3-$ represents the five atom bridge: $-O-(CH_2)_3-O-$

the energy level shift can be calculated for porphyrin dimers with restricted rotational freedom.

In an accompagnying paper /38/ we have used these results together with those from EPR and fluorescence measurements to determine the relative orientation of the porphyrin rings for three types of TTP dimers. In this paper we present a more detailed theory for the excitonic shifts in the absorption spectra of TTP dimers and a doubly linked meso-dimer. By comparing the experimental and theoretical spectra the geometry of these dimers can be determined. We have also studied the influence of the polarity of the solvent on the orientational distribution of the porphyrin rings w.r.t. each other.

6.2 THEORY.

Because the presence of ligands at the central metal ion in metallo porphyrins may affect the distribution of possible conformations in porphyrin dimers containing one or two metal ions, we have only considered free base (H_2) porphyrins.

For symmetrically substituted free base porphyrins the x- and y-polarized transitions in the Soret region are almost degenerate /54-56/. For the calculation of the exciton shifts, we have to include both types of transitions. Nevertheless, we need to consider only transitions directed along one particular the H-H axis. Because of the ground state N-H tautomerism in free base porphyrins /57-59/ at room temperature, the H-H axis in each of the porphyrin rings has two possible mutually perpendicular directions, occurring with about equal probability. This results again in two different directions of each transition dipole moments in both porphyrin rings in the dimer. Taking into account the relative phase of the transition dipoles, four different dipole-dipole interactions are possible in these dimers, at the same time covering excitonic interactions between x and y transitions of both porphyrin macrocycles within the Soret-band.

We place the dimer in an x,y,z- coordinate system, so that one of the porphyrin macrocycles lies in the x,y plane. The position of a dimer in the x,y,z coordinate system is presented in fig. 2 for the o,p-C_3-$(TTP)_2$ dimer. The coordinates of the second porphyrin macrocycle is represented by the vector $\vec{r}$, joining both centres of the porphyrin rings and the angle α, being the angle between $\vec{r}$ and the x,y plane. All dimer conformations can now be described by one or at

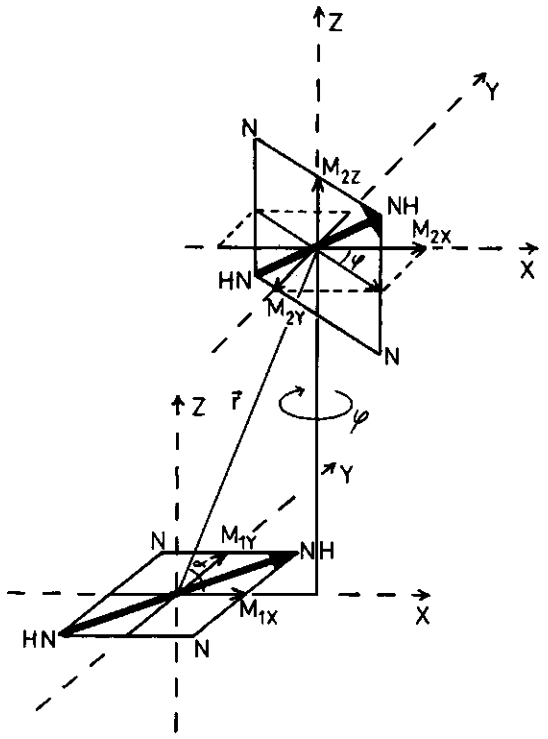

Fig. 2 Position of the o,p-C_3-$(TTP)_2$ dimer in an x,y,z coordinate system. One porphyrin ring is placed in the x,y plane; the position of the second macrocycle is defined by r, the vector joining both centres and α, the angle between r and the x,y plane. ϕ is the rotation angle used in the calculations.

most two rotation angles, as is shown in fig. 3.

The vectors of the transition dipoles in both porphyrin rings are resolved into their components along the axes of the mainframe. Dipole-dipole interactions can then be considered as the sum of the interactions of all individual vector components in its specific case.

The effects of solvent polarity on the folding of the dimer have been neglected in this treatment by asuming that all compounds are dissolved in one and the same solvent. In this way the excitonic interactions in all three TTP dimers can be compared.

The excited state energies of dimers can be calculated w.r.t. those of the

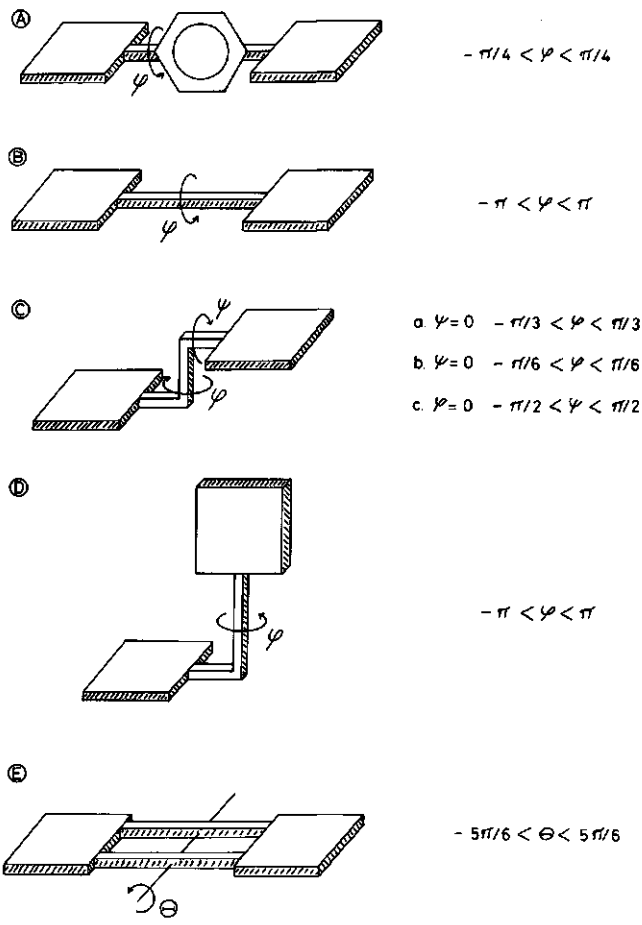

Fig. 3 Conformations of the various dimers: phenyl bridged dimer (A), p,p (B), o,o (C) and o,p-C_3-$(TTP)_2$ dimer (D) and meso-dimer2 (E) as used for the calculation of the shifts of the Soret absorption bands. ϕ, ψ and Θ define the relative orientations of both porphyrin rings; (angular boundaries indicated). The figure represent a situation with ϕ, Θ and $\psi = 0$. (For the relative position of both rings for the o,p-C_3-$(TTP)_2$ dimer in a coordinate system x,y,z see fig. 2).

corresponding monomer from eqn. (1), containing the transition dipole moments $\vec{M}_1$ and $\vec{M}_2$ of the porphyrin moieties 1 and 2, separated by a centre-to-centre distance r:

$$\Delta E = \frac{\vec{M}_1 . \vec{M}_2}{r^3} - 3 \frac{(\vec{M}_1 . \vec{r})(\vec{M}_2 . \vec{r})}{r^5} \qquad (1)$$

The exciton interaction V is defined by $V = 2|\Delta E|$.

As an example we present here the calculation of the energy level shift ΔE as the result of exciton interaction in o,p-C_3-$(TTP)_2$, with transition dipoles as shown in fig. 2. For this dimer, rotation of one macrocycle w.r.t. the other is possible around the linking chain over an angle ϕ ($-\pi < \phi < \pi$). We have used a single rotation angle, because other possible rotations are highly sterically hindered as can be concluded from space filling models. The set of dipole-dipole interactions, as shown in fig. 2, yield the following energy shifts:

$$\Delta E_{1a} = \frac{M_{1x} . M_{2x}}{r^3} - \frac{(M_{1x} . r)(M_{2x} . r)}{r^5} = \frac{M^2}{r^3} (\tfrac{1}{2} \cos \phi - \frac{3}{2} \cos^2 \alpha \cos \phi) \qquad (2a)$$

$$\Delta E_{1b} = \frac{M_{1x} . M_{2y}}{r^3} - \frac{(M_{1x} . r)(M_{2y} . r)}{r^5} = 0 \qquad (2b)$$

$$\Delta E_{1c} = \frac{M_{1x} . M_{2z}}{r^3} - \frac{(M_{1x} . r)(M_{2z} . r)}{r^5} = \frac{M^2}{r^3} (-\frac{3}{2} \sin \alpha \cos \alpha) \qquad (2c)$$

$$\Delta E_{1d} = \frac{M_{1y} . M_{2x}}{r^3} - \frac{(M_{1y} . r)(M_{2x} . r)}{r^5} = 0 \qquad (2d)$$

$$\Delta E_{1e} = \frac{M_{1y} . M_{2y}}{r^3} - \frac{(M_{1y} . r)(M_{2y} . r)}{r^5} = \frac{M^2}{r^3} (-\tfrac{1}{2} \sin \phi) \qquad (2e)$$

$$\Delta E_{1f} = \frac{M_{1y} . M_{2z}}{r^3} - \frac{(M_{1y} . r)(M_{2z} . r)}{r^5} = 0 \qquad (2f)$$

with $|M_{1x}| = |M_{1y}| = |M_{2z}| = M \cos(\pi/4) = \frac{1}{2}\sqrt{2}\, M$

$|M_{2x}| = M \cos(\pi/4) \cos \phi = \frac{1}{2}\sqrt{2}\, M \cos \phi$

$|M_{2y}| = M \cos(\pi/4) \sin \phi = \frac{1}{2}\sqrt{2}\, M \sin \phi$

For the o,p-C_3-$(TTP)_2$ dimer $\alpha = \pi/3$ as found from space filling models. The sum of eqns. (2a) - (2f) result in the total energy shift, as given by:

$$\Delta E_{1\ \text{total}} = \frac{M^2}{r^3} \left(\frac{1}{8} \cos\phi - \tfrac{1}{2} \sin\phi - \frac{3}{8}\sqrt{3}\right) \qquad (3)$$

The corresponding transition probability P_1 is proportional to M^2 and is thus a function of the rotation angle ϕ. P_1 is found to be given by:

$$P_1 \ (:)\ M^2\ (2 + \cos\phi - \sin\phi) \qquad (4)$$

For our calculations, we assume that all rotation angles have equal probability of occurence within the boundaries, given in fig. 2.

The complete set of equations for ΔE and P for o,p-C_3-$(TTP)_2$, taking into account the relative orientations of $\vec{M}_1$ and $\vec{M}_2$ resulting from N-H tautomerism and the relative phase of the transition dipoles is given in Table 1. Eqns. (2a) -

Table 1.

The energy level shifts (ΔE) and the corresponding transition probabilities (P) of the four different dipole-dipole interactions in o,p-C_3-$(TTP)_2$ as function of the rotation angle ϕ around the linking chain.

$\Delta E_1 = \frac{M^2}{r^3}\left(\frac{1}{8}\cos\phi - \frac{1}{2}\sin\phi - \frac{3}{8}\sqrt{3}\right)$	$P1\ (:)\ M^2\ (2 + \cos\phi - \sin\phi)$
$\Delta E_2 = \frac{M^2}{r^3}\left(\frac{1}{8}\cos\phi - \frac{1}{2}\sin\phi + \frac{3}{8}\sqrt{3}\right)$	$P_2\ (:)\ M^2\ (2 + \cos\phi - \sin\phi)$
$\Delta E_3 = \frac{M^2}{r^3}\left(-\frac{1}{8}\cos\phi + \frac{1}{2}\sin\phi + \frac{3}{8}\sqrt{3}\right)$	$P_3\ (:)\ M^2\ (2 - \cos\phi + \sin\phi)$
$\Delta E_4 = \frac{M^2}{r^3}\left(-\frac{1}{8}\cos\phi + \frac{1}{2}\sin\phi - \frac{3}{8}\sqrt{3}\right)$	$P_4\ (:)\ M^2\ (2 - \cos\phi + \sin\phi)$

(2f) represent only one part of this Table (cf. eqn (3)). The total result is two absorption profiles, one of which is redshifted ($\Delta E_1 < 0$, $\Delta E_4 < 0$) and a second one blueshifted ($\Delta E_2 > 0$, $\Delta E_3 > 0$) w.r.t. the monomeric absorption taken as a reference. Fig. 5D represents the calculated absorption profiles resulting from a rotation of ϕ over a full 2π cycle. These profiles can be compared with

the experimental 2nd derivative absorption spectra in the same figure.

For the p,p-C_3-$(TTP)_2$ dimer the situation is simpler, since the vector, joining the two centres of both porphyrin macrocycles lies in the plane of one of these macrocycles, and $\vec{M}_1$ and $\vec{M}_2$ have angles of $\pi/4$ with this vector. Note that rotation of one prophyrin ring w.r.t. the other over π, transformes one N-H tautomer into its partner. Considering a ϕ-rotation over the full 2π range, one finds that the four situations corresponding to four different orientations of $\vec{M}_2$ w.r.t. $\vec{M}_1$, due to N-H tautomerism and the relative phase of the transition dipole moments, reduces to two, as shown in fig. 4. In this figure the two orientations of $\vec{M}_2$ w.r.t. $\vec{M}_1$ are represented by solid arrows; the other two (broken arrows) are found by a ϕ-rotation of one porphyrin ring over π radians. The two situations in fig. 4 are denoted as: i) an in-phase orientation (A) and ii) an out-of-phase orientation (B) of both transition dipole moments.

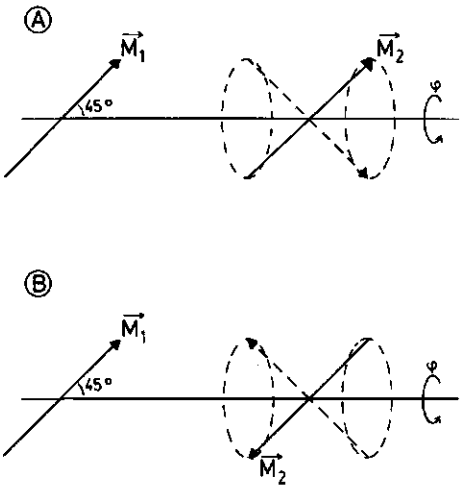

Fig. 4 Relative orientations of transition dipole moment $\vec{M}_2$ w.r.t. $\vec{M}_1$ in the p,p dimer. The plane of one porphyrin macrocycle is in the plane of the drawing; the second porphyrin is rotated over ϕ.

For the phenyl bridged dimer the same holds; however, due to the steric hindrance of the rotation of one porphyrin ring w.r.t. the other, we assume the rotation angle to be in the range of $0 < \phi < \pi/2$. Now we have to take into account all four orientations of $\vec{M}_2$ w.r.t. $\vec{M}_1$.

TABLE 2.

The energy level shifts (ΔE) and the corresponding transition probabilities (P) for all dimers as function of the rotation angles as defined in fig. 3.

Phenyl bridge dimer (A)	
$\Delta E_1 = \frac{M^2}{r^3} (\frac{1}{2} \cos \phi - 1)$	P_1 (:) M^2 $(3 + \cos \phi)$
$\Delta E_2 = \frac{M^2}{r^3} (-\frac{1}{2} \cos \phi - 1)$	P_2 (:) M^2 $(3 - \cos \phi)$
$\Delta E_3 = - \Delta E_1$	P_3 (:) M^2 $(1 - \cos \phi)$
$\Delta E_4 = - \Delta E_2$	P_4 (:) M^2 $(1 + \cos \phi)$
p,p - C_3- $(TTP)_2$ (B)	
$\Delta E_1 = \frac{M^2}{r^3} (\frac{1}{2} \cos \phi - 1)$	P_1 (:) M^2 $(3 + \cos \phi)$
$\Delta E_2 = \frac{M^2}{r^3} (1 - \frac{1}{2} \cos \phi)$	P_2 (:) M^2 $(1 - \cos \phi)$
o,o - C_3 - $(TTP)_2$ (C) ϕ - rotation	
$\Delta E_1 = \frac{M^2}{r^3} (\cos \phi - \frac{9}{16} (\sin \phi + 1)(\cos \phi + 1)[1 + \frac{3}{8} (\cos \phi - 1)]^{-5/2})$	
	P_1 (:) M^2 $(2 + 2 \cos \phi)$
$\Delta E_2 = \frac{M^2}{r^3} (- \sin \phi + \frac{9}{16} \cos \phi (\cos \phi + 1)[1 + \frac{3}{8} (\cos \phi - 1)]^{-5/2})$	
	P_2 (:) M^2 $(2 - 2 \sin \phi)$

$\Delta E_3 = - \Delta E_1$ $\quad P_3$ (:) M^2 (2 - 2 cos ϕ)

$\Delta E_4 = - \Delta E_2$ $\quad P_4$ (:) M^2 (2 + 2 sin ϕ)

ψ - rotation

$\Delta E_1 = \frac{M^2}{r^3} (\frac{1}{2} \cos \psi - \frac{3}{8} \sqrt{3} \sin \psi - \frac{5}{8})$ $\quad P_1$ (:) M^2 (3 + cos ψ)

$\Delta E_2 = \frac{M^2}{r^2} (- \frac{1}{2} \cos \psi + \frac{3}{8} \sqrt{3} \sin \psi - \frac{5}{8})$ $\quad P_2$ (:) M^2 (3 - cos ψ)

$\Delta E_3 = - \Delta E_1$ $\quad P_3$ (:) M^2 (1 - cos ψ)

$\Delta E_4 = - \Delta E_2$ $\quad P_4$ (:) M^2 (1 + cos ψ)

---

o,p - C_3 - $(TTP)_2$ (D)

$\Delta E_1 = \frac{M^2}{r^3} (\frac{1}{8} \cos \phi - \frac{1}{2} \sin \phi - \frac{3}{8} \sqrt{3})$ $\quad P_1$ (:) M^2 (2 + cos ϕ - sin ϕ)

$\Delta E_2 = \frac{M^2}{r^3} (\frac{1}{8} \cos \phi - \frac{1}{2} \sin \phi + \frac{3}{8} \sqrt{3})$ $\quad P_2$ (:) M^2 (2 + cos ϕ - sin ϕ)

$\Delta E_3 = \frac{M^2}{r^3} (- \frac{1}{8} \cos \phi + \frac{1}{2} \sin \phi + \frac{3}{8} \sqrt{3})$ $\quad P_2$ (:) M^2 (2 - cos ϕ + sin ϕ)

$\Delta E_4 = \frac{M^2}{r^3} (- \frac{1}{8} \cos \phi + \frac{1}{2} \sin \phi - \frac{3}{8} \sqrt{3})$ $\quad P_3$ (:) M^2 (2 - cos ϕ + sin ϕ)

---

meso-dimer 2 (E)

$$\Delta E_1 = \frac{M^2}{r^3} \{ \tfrac{1}{2}(\cos\theta + 1) \cos^{-3}(\tfrac{1}{2}\theta) - \tfrac{3}{2} \cos^{-1}(\tfrac{1}{2}\theta)\}$$

$$P_1 (:)\ M^2 (3 + \cos\theta)$$

$$\Delta E_2 = \frac{M^2}{r^3} \{ \tfrac{1}{2}(\cos\theta + 1) \cos^{-3}(\tfrac{1}{2}\theta) - \tfrac{3}{2} \cos^{-1}(\tfrac{1}{2}\theta)\}$$

$$P_2 (:)\ M^2 (1 + \cos\theta)$$

$$\Delta E_3 = -\Delta E_1 \qquad P_3 (:)\ M^2 (1 - \cos\theta)$$

$$\Delta E_4 = -\Delta E_2 \qquad P_4 (:)\ M^2 (3 - \cos\theta)$$

In Table 2 the calculated energy level shifts (ΔE) and relative transition probabilities (P) are given as a function of the rotation angle ϕ (see fig. 2). Where rotation is allowed, variations in the rotation angle of the plane of the phenyl group w.r.t. the porphyrin plane is neglected; this angle (50 - 60° /60, 61/) is considered to be included in the rotation angle ϕ. For the o,o-C_3-$(TTP)_2$ dimer ΔE and P are also given as a function of ψ, the rotation angle of one porphyrin plane w.r.t. the linking tolyl group, see fig. 2, in this case $\phi = 0$. For $\phi \neq 0$ the porphyrin plane cannot rotate w.r.t. the linking tolyl group (ψ), due to sterical hindrance. This situation results in a stretched conformation, very similar to that for the p,p-C_3-$(TTP)_2$ dimer. For the meso-dimer2 no rotation around the linking chain is possible, because of the double linkage, and the results are given as a function of θ only (see fig. 2). Space filling models of meso-dimer1 exhibit a large degree of freedom of one porphyrin plane w.r.t. the other. It is therefore not possible to describe all possible conformations by a single rotation angle, and no theoretical absorption profile has been calculated for this compound. Fig. 5 contains calculated profiles for the Soret absorption band for the various dimers. Except for the meso-dimer2 all calculated spectra are corrected for differences in the centre-to-centre distance r, in view of the results obtained from space filling models. For the meso-dimer2 the absolute values of the shifts cannot be compared to those of the tetra-aryl dimers.

Because we neglected any substitutional effects on the spectra of the por-

phyrin monomers in our calculations, shifts from the monomer position may not always be of the same magnitude as calculated. Also, the 'inhomogeneous solvent broadening' of the spectra has not been taken into account.

6.3 EXPERIMENTAL.

Free base meso α,β,γ,δ - tetratolylporphyrin (H_2-TTP) monomers and dimers p,p-C_3-$(TTP)_2$, o,p-C_3-$(TTP)_2$ and o,o-C_3-$(TTP)_2$ (see fig. 1) were synthesized according to the literature /33,62/, and purified by adsorption chromatography on silica gel (Merck, Kieselgel 60) with chloroform as the eluent and gel permeation chromatography (Biorad Laboratories, Biobeads SX2 with toluene). The purity of the samples was checked by TLC on silica gel plates (Merck, Kieselgel 60) with toluene. Meso porphyrin IX dimethylester (meso IX) was purchased from Sigma Chemicals Co. and was used without further purification. Meso-dimer1 and meso-dimer2 (see fig. 1) were a generous gift of Dr. K. Ichimura of the Research Institute for Polymers and Textiles in Yokohama, Japan. The meso compounds were also checked on purity using TLC, but with dichloromethane as the eluent. The phenyl bridged dimer was a gift of dr. M.R. Wasielewski of the Argonne National Laboratory, Argonne, USA.

The possibility for intermolecular aggregation of the TTP monomer and its dimers was checked by taking concentration dependent fluorescence spectra at room temperature and at 77 K in toluene. Up to a concentration of 10^{-3} M we found no evidence of dimerization or aggregation. This is in sharp contrast with the aggregation behaviour of other types of porphyrins, where aggregation already occurs at lower concentrations. The lower tendency to aggregate for TTP is most likely due to the steric hindrance of the tolylgroups. For the meso-dimers no dimerization was seen at concentrations $< 5.10^{-5}$ M.

Absorption spectra and their 2^{nd} derivative spectra were recorded at room temperature using a Kontron Uvikon 810 double beam spectrophotometer. The slitwidth of the monochromator was 1 nm, and the wavelength interval for 2^{nd} derivative spectra 2 nm, except for the meso compounds where we used 4 nm. The sample concentrations were $\simeq 10^{-6}$ M. All solvents (PA grade) were used without further purification. We recorded 2^{nd} derivative absorption spectra to visualize splitted absorption bands, because mostly exciton bands could not be well resolved in normal absorption spectra. For some compounds the relative transition probabilities of the dimer excited states could be quantitatively measured as relative intensities of dimer absorption peaks in the Soret region.

6.4 RESULTS.

B(0,0) (Soret) bands of the tetraarylporphyrins exhibit a redshift w.r.t. the corresponding monomer, see Table 3. The magnitude of this shift depends on the dimer configuration and the solvent polarity. The o,o-C_3-$(TTP)_2$ dimer exhibits almost no shift. In the phenyl bridged dimer the redshift is $\simeq$ 6 times larger than in the C_3-linked dimers, due to the much shorter distance in the phenyl bridged dimer. A small blueshifted component can be seen. A p,p dimer with a $-(CH_2)_{10}-$ instead of a $-(CH_2)_3-$ bridge does not exhibit a measurable shift.

By contrast, the meso-dimers show a blueshift w.r.t. the position of the mon-

TABLE 3.

Position (cm^{-1}) of the 2^{nd} derivative peak of the Soret absorption band of porphyrin monomers and shifts (cm^{-1}) of the peak positions of the dimers studied w.r.t. the monomer position. A - sign denotes a redshifted, a + sign a blueshifted component. (Solutions $\simeq 10^{-6}$ M; room temperature).

Error in the position ± 7 cm^{-1}; in the shift ± 14 cm^{-1}.

Compound Solvent:	toluene	THF	acetone
TTP	23810	23981	24091
p,p-C_{10}-$(TTP)_2$	+16	+11	+17
p,p-C_3-$(TTP)_2$	-85	-98	-110
o,o-C_3-$(TTP)_2$	+5	-6	-12
o,p-C_3-$(TTP)_2$	+131	+104	+163
	-292	-324	-270
TPP	23906	24067	24196
phenyl bridged dimer	+92	+82	+82
	-531	-559	-571
meso IX	24907	25157	25317
meso-dimer1	+442	+64	+128
	0		-214
meso-dimer2	+701	+517	+490
	-62	0	-223

omer (Table 4). Comparing the solvent effects on the shifts of p,p-C_3-$(TTP)_2$ and the meso-dimers, we note that for the meso-dimer the shift is decreasing with increasing solvent polarity, whereas the tetra-aryl dimer shows opposite behaviour.

In Table 3 2^{nd} derivative absorption spectral data are summarized, whereas in fig. 5 also the observed 2^{nd} derivative spectra are shown for all dimers in the same solvent (toluene).

6.5 DISCUSSION.

In order to interpret the excitonic interactions in the C_3-$(TTP)_2$ dimers, we have used the phenyl bridged dimer as a standard. This dimer has a stretched geometry and the only possible intramolecular motion is a rotation of both porphyrin rings w.r.t. each other. This rotation is, however, sterically hindered, due to the fact that the angle between the phenyl group and the porphyrin ring is $\tilde{}$ 50° /60,61/, which is taken as 45° for convenience. Applying Table 2 to the phenyl bridged dimer a red- and a blueshifted component in the absorption band are predicted, in agreement with the experimental results, where a component redshifted with $\tilde{}$ 10 nm is found, and a second 1.5 nm blueshifted component. It must be noted, that the determination of the monomer position is rather critical; we have used the tetraphenylporphyrin (TPP) macrocycle as the reference for the phenyl bridged dimer.

The p,p-C_3-$(TTP)_2$ dimer can be compared with the phenyl bridged dimer. From space filling models it can be concluded, that also this compound has only one major intramolecular rotation: i.e. around the linking axis. Apart from the larger distance between both centres of the porphyrin macrocycles in this dimer (2.5 nm) w.r.t. the phenyl bridged dimer (1.5 nm), one could expect the same excitonic interactions; a redshifted and a small blueshifted component. In our experiment we cannot resolve these two components, and we only detect a small net redshift of $\tilde{}$ 1.5 nm. This is what is predicted, taking into account the redshift for the phenyl bridged dimer and the effect of the r^{-3} dependence of the excitonic interaction. With the centre-to-centre distances as given above, for the p,p-C_3-$(TTP)_2$ dimer a redshift of $\tilde{}$ 2 nm is expected. We can conclude that this p,p dimer has a stretched geometry, but in more polar solvents the interaction between both porphyrin rings is found to be somewhat larger. This means that this dimer has a tendency to fold in more polar solvents.

The o,o-C_3-$(TTP)_2$ dimer can exist in two conformations, i) a cofacial (endo)

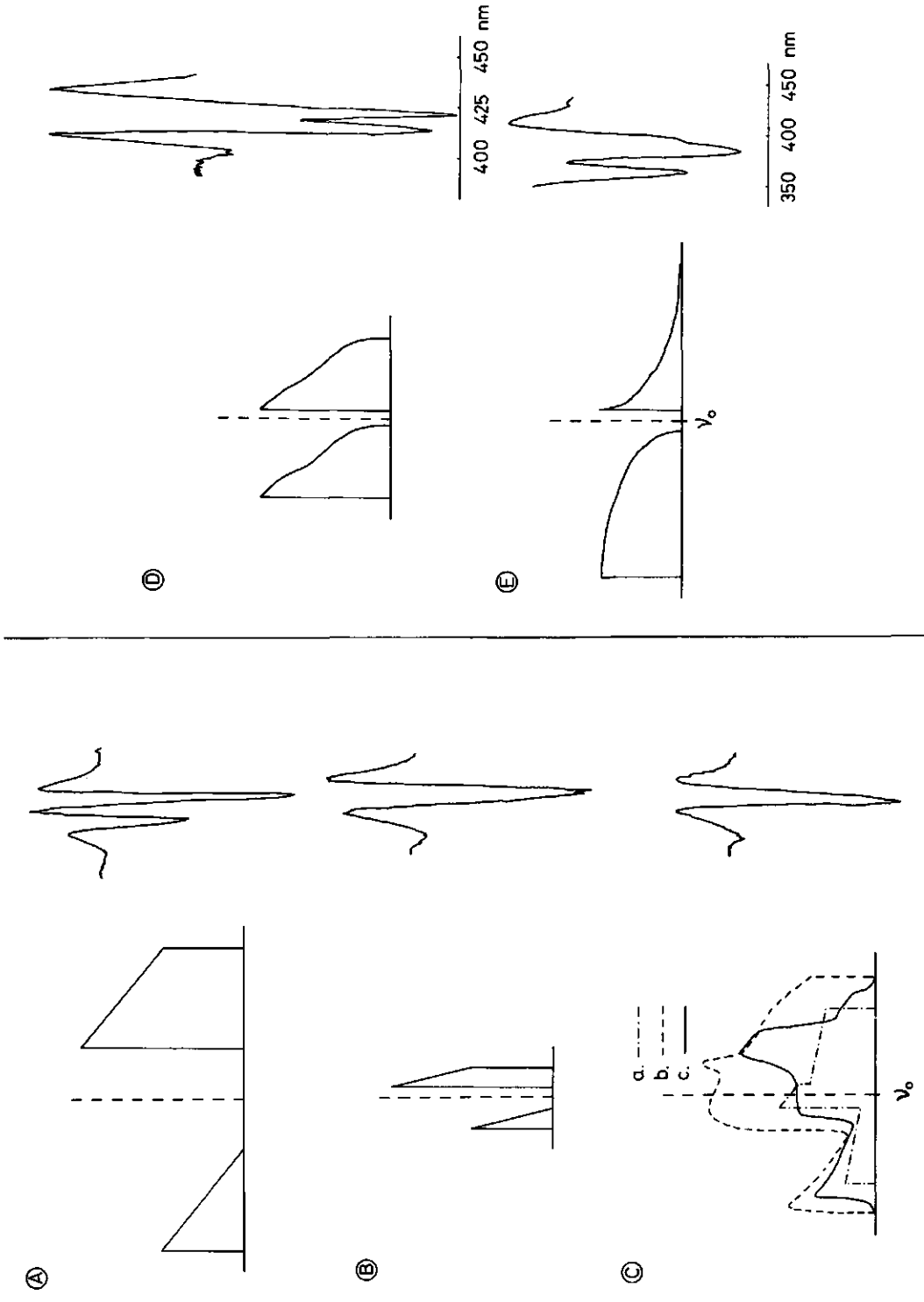

Fig. 5 Calculated profiles and experimental 2nd derivative Soret absorption bands for phenyl bridged (A), the p,p (B), o,o (C) and o,p-C_3-$(TTP)_2$ dimer (D) and meso-dimer2 (E). The boundaries of ϕ, ψ and Θ are given in fig. 2.

form and ii) a rotation of 180° around the linking axis of one porphyrin ring (exo-conformation). Applying the exciton model to the endo-form, a large blue-shift, due to the relatively short centre-to-centre distance of 0.9 nm /38/ is expected. For the exo-conformation a small net blue- or redshift is predicted. We have calculated spectra for three possible conformations, corresponding to: i) a ϕ-rotation around the linking chain over +/- $\pi/3$, ii) a ϕ-rotation over +/- $\pi/6$ and iii) no rotation around the linking chain ($\phi = 0$), but a rotation of one porphyrin ring w.r.t. the other over the range ($-\pi < \psi < \pi$). The results

TABLE 4.

Soret absorption band maxima (nm) of $\tilde{}$ 10^{-6} M solutions of the porphyrin monomers and shifts (nm) of the dimers studied in several solvents at room temperature. A - sign denotes a redshifted, a + sign a blueshifted band (Bandwidth $\tilde{}$ 15 nm).

Compound	Solvent:	toluene	THF	acetone
TTP		420.0	417.0	414.7
p,p-C_{10}-$(TTP)_2$		+0.3	+0.3	-0.2
p,p-C_3-$(TTP)_2$		-1.5	-1.5	-1.7
o,o-C_3-$(TTP)_2$		+0.2	-0.2	-0.4
o,p-C_3-$(TTP)_2$ [a]		+2.3	+1.8	+2.4
		-5.2	-4.7	-5.1
TPP		418.4	415.4	413.2
phenyl bridged dimer		-0.1	-0.3	-0.2
		-8.2	-9.0	-9.2
meso IX [b]		401.1	396.2	393.9
meso-dimer 1 [c]		+5.7	+1.0	+4.7
meso-dimer 2 [c]		+10.7	+9.4	+9.8

a) calculated from 2nd derivative spectra
b) bandwith $\tilde{}$ 20 nm
c) bandwith $\tilde{}$ 45 nm

are given in fig. 5C. From our experimental results, as presented in Tables 3 and 4, we can conclude that the o,o-C_3-$(TTP)_2$ dimer has an exo-conformation and that a rotation around the linking axis is largely hindered preventing rotation over the full 2π range. Our experimental results are only consistent with small deviation from $\phi = 0$ and a small rotation of one porphyrin ring w.r.t. the other is possible.

For the o,p-C_3-$(TTP)_2$ dimer space filling models reveal that free rotation over 2π radians around the linking chain is possible. From our theoretical results we expect then to observe a split absorption band, and shifts that are larger than in the p,p dimer (see fig. 5). This is in agreement with our experimental results. Tables 3 and 4 demonstrate that changing the polarity of the solvent has a distinct effect on the energy shifts, but there is no systematic trend. We have not analyzed the influence of the folding of the dimer on the spectra as a result of the solvent polarity in view of the possible presence of of several, slightly different conformations.

For all three C_3-$(TTP)_2$ dimers, the conclusions are confirmed by NMR experiments /39/. The p,p dimer is found to have a stretched geometry; the o,o dimer has an exo-conformation and for the o,p dimer the data are consistent with a rotation around the linking chain.

Of the meso-dimers we have only calculated the energy level shifts of meso-dimer2. For the singly linked meso-dimer1 no simple calculation is possible, due to the very large internal freedom. For the meso-dimer2, assuming a rotation over $-150 < \theta < 150°$ (see fig. 3), we conclude that a blueshifted absorption band with a small redshifted component should be found, in agreement with the experimental results. This has also been found experimentally for doubly linked cofacial porphyrin dimers /63/.

In solvents of increasing polarity the interactions between both meso-porphyrin rings decreases. This implies that in more polar solvents the dimer unfolds (the boundaries of θ will be narrower), in sharp contrast with the behaviour of the p,p-C_3-$(TTP)_2$ dimer, which folds in more polar solvents. These effects can be understood by realizing that for the TTP dimers the apolar porphyrin macrocycles and the alkyl-chain are forced together in a polar environment. The meso-dimer is linked by more a polar chain containing ester-groups (see fig. 1), which unfolds in a polar environment. Thus, there are two counteracting effects, when the solvent polarity is increased: unfolding of the polar chain and folding due to hydrophobic interactions between both porphyrin rings. For both meso-dimers we find the net effect of increasing solvent polarity to be unfolding.

6.6 CONCLUSIONS.

A simple exciton model can describe the effects of the dimer-conformation on spectral shifts and band-shapes. The excitonic interactions result in a shift and/or splitting of the dimer absorption bands w.r.t. the monomer position. There is semi-quantitative agreement of the experimental and calculated spectra.

Changing the polarity of the solvent influences the folding or unfolding of the dimer. From our experiments can be concluded that TTP dimers have a tendency to fold in more polar solvents, whereas the meso-dimers are unfolding. Both the structure and solvent polarity affect the average orientation and angular distribution of the porphyrin macrocycles w.r.t each other. This is in agreement with other experimental results /38,39/.

6.7 ACKOWLEDGEMENT.

We thank dr. K. Ichimura for his generous gift of the meso-dimers, and dr. M.R. Wasielewski for the phenyl bridged dimer.

This investigation was partly supported by the Netherlands Foundation for Chemical Research (S.O.N.) with financial aid from the Netherlands Organization for the Advancement of Pure Research (Z.W.O.).

6.8 REFERENCES.

1. K. Sauer, in Bioenergetics of photosynthesis, Govindjee (ed.), (Academic Press, New York, 1975), Ch. 3.
2. F.K. Fong and V.J. Koester, Biochim.Biophys.Acta, 423 (1976) 52-64.
3. V.J. Koester and F.K. Fong, J.Phys.Chem., 80 (1976) 2310-2312.
4. L.L. Shipman, T.M. Cotton, J.R. Norris and J.J. Katz, Proc.Natl.Acad.Sci. USA, 73 (1976) 1791-1794.
5. F.K. Fong, V.J. Koester and J.S. Polles, J.Am.Chem.Soc., 98 (1976) 6406.
6. M.R. Wasielewski, U.H. Smith, B.T. Cope and J.J. Katz, J.Am.Chem.Soc., 99 (1977) 4172.
7. H. Ogoshi and H. Sugimoto, Tetrahedron Lett., 2 (1977) 169.
8. C.K. Chang, M.-S. Kuo and C.-B. Wang, J.Heterocycl.Chem., 14 (1977) 943.
9. C.K. Chang, J.Heterocycl.Chem., 14 (1977) 1285.

10. M.R. Wasielewski, W.A. Svec and B.T. Cope, J.Am.Chem.Soc., 100 (1978) 1961.
11. J.P. Collman, C.M. Elliot, T.R. Halbert and B.S. Tovrog, Proc.Natl.Acad.Sci. USA, 74 (1977) 18-22.
12. N.E. Kagan, D. Mauzerall and R.B. Merrifield, J.Am.Chem.Soc., 99 (1977) 5484.
13. C.K. Chang, Adv.Chem.Ser., 173 (1979) 162-177.
14. T.L. Netzel, P. Kroger, C.K. Chang, I. Fujita and J. Fajer, Chem.Phys.Lett., 67 (979) 223-228.
15. T.L. Netzel, M.A. Bergkamp, C.K. Chang and J. Dalton, J.Photochem., 17 (1981) 451.
16. M.A. Bergkamp, J. Dalton and T.L. Netzel, J.Am.Chem.Soc., 104 (1982) 253-259.
17. I. Fujita, T.L. Netzel, C.K. Chang and C.-B. Wang, Proc.Natl.Acad.Sci. USA, 79 (1982) 413-417.
18. T.L. Netzel, M.A. Bergkamp and C.K. Chang, J.Am.Chem.Soc., 104 (1982) 1952-1957.
19. M.A. Bergkamp, C.K. Chang and T.L. Netzel, J.Phys.Chem., 87 (1983) 4441-4446.
20. M.R. Wasielewski, M.P. Niemczyk and W.A. Svec, Tetrahedron Lett., 23 (1982) 3215-3218.
21. R.R. Durand, C.S. Bencosme, J.P. Collman and F.C. Ansom, J.Am.Chem.Soc., 105 (1983) 2710-2718.
22. R.R. Bucks and S.G. Boxer, J.Am.Chem.Soc., 104 (1982) 340-343.
23. F. Gueckel, D. Schweitzer, J.P. Collman, S. Bencosme, E. Evitt and J. Sessler, Chem.Phys., 86 (1984) 161-172.
24. J.S. Connolly, in Photochemical conversion and storage of solar energy, part A, J. Rabani (ed.), (The Weizmann Science Press of Israel, 1982), p. 175-204.
25. S.G. Boxer and G.L. Closs, J.Am.Chem.Soc., 98 (1976) 5406.
26. M.R. Wasielewski, M.H. Studier and J.J. Katz, Proc.Natl.Acad.Sci. USA 73 (1976) 4282-4286.
27. F.P. Schwartz, M. Gouterman, Z. Muljiani and D.H. Dolphin, Bioinorg.Chem., 2 (1972) 1-32.
28. J.A. Anton, P.A. Loach and Govindjee, Photochem.Photobiol., 28 (1978) 235-242.
29. R. Selensky. D. Holten, M.W. Windsor, J.B. Paine III, D. Dolphin, M. Gouterman and J.C. Thomas, Chem.Phys., 60 (1981) 33-46.

30. R.E. Overfield, A. Scherz, K.J. Kaufmann and M.R. Wasielewski,
J.Am.Chem.Soc., 105 (1983) 5747-5752.
31. P. Krausz and C. Gianotti, J.Chim.Phys., 80 (1983) 299-303.
32. B.S. Sudhindra and J.-H. Fuhrhop, Int.J.Quant.Chem., 20 (1981) 747-753.
33. R.G. Little, J.Heterocycl.Chem., 15 (1978) 203-208.
34. P. Maillard, S. Gaspard, P. Krausz and C. Gianotti,
J.Organomet.Chem., 212 (1981) 185-191.
35. M. Okamoto, N. Oishi, Y. Nishida and S. Kida, Inorg.Chim.Acta,
64 (1982) L217.
36. K. Ichimura, Chem.Lett., (1977) 641-644.
37. K. Ichimura and S. Takeuchi, Heterocycl., 1 (1978) 96.
38. L. Benthem, R.B.M. Koehorst, L.H. de Graaff and T.J. Schaafsma,
to be published
Chapter 4 of this thesis.
39. L. Benthem, R.B.M. Koehorst and T.J. Schaafsma,
to be published
Chapter 5 of this thesis.
40. M. Kasha, in Spectroscopy of the excited state, B. Di Bartolo (ed.),
(Plenum Press, New York, 1976), p. 337-363
and references therein.
41. M. Kasha, H.R. Rawls and M. Ashraf El-Bayoumi,
in Molecular Spectroscopy VIII, (IUPAC, Butterworths, London, 1965),
p. 371-392
42. R.P. Hemeger, J.Chem.Phys., 66 (1977) 1795.
43. M.Z. Zgierski, Chem.Phys.Lett., 21 (1973) 525.
44. W.T. Simpson and D.L. Peterson, J.Chem.Phys., 26 (1957) 588.
45. M.R. Philpott, J.Chem.Phys., 53 (1970) 968.
46. R.L. Fulton and M. Gouterman, J.Chem.Phys., 41 (1964) 2280.
47. L.L. Shipman and J.J. Katz, J.Phys.Chem., 81 (1977) 477.
48. L.L. Shipman, J.R. Norris and J.J. Katz, J.Phys.Chem., 80 (1976) 877.
49. N.S. Hush and L.S.Woolsey, Mol.Phys., 21 (1970) 465.
50. K.A. Zachariasse and D.G. Whitten, Chem.Phys.Lett., 22 (1973) 527.
51. C.W. Tang and A.C. Albrecht, J.Chem.Phys., 62 (1975) 2139.
52. F.J. Kampas and M. Gouterman, L.Lumin., 14 (1976) 121.
53. M. Gouterman, D. Holten and E. Lieberman, Chem.Phys., 25 (1977) 139-153.
54. G.D. Dorough, J.R. Miller and F.M. Huennekens,
J.Am.Chem.Soc., 73 (1951) 4315-4320.
55. M. Gouterman, J.Mol.Spectr., 6 (1961) 138-163.

56. C. Rimington, S.F. Manson and O. Kennard, Spectrochim.Acta, 12 (1958) 65.
57. C.B. Storm and Y. Teklu, J.Am.Chem.Soc., 94 (1972) 1745-1747.
58. P. Stilbs and M.E. Moseley, J.C.S. Faraday II, 76 (1980) 729-731.
59. H.-H. Limbach and J. Henning, J.Chem.Phys., 71 (1979) 3120-3124.
60. R.J. Abraham, A.H. Jackson, G.W. Kenner and D. Warburton, J.Chem.Soc., (1963) 853-862.
61. S.J. Silvers and A. Tulinsky, J.Am.Chem.Soc., 89 (1967) 3331-3337.
62. A.D. Adler, F.R. Longo, J.D. Finarelli, J. Goldmacher, J. Assour and L. Korsakoff, J.Org.Chem., 32 (1967) 476.
63. J.P. Collman, A.O. Chong, G.B. Jameson, R.T. Oakley, E. Rose, E.R. Schmittou and J.A. Ibers, J.Am.Chem.Soc., 103 (1981) 516-533.

APPENDIX I

THE FLUORESCENCE FADING METHOD

For a theoretical description of the fluorescence fading method (FF), we consider the ground state (S_0) and the first excited singlet (S_1) and triplet (T_0) state. Even when a molecule is excited into Soret-states, it is not necessary to include the population of these states into the kinetic model, since their lifetime is very short w.r.t. the lifetime of the S_0,S_1 and T_0 states.

The rate equations for the S_0 and S_1 state are respectively:

$$\dot{S}_0 = - k_e S_0 + k_f S_i + k_T T_0 \qquad (1a)$$

$$\dot{S}_1 = k_e S_0 - (k_f + k_{ISC}) S_1 \qquad (1b)$$

The kinetic constants are defined in fig. A. The total number of molecules (N) is given by:

$$N = S_0 + S_1 + T_0 \qquad (2)$$

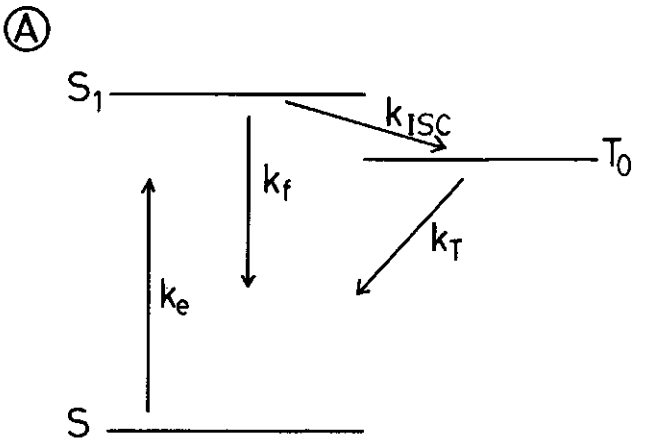

The response of the fluorescence intensity to an excitation step can be obtained by solving the rate equations (1a) and (1b) and using the relation (2). This results in:

$$\ddot{S}_1 + (k_e + k + k_T)\dot{S}_1 + [\,k_e(k_{ISC} + k_T) + k_T k\,]S_1 - k_e k_T N = 0 \qquad (3)$$

with $k = k_f + k_{ISC}$. The general solution of eqn. (3) is:

$$S_1(t) - S_1(\infty) = A \exp(r_1 t) + B \exp(r_2 t) \qquad (4)$$

where $r_1 = - k - k_e(1 - \phi_T)$ (5a)

$$r_2 = k_T - k_e\phi_T \qquad (5b)$$

and $A = (r_1 - r_2)^{-1}(k_e N + r_2 S_1(\infty))$ (6a)

$$B = -(r_1 - r_2)^{-1}(k_e N + r_1 S_1(\infty)) \qquad (6b)$$

The roots r_1 and r_2 represent approximate solutions, retaining only terms linear in the excitation rate k_e, which is assumed to be small w.r.t. $k_f + k_{ISC}$; the triplet quantum yield $\phi_T = k_{ISC}/k$. The constants A and B are obtained from the boundary condition $S_1(0) = 0$ and $\dot{S}_1(0) = k_e N$. Noting that in general $r_1 >> r_2$, eqn. (4) can be transformed into:

$$S_1(t) = k_e N k^{-1}\,[\,1 - \exp(r_1 t) - k_e k_{ISC} k^{-1} k_T^{-1}\,\{1 - \exp(r_2 t)\}] \qquad (7)$$

In steady state it follows that:

$$T_0(\infty) = S_1(\infty)\, k_{ISC} k_T^{-1} \qquad (8a)$$

and $S_1(\infty) = k_e N k^{-1}$ (8b)

Converting $S_1(t)$ into $I_f(t)$ - the fluorescence intensity - by $I_f = k_f S_1 = \phi_f k S_1$, where ϕ_f is the fluorescence quantum yield, eqn. (7) takes the convenient form:

$$I_f(t) = k_e N \phi_f\,[\,1 - \exp(r_1 t) - \frac{T_0(\infty)}{N}\,\{1 - \exp(r_2 t)\}] \qquad (9)$$

Eqn. (9) reveals the presence of two different processes: i) a rapid rise of the fluorescence to a steady state level, due to populating of S_1 immediately after the onset of excitation, i.e. in a time interval $k^{-1} < t < k_T^{-1}$, ii) a much slower decrease of $I_f(t)$, due to populating T_0 - referred to as 'fluorescence fading'. Assuming $k >> k_T$, we choose to ignore the first process for $I_f(t)$, i.e. we choose the time interval such

that it only refers to process ii), implying that effectively t = 0 somewhere in the interval $k << t < k_T$. Then, eqn. (9) can be rewritten as:

$$I_f(t) = I_f(0) \left[1 - \frac{T_0(\infty)}{N} \{1 - \exp(r_2 t)\} \right] \quad (10)$$

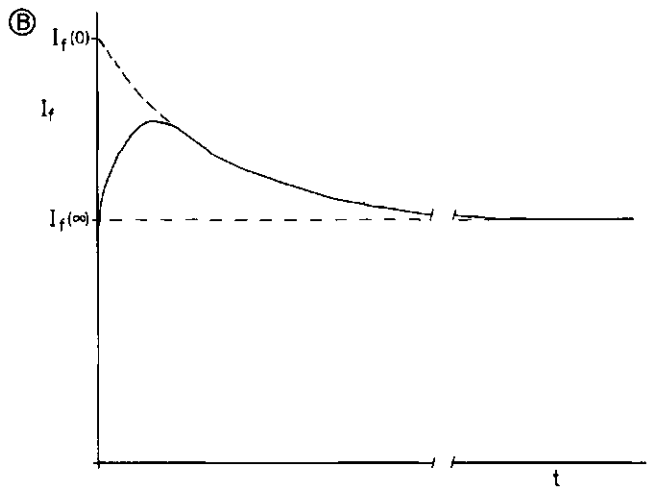

where $I_f(0)$ is the fluorescence intensity, found by extrapolating the fluorescence fading curve to t = 0 (see fig. B). From eqn. (10) we obtain now two important results:

$$I_f(t) - I_f(\infty) = [I_f(0) - I_f(\infty)] \exp(r_2 t) \quad (11)$$

$$\frac{I_f(\bar{0}) - I_f(\infty)}{I_f(0)} = T_0(\infty)/N \quad (12)$$

These results are a simplified version of those obtained by Avarmaa/1/.

By combining eqns. (8a) and (8b), it can be easily seen that r_2 in eqn. (5b) can also be written as:

$$r_2 = - k_T \left[1 - \frac{T_0(\infty)}{N} \right] \quad (13)$$

at low excitation rates. Thus, the true molecular triplet decay rate k_T can be simply obtained from the experimental FF curve by subtracting a fraction $\frac{T_0(\infty)}{N}$ from the measured value of r_2. This fraction also represents the experimental fractional decrease of the fluorescence intensity

from its initial to its steady state value, due to transfer of molecules to T_0 during excitation.

A similar treatment as given above applies to the case, where we take into account the presence of three sublevels in T_0. Now the $I_f(t)$ curve contains the roots $k_i + \phi_T^i k_e$ (i = x,y,z), analogous to (5b). The amplitudes of these three roots in $I_f(t)$ in fact are a direct measure for the corresponding steady state populations $n_i(\infty)$. However, the decay constant of a particular triplet sublevel cannot be determined from the FF curve, if it does not carry any population, e.g. because ϕ_T for that level is close to zero.

REFERENCE.

1. R. Avarmaa, Mol.Phys., 37(1979)441-454.

APPENDIX 2

TRIPLET DECAY IN THE PRESENCE OF TRIPLET-TRIPLET ENERGY TRANSFER

For a homodimer we have an energy level scheme as shown in fig. A.

Ⓐ

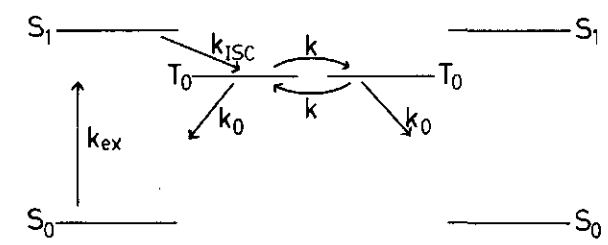

Ⓑ

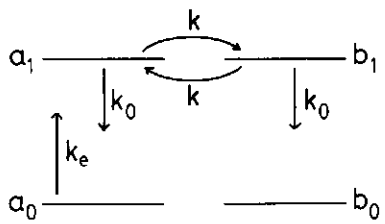

In the presence of a finite Stokesshift between the 0-0 absorption- and fluorescence maxima, energy transfer can only be endothermic and thus singlet-singlet energy transfer is highly improbably between both units. It is further assumed that the triplet exciton splitting is much smaller than the zero field splitting, since the oscillator strength of the S_0 - T_0 transition is very small. The hopping rate for triplet excita-

tion between both halves of the [illegible]

SUMMARY.

Tetraphenylporphyrin (TPP) molecules have been linked together to form dimers, using two positions of the phenyl groups at which the linking chain, which consisted mostly of 5 atoms, is attached (ortho or para position). The resulting dimers have different relative orientations of the porphyrin macrocycles w.r.t. each other and different centre-to-centre distances. Using standard procedures, metal ions have been inserted into the porphyrin ring; depending on the type of experiment different metal ions have been chosen. This thesis describes the effect of varying the geometry of these dimers on singlet-singlet energy transfer, excitonic- and spin-spin interaction and triplet state parameters.

Using the optically detected magnetic resonance technique and the fluorescence fading method, the zero field splitting parameters (D and E) and the kinetic constants of the lowest excited triplet state have been determined for homo-dimers of the free base $(H_2TPP)_2$, of the zinc-compound $(ZnTPP)_2$ and for mixed dimers. These triplet state parameters can be compared with the results for both monomers. It is found that for the homodimers the results are the same as for the corresponding monomers. Also, no singlet-singlet energy transfer is observed, due to a very small overlap of the fluorescence and absorption spectra. For the mixed dimers we find the same triplet state parameters as for H_2TPP, due to efficient singlet-singlet energy transfer (vide infra). From our results it can be concluded that the triplet states of both macrocycles in a TPP dimer can be considered as isolated from each other. This is not unexpected, since the triplet excitonic interaction is predicted to be small, due to the small S_0-T_0 oscillator strength. Thus triplet-triplet energy transfer is unlikely to occur. Triplet excitonic interactions are expected to be observable by magnetic resonance techniques for much shorter distances between both porphyrin rings, than occur in our dimers.

The average distance between the centres of both porphyrin macrocycles can be determined, using the spin-spin interaction between two paramagnetic ions, inserted into each of the porphyrin rings. This interaction is observable as a broadening in the solid state EPR powder spectra of Cu-Cu dimers. From these measurements the distances between ring centres in apolar solvents can be determined as: para-para (p,p) dimer 2.7, ortho-para (o,p) dimer 2.2 and ortho-ortho

(o,o) dimer 2.1 nm. In polar solvents the relatively apolar porphyrin macrocycles are forced together, resulting in a shorter ring-ring distance. Steric hindrance of the phenyl groups can prevent this folding, however, for some of the dimers. The results obtained by this method are in good agreement with the distances derived from space filling models. It can also be concluded that an endo-conformation (cofacial) for the o,o dimer is highly unlikely and that the preferential orientation is the exo-conformation, a situation very similar to the p,p dimer. These results are also confirmed by NMR measurements.

We have performed a theoretical analysis of excitonic interaction on the Soret absorptionband. From this analysis, taking into account the presence of proton tautomers in free base porphyrin monomers and -dimers, the energy level shifts are determined as a function of the rotational angle around the linking chain. Comparing the theoretical and experimental data, the preferential orientation, determined from the shift and/or splitting of the absorption band, and the rotational angular distribution, determined by the bandwidth w.r.t. that of the monomer, can be found. For the p,p dimer the porphyrin macrocycles are approximately coplanar with a narrow orientational distribution; the o,o dimer has an exo-conformation and also coplanar macrocycles with a very narrow angular distribution. For the o,p dimer the result is an average perpendicular position of the porphyrin rings, but with a large rotational freedom. Because of steric effects of the bulky phenyl groups the spread in rotation does not extend over the full 2π range.

In covalently linked metal porphyrins, containing two different metal ions or consisting of a mixed metallo-free base porphyrin, singlet-singlet energy transfer occurs. We have analyzed S-S energy transfer between the zinc-containing and free base moieties in TPP dimers by emission spectroscopy and fluorescence kinetics. From fluorescence and fluorescence-excitation spectra the energy transfer efficiency, the rate of energy transfer, the lifetime of the donor fluorescence and the donor-acceptor distance can be calculated and compared with the results from fluorescence decay experiments. Both sets of values are in very good agreement. The donor-acceptor distance is also in agreement with the distance found by other methods. For the dimers the energy transfer rate constant is $\tilde{}$ 2 magnitudes higher than that for intersystem crossing and the fluorescence decay, corresponding to an energy transfer efficiency of $\tilde{}$ 85%. The energy transfer rate constant is dependent on $\langle r^{-6} \rangle$, as well as on the relative orientation of the transition dipole moments. Due to the perpendicular position of both porphyrin macrocycles in the o,p dimer the energy transfer rate constant is lower than in the p,p dimer, although the distance between both rings is much shorter.

From all measurements, it can be concluded that the properties of the singlet and triplet states of the o,o dimer, are very similar to those of the p,p dimer, apart from the distance effect. The o,p dimer has in some cases a different behaviour, due to the different position and orientation of the porphyrin macrocycles w.r.t. each other in comparison with the other two dimers.

The appendices contain the mathematical formalism for the fluorescence fading method (appendix 1) and triplet decay in the presence of triplet-triplet energy tranfer (appendix 2) are presented.

SAMENVATTING.

Dimeren van tetrafenylporfyrine (TPP) moleculen zijn gemaakt, door de brug, die meestal uit 5 atomen bestond, aan twee plaatsen van de fenylring te bevestigen (op de ortho of para plaats). De porfyrine-ringen in de zo ontstane dimeren hebben verschillende relatieve orientaties t.o.v. elkaar en verschillende ring-ring afstanden. Metallering van de ring vond plaats via standaard methodes; afhankelijk van het experiment zijn verschillende metaalionen gebruikt. Dit proefschrift beschrijft het effect van veranderingen in de geometrie van deze dimeren op singlet-singlet energie overdracht, exciton- en spin-spin interacties en de eigenschappen van de laagste triplet toestand.

Met de optisch gedetecteerde magnetische resonantie techniek en de 'fluorescence fading' methode zijn de nulveld splitsings parameters (D en E) en de kinetische constanten van de laagst aangeslagen triplet toestand van de homodimeren van de vrije base $(H_2\text{-TPP})_2$, de zinkverbinding $(Zn\text{-TPP})_2$ en van de gemengde dimeren ($ZnTPP\text{-}H_2TPP$). De resultaten zijn vergeleken met die van de beide monomeren. Er is gevonden dat voor de homo- dimeren de resultaten hetzelfde zijn als voor hun monomeren. Singlet-singlet energie kan worden verwaarloosd als gevolg van de geringe overlap van de fluorescentie- en absorptiespectra. De gemengde dimeren hebben dezelfde eigenschappen van de triplettoestand als het H_2TPP monomeer, als gevolg van efficiente singlet-singlet energie overdracht. Verder kan geconcludeerd worden dat de triplet toestanden van beide porfyrine ringen in een TPP dimeer van elkaar geisoleerd zijn. Dit is niet onbegrijpelijk, omdat de triplet exciton interactie klein verondersteld kan worden, als gevolg van de kleine $S_0 - T_0$ oscillator sterkte, zodat triplet-triplet energie overdracht onwaarschijnlijk is. Triplet exciton interacties kunnen met magnetische resonantie technieken pas worden waargenomen bij veel kleinere afstanden tussen de beide porfyrine ringen, dan in de in dit proefschrift beschreven dimeren.

De gemiddelde afstand tussen de middelpunten van beide porfyrine ringen kan bepaald worden uit de spin-spin interactie tussen twee paramagnetische ionen, die zich in de porfyrine ring bevinden. Deze interactie wordt waargenomen als een lijnverbreding van ESR poeder spectra van Cu-Cu dimeren. Uit deze metingen zijn in apolaire oplosmiddelen de volgende afstanden bepaald: para-para (p,p) dimeer 2.7 nm, ortho-para (o,p) dimeer 2.2 nm en ortho-ortho (o,o) dimeer 2.1 nm

In polaire oplosmiddelen wordt de gemiddelde afstand tussen de relatief apolaire porfyrine ringen kleiner. Sterische hindering van de fenylgroepen deze vouwing echter tegengaan. De verkregen resultaten komen goed overeen met de afstanden die in molecuul-modellen gevonden worden. Voor het o,o dimeer is tevens gevonden, dat de endo-conformatie ('sandwich'-struktuur) onwaarschijnlijk is en dat de voorkeursorientatie de exo-vorm (uitgevouwen struktuur) is; een situatie die erg veel lijkt op die van het p,p dimeer. Deze resultaten zijn door NMR metingen bevestigd.

Een theoretische analyse is gemaakt van de exciton interactie op de Soret absorptie band. Rekening houdend met de waterstof tautomeren in vrije base monomeren en -dimeren, zijn de verschuivingen van de energie niveau's als functie van rotatiehoek rond de bindingsketen bepaald. Vergelijking van de theoretische en experimentele resultaten levert de voorkeurs orientatie op, die uit de verschuiving en/of de splitsingven het maximum van de absorptie band wordt bepaald. De breedte van de distributie van de rotatiehoeken is gerelateerd aan de spectrale bandbreedte t.o.v. die van het monomeer. Voor het p,p dimeer liggen de porfyrine ringen ongeveer in een vlak met een smalle rotatie hoekverdeling; het o,o dimeer heeft een exo-vorm en evenwijdige ringen met vrijwel geen rotatievrijheid. Voor het o,p dimeer is het resultaat, dat de porfyrine ringen loodrecht op elkaar staan, maar een grote rotatie vrijheid hebben. Door sterische hindering van de fenyl groepen kan de rotatie niet geheel over 360° plaats vinden.

In covalent gebonden metaal porfyrines, die of twee verschillende metaal ionen bevatten of bestaan uit gemengde metaal-vrije base porfyrines vindt singlet-singlet energie overdracht plaats. De S-S energie overdracht is bestudeerd tussen het zink (II) en het vrije base gedeelte in een TPP dimeer m.b.v. emissie spectroscopie en door de fluorescentie-kinetiek. Uit de fluorescentie- en fluorescentie-excitatie spectra kan de efficientie en de snelheid van energie overdracht, de levensduur van de donor fluorescentie en de 'donor-acceptor' afstand berekend en vergeleken worden met de resultaten uit fluorescentie verval metingen. Er is goede overeenstemming gevonden. De hieruit berekende afstanden kloppen ook goed met die welke uit andere metingen verkregen zijn. Voor de dimeren blijkt de snelheidsconstante voor S-S van energie overdracht ongeveer 2 ordes groter te zijn dan de snelheidsconstante voor intersystem crossing en fluorescentie, overeen komend met een energie overdrachts efficientie van $\tilde{}$ 85 %. De snelheidscontante voor energie overdracht is evenredig met r^{-6} en afhankelijk van de relatieve orientatie van de overgangs dipoolmomenten. Als gevolg van de loodrechte stand van de beide porfyrine ringen in het o,p dimeer is de snelheid

van energie overdracht lager dan die in het p,p dimeer, hoewel de ring-ring afstand kleiner is.

Uit alle metingen volgt dat de eigenschappen van de singlet en triplet toestanden van het o,o dimeer in uitgevouwen vorm goed overeen komen met die van het p,p dimeer, afgezien van het afstandseffect. Het o,p dimeer heeft steeds een afwijkend gedrag door de andere stand van de ringen t.o.v. elkaar in vergelijking met de ander dimeren.

In de appendices zijn wiskundige afleidingen gegeven van de 'fluorescence fading' methode (appendix 1) en triplet verval in aanwezigheid van triplet-triplet energie overdracht (appendix 2).

NAWOORD.

Een proefschrift is zelden het werk van een enkele onderzoeker. Ook deze dissertatie is ontstaan uit de samenwerking van velen. Zonder de ongenoemden tekort te willen doen, wil ik enkele met name noemen.

In de eerste plaats Tjeerd Schaafsma; dank zij alle discussies, aanwijzingen voor nieuwe experimenten en verklaringen - waarvan soms de meest wilde - van waargenomen signalen en correcties op de tekst is dit boekje geworden zoals het er nu ligt.

Grote dank ben ik verschuldigd aan Rob Koehorst, door wiens synthetisch werk de metingen uitgevoerd konden worden aan goed gedefinieerde verbindingen. De vele mogelijkheden, die jij steeds opnieuw bood door weer andere, leuke en interessante stofjes te synthetiseren heb ik nooit volledig kunnen uitbuiten.

Arie van Hoek (voor het optische deel) en Adrie de Jager (voor het microgolfwerk) hebben er steeds weer voor gezorgd dat vele technische problemen werden opgelost.

Als hoofdvakstudenten hebben Leo van de Graaff en Jan Kielstra een aandeel in de metingen gehad. De resultaten van hun werk zijn voor een belangrijk deel in dit proefschrift terug te vinden.

Geoff Searle heeft vaak geholpen het modelwerk en het 'in vivo'-werk te vergelijken.

Alle (oud-) medewerkers van de vakgroep Moleculaire Fysica dank ik voor alle wetenschappelijke en/of sociale contacten.

De firma Gardner in Vilvoorde (Belgie) zorgde voor een vrijwel onberispelijke aanvoer van vloeibaar helium, zonder welk de meeste experimenten onmogelijk zouden zijn.

De instrumentmakerij o.l.v. Hennie van Beek, Alfred van Baren en zijn staf voor het fotowerk en alle anderen, die hun steentje (groot of klein) voor dit boekje hebben aangedragen verdienen veel dank.

De afdeling tekstverwerking van de LH dank ik voor het camera-ready maken van mijn eigen ruw aangeleverde tekstfiles.

Tot slot, Lyda bedankt voor alle rust en hulp gedurende deze bijna vijf jaar, je hebt tot het eind toe geprobeerd de essentie van het werk te begrijpen, misschien dat het m.b.v. de samenvatting toch gelukt is. Marco en Rob, bedankt voor

je afleiding, hoewel jullie eerste levensjaar mij soms wel wat erg ver van de wetenschap hield. De medewerkers van de afd. Neonatologie van het Sint Radboud Ziekenhuis te Nijmegen hebben in de eerste helft van 1982 voor ons veel betekend.

Het in dit proefschrift beschreven onderzoek werd ondersteund door de Stichting Scheikundig Onderzoek Nederland (SON) met financiele steun van de Nederlandse Organisatie voor Zuiver Wetenschappelijk Onderzoek (ZWO).

CURRICILUM VITAE.

Lambertus Benthem werd op 4 december 1953 te Groningen geboren. In 1971 behaalde hij het HBS-B diploma aan de Scholengemeenschap 'Kamerlingh Onnes' te Groningen. In datzelfde jaar begon hij de studie scheikunde aan de Rijks Universiteit te Groningen. Na het afleggen van het kandidaatsexamen S1 in april 1975, begon hij aan z'n hoofdvakstudie o.l.v. prof. dr. D.A. Wiersma bij het laboratorium voor Fysische Chemie. Het onderzoek (dat tot een publicatie leidde) betrof een ODMR en ENDOR studie aan p-benzochinon, en werd onder de directe begeleiding van drs. J.H. Lichtenbelt uitgevoerd. Tevens werd een scriptie gemaakt over het onderwerp 'Supersone moleculaire bundels'. Voor van het bijvak Sterrenkunde werd een 6-maands theoretisch onderzoek gedaan aan planetaire nevels. Tijdens zijn studie was hij gedurende 2 jaar voor 3/10 weektaak in dienst van de R.U. Groningen als student-assistent op het praktikum Fysische Chemie. Het doctoraalexamen (met onderwijsbevoegdheid in de natuur- en scheikunde) werd afgelegd op 24 april 1979.

Op 1 december 1979 trad hij voor een periode van 4 jaar in dienst bij de Nederlandse Organisatie voor Zuiver Wetenschappelijk Onderzoek Z.W.O. (Stichting Scheikundig Onderzoek Nederland) en werd tewerk gesteld bij de vakgroep Moleculaire Fysica van de Landbouw Hogeschool te Wageningen. Naast het in dit proefschrift beschreven onderzoek was hij nauw betrokken bij het praktikum Chemische Binding en verzorgde gedurende 3 jaar het college 'Principes van Straling'. Tevens maakte hij gedurende 3 jaar deel uit van het vakgroepbestuur.

VERANTWOORDING.

INLEIDING.

Wie de resultaten van een aantal jaren wetenschappellijk werk in de vorm van een proefschrift publiceert heeft vaak een enorm communicatieprobleem met 'leken'. Het blijkt dat er een wijde kloof bestaat tussen de vragen van de wetenschapper en die van de hem omringende wereld. Dit geldt vooral voor het wetenschappelijk onderzoek in de zogenaamde exacte vakken. Een scheikundige bijvoorbeeld die afgestudeerd is in de fysische chemie, loopt al snel tegen dit probleem aan. Voor zijn omgeving is een scheikundige - of die nu wetenschappelijk gevormd is of niet - iemand die stofje A bij stofje B doet om zodoende een nieuw stofje C te kunnen maken, terwijl een fysisch-chemicus eigenlijk veel meer natuurkunde bedrijft. Omdat dit beeld onvolledig is wil ik proberen om in deze samenvatting de problemen, waar ik mij zo'n vier jaar mee heb bezig gehouden, iets meer te verduidelijken voor hen die niet op dit onderzoeksterrein thuis zijn.

Voor het gemak is aan het eind van dit stukje tekst een verklarende woorden- en begrippen lijst opgenomen.

LICHT EN MOLEKULEN.

De ons omringende natuur demonstreert heel duidelijk de wisselwerking tussen licht en planten. In het voorjaar, als de lichtintensiteit toeneemt krijgt een plant groene bladeren en begint te groeien. In de herfst worden de bladeren bruin en vallen vervolgens af. De groei van de plant zal nu vertragen of stopt zelfs geheel. Zouden we een plant helemaal geen licht meer geven, dan sterft deze zelfs af. Maar wat gebeurt er nu precies? Laten we een groen blad eens onder een steeds sterker vergrotende microscoop leggen (voor zover dat in de laatste stappen mogelijk zou zijn). Allereerst zien we een wirwar van nerven en vervolgens talloze celletjes. Elk van die celletjes bestaat weer uit verschillende onderdelen en deze celonderdelen blijken tenslotte weer opgebouwd te zijn uit verschillende molekulen. Wat is nu een molekuul van bijvoorbeeld water; dit is

de kleinste hoeveelheid (= deeltje), dat nog net water is. En wat is dan licht? Ook dat blijkt, als je het heel nauwkeurig gaat bekijken, samengesteld te zijn uit verschillende deeltjes, fotonen genaamd. Elke kleur licht is zo een ander soort foton. Nu kennen we allemaal het zichtbare licht, maar er zijn ook soorten onzichtbaar 'licht', zoals bijvoorbeeld radiostraling en rontgenstraling, dat eveneens uit verschillende soorten fotonen bestaat. De wisselwerking van een groen blad met licht is dus bij nadere beschouwing een wisselwerking van fotonen en molekulen.

Verschillende kleuren licht bestaan uit fotonen met een verschillende energie-inhoud. Zo is ultra-violet licht bijvoorbeeld veel energie-rijker en daardoor veel schadelijker voor mens en dier dan rood licht, dat op zijn beurt weer veel energie rijker is dan radiostraling. Een molekuul is een bouwwerk van een heleboel elektrisch geladen deeltjes (atoomkernen en elektronen). Het is niet een rotsvast bouwwerk, maar de verschillende deeltjes zijn onderling in beweging, sommige meer, andere minder. Desondanks blijft het wel een geheel. Het blijkt nu dat zo'n molekuul ook een bepaalde energie-inhoud heeft. Elk molekuul bezit een bepaalde toestand waarin het zich het liefste bevindt. Dit is de toestand waarin de geladen deeltjes zo ten opzichte van elkaar 'zitten' en bewegen, dat de energie-inhoud van het molekuul zo klein mogelijk is. Dit noemen we de grondtoestand. Er zijn echter veel meer toestanden. Elke verschillende manier van bewegen van de geladen deeltjes heeft een hogere energietoestand van het molekuul tot gevolg. Zo'n hogere energie-toestand heet een aangeslagen toestand. Het verschil tussen de grond- en aangeslagen toestand is dus een energie verschil. Normaal bevindt het molekuul zich in de grondtoestand, maar als er nu een foton opvalt met een energie-inhoud (=kleur) die precies past bij het energie verschil tussen de grond- en aangeslagen toestand, dan raakt het molekuul uit zijn gewone doen: het molekuul kan dit foton absorberen. Het foton houdt dan op te bestaan en het molekuul komt in een aangeslagen toestand. De energie van het licht is dus door het molekuul opgenomen.

Dit is nu precies wat er in een groen blad van een plant gebeurt. De energie van het zonlicht wordt door de molekulen in het blad (de chlorofyl-molekulen) geabsorbeerd en deze energie wordt gebruikt om nieuwe bouwstoffen te maken zodat de plant kan groeien. Het blad is dus eigenlijk een chemische fabriek, die draait op licht. Dit proces, het omzetten van lichtenergie in energie die de plant in z'n fabriekje gebruikt, wordt de fotosynthese genoemd en is van levensbelang voor alle levende wezens op aarde. Het is dus erg belangrijk om te weten en te begrijpen wat er op molekulaire schaal gebeurt. Nu is de fotosynthese een erg ingewikkeld proces en daarom proberen we er eerst achter te komen, wat er in

modelsystemen gebeurt. We bestuderen in het laboratorium dus de wisselwerking van licht met een molekuul, dat ongeveer dezelfde eigenschappen heeft als chlorofyl, maar veel eenvoudiger van opzet is. We zouden dan natuurlijk een kristal kunnen nemen van ons modelmolekuul, maar dit leidt tot complicaties: de molekulen blijken niet als afzonderlijk te kunnen worden beschouwd, de molekulen hebben onderling wisselwerkingen met elkaar die we nu juist niet willen onderzoeken. Bovendien zijn in de natuur de molekulen ook niet zo regelmatig gerangschikt als in een kristal. We nemen daarom een oplosmiddel, waarin we een kleine hoeveelheid van onze modelmolekulen oplossen en deze sterk verdunde oplossing vriezen we in voor bepaalde soorten metingen, of we gebruiken de vloeibare oplossing bij kamertemperatuur. In deze oplossing kunnen we wel de wisselwerking van licht met ons modelmolekuul bestuderen. Sommige experimenten zijn bij kamertemperatuur gedaan, dezelfde temperatuur als waarbij een plant ook 'werkt', maar sommige experimenten hebben we bij zeer lage temperatuur uitgevoerd (-150 °C, -196 °C of zelfs -269 °C). Dit gebeurde om een paar redenen: I) in een oplossing bewegen de molekulen, terwijl we dat soms niet kunnen gebruiken en II) bij kamertemperatuur treden effecten op, die een meting geheel kunnen verstoren. De oplossing, of die zich nu in vaste of vloeibare vorm bevindt en waaraan de metingen worden gedaan, noemen we het monster.

Wat gebeurt er nu als we het modelmolekuul door bestraling met een bepaalde kleur licht in een aangeslagen toestand brengen. Er zijn dan verschillende manieren voor het molekuul, om weer naar de grondtoestand terug te keren. Het molekuul kan na een poosje hetzelfde foton weer uitzenden, dit heet emissie. Het raakt dan de extra energie weer kwijt, die in het foton gaat zitten en het molekuul keert terug naar de grondtoestand. Het molekuul kan de extra energie ook kwijt raken zonder een foton uit te zenden. Het heeft immers zeer veel verschillende aangeslagen toestanden die onderling een zeer klein energie verschil hebben. Vandaar dat het molekuul vanuit z'n aangeslagen toestand telkens in een lagere aangeslagen toestand kan komen door zijn energie beetje bij beetje af te staan. Dit is te vergelijken met een ladder; je kunt beneden komen door van de bovenste sport te springen maar ook door steeds een sport lager te gaan. De energie wordt op deze manier doorgegeven aan de buurmolekulen, die daardoor in een aangeslagen toestand komen die iets hoger in energie ligt dan de grondtoestand. Het monster wordt door dit proces een ietsje warmer.

EXPERIMENTEREN MET LICHT EN MOLEKULEN.

Hoe kunnen we nu experimenteel (dus door het doen van proeven) vaststellen welke aangeslagen toestanden ons molekuul precies heeft en wat er na het aanslaan ervan gebeurt. We sturen daarvoor licht door het monster en daarna valt het op een detector. Dit is een apparaat dat licht kan omzetten in een electrisch stroompje en met een recorder kunnen we het spectrum op papier tekenen.

Elke aangeslagen toestand van een molekuul kunnen we in een zeer eenvoudige beschrijving karakteriseren door een bepaalde trillingsfrequentie (dat is het aantal trillingen per seconde), want een aangeslagen toestand was niets anders dan het bewegen van de geladen deeltjes (dit zijn de trillingen) in het molek uul. Een bepaalde trillingsfrequentie komt dus overeen met de energie van de betreffende aangeslagen toestand. We spreken daarom in de praktijk vaak van de frequentie van de aangeslagen toestand. Zo kunnen we ook de kleur van het licht karakteriseren door een frequentie. Als we dus willen weten welke aangeslagen toestand ons molekuul heeft, moeten we eigenlijk bepalen welke frequenties van het licht passen bij ons molekuul. We laten daarom licht op ons molekuul vallen, waarvan we de frequentie langzaam veranderen, bijvoorbeeld van blauw naar rood. Zolang er in het monster niets gebeurt zal de stroom uit de detector niet veranderen en tekent de recorder een rechte lijn op het papier. Elke keer als een lichtfrequentie precies overeen komt met de frequentie van de aangeslagen toestand van het molekuul dan wordt er licht geabsorbeerd. De hoeveelheid licht (de intensiteit) wat de detector dan bereikt wordt eventjes minder, het recorderpennetje slaat naar een kant uit. Zijn we met de frequentie van het licht de frequentie van de aangeslagen toestand weer voorbij dan valt al het licht weer op de detector en het pennetje gaat weer naar zijn oorspronkelijke stand. We hebben nu een zogeheten absorptiespektum opgenomen en hieruit kunnen we de frequenties van de aangeslagen toestanden bepalen.

Met deze apparatuur kunnen we ook kijken naar de manier waarop het molekuul weer van de aangeslagen toestand naar de grondtoestand terug keert. We laten dan heel eventjes licht met precies de goede freqentie op het kristal vallen, zodat de molekulen in de aangeslagen toestand komen. Als het licht weer uit is, kan het molekuul het geabsorbeerde foton weer uitzenden. Dit kan in principe op elk willekeurig tijdstip gebeuren. Het kristal bevat echter vele miljarden modelmolekulen. Op elk moment nadat het opvallende licht is gedoofd, zijn er wel een paar die hun foton weer uitzenden. Dit worden er natuurlijk wel steeds minder, zodat de intensiteit van het uitgestraalde licht ook steeds minder wordt. Op de recorder zien we dan een hele snelle uitwijking en vervolgens keert het pennetje

weer langzaam naar de oorpronkelijke stand terug. Zo kunnen we meten hoe lang de molekulen er over doen om hun aanslag-energie weer kwijt te raken, ofwel hoe lang bevinden de molekulen zich in de aangeslagen toestand (de levensduur van de aangeslagen toestand).

We kunnen dus onze experimenten doen als funktie van de frequentie, d.w.z. door de frequentie te varieren en daarmee bepalen we de energie-inhoud van een aangeslagen toestand of als functie van de tijd ofwel hoe lang duurt het voor het molekuul weer in de grondtoestand is terug gekeerd.

Welke experimenten worden er in dit boekje beschreven. Behalve de al genoemde absorptie metingen wil ik nog een paar in detail bespreken.

ENERGIE OVERDRACHT.

We hebben gezien dat een molekuul een foton met een bepaalde frequentie kan absorberen en vervolgens dit foton weer kan uitzenden. Nu blijkt echter dat in het algemeen het uitgezonden foton een iets kleinere frequentie heeft dan het geabsorbeerde foton. In kleuren uitgedrukt: het uitgezonden foton is iets roder van kleur dan het geabsorbeerde foton. Stel nu dat er in ons monster zich nog een tweede, een ander soort modelmolekuul (B) bevindt dat een aangeslagen toestand heeft met een energie-inhoud die precies overeen komt met het uitgezonden foton van het eerste soort molekuul (A). Dit molekuul B zal dan in die aangeslagen toestand komen en na enige tijd weer terugvallen naar de grondtoestand onder uitzenden van weer een iets roder foton.

Dit proces, wat hier zeer simplistisch beschreven is en waarbij de extra energie van molekuul A wordt 'overgedragen' naar molekuul B heet energie overdracht. Wanneer we het monster nu belichten met licht met de frequentie van foton 1 en we zetten de detector zo dat deze alleen licht ziet met de frequentie van foton 2 dan kunnen we bepalen of er energie overdracht is en tevens de snelheid en efficientie hiervan.

Dit soort experimenten worden gedaan, omdat deze energie overdrachtsprocessen zich ook in een plantenblad afspelen. Het chlorofyl-molekuul neemt de energie uit het zonlicht op en geeft dit door aan molekulen die dit niet kunnen, maar die wel in staat zijn om de bouwstoffen te maken die de plant nodig heeft en dat is iets wat het chlorofylmolekuul weer niet kan. Met behulp van ons modelmolekuul kunnen we dus iets leren over dit soort processen.

FDMR OF ODMR EXPERIMENTEN.

Deze letters zijn de beginletters van de engelse termen voor fluorescentie gedetecteerde magnetische resonantie en optisch gedetecteerde magnetische resonantie. Als we nu het magnetisch resonantie deel eerst even weglaten, dan houden we over fluorescentie en optisch gedetecteerd. Optisch gedetecteerd wil zeggen: waarnemen (detecteren) van zichtbaar licht (optisch). We hebben gezien dat het molekuul naar de grondtoestand kan terug keren door het uitzenden van een foton en hebben dat emissie genoemd. Nu zijn er vele soorten emissies en een daarvan is de fluorescentie. Fluorescentie gedetecteerd is dus een nauwkeuriger gedefinieerde methode dan optisch gedetecteerd.

En dan het magnetisch resonantie deel. We weten al dat er vele aangeslagen toestanden zijn. Nu komen er ook groepjes van drie voor, die heel dicht bij elkaar liggen en dat noemen we een triplet toestand (tri = drie). Een triplet aangeslagen toestand is een beetje vreemd soort aangeslagen toestand. Een molekuul wil het liefst zo snel mogelijk terug keren naar de grondtoestand omdat hij zich daar het prettigste voelt. Een triplet toestand is voor een molekuul echter ook een redelijke toestand om in te verblijven en het zal dan ook relatief lang duren voordat het hieruit weer naar de grondtoestand zal terugkeren. Wel maakt het een heel klein beetje uit, uit welke het molekuul terugvalt, omdat er een klein verschil tussen de drie toestanden onderling is; het molekuul voelt zich in elke toestand niet even lekker.

De energie-inhoud van de drie toestanden verschilt maar een heel klein beetje van elkaar. Willen we nu van de ene naar de andere toestand gaan, dat kunnen we dit niet doen met zichtbaar licht omdat de frequentie hiervan veel te groot is. We hebben hiervoor 'licht' met een veel kleinere frequentie nodig en wel een vorm van radiostraling. Volgens het woordenboek is resoneren trillen. Als we nu de juiste frequentie radiostraling op ons monter laten vallen, dan zal het molekuul heel snel van de ene naar de andere toestand van het triplet gaan. Het trilt als het ware tussen twee van de drie toestanden heen en weer. Het soort

experimenten, waarbij we molekulen met behulp van radiostraling tussen twee toestanden laten trillen worden magnetische resonantie experimenten genoemd.

Hiermee hebben we de term FDMR verklaard, maar hoe werkt nu zo'n experiment. Voor het gemak verwaarlozen we het terugvallen naar de grondtoestand zonder het uitzenden van een foton; het proces waarbij het monster een ietsje warmer werd. We hebben al eerder gezien dat ons monster miljarden modelmolekulen bevat. We kijken dus nooit naar een molekuul maar naar zeer, zeer vele. Als we het monster nu continu belichten met de juiste frequentie licht, dan kunnen we de fluorescentie detecteren. De intensiteit hiervan heeft dan een bepaalde waarde (I_0). Echter een bepaald percentage molekulen zal geen foton uitzenden maar zal in de triplet toestand terecht komen. De intensiteit van de fluorescentie neemt hierdoor af tot de waarde I_1, omdat nu niet 100% van de aangeslagen molekulen fluoresceren, maar bijvoorbeeld slechts 75%. In de triplet toestand bevinden zich dan 25% van de aangeslagen molekulen, die slechts langzaam naar de grondtoestand zullen terugvallen en dan het spelletje weer van voren af aan gaan spelen.

Wat gebeurt er nu als we ook nog de juiste frequentie radiostraling op het kristal laten vallen, zodat het molekuul tussen twee van de drie toestanden van het triplet kan gaan trillen. De triplet toestanden hebben onderling een iets verschillende tijd nodig om naar de grondtoestand terug te vallen en door deze resonantie kan het terugvallen worden versneld of vertraagd, iets wat door het molekuul bepaald wordt. Nemen we even aan dat het proces versneld wordt. Dit betekent dan dat deze molekulen, die uit de triplet toestand komen eerder weer in de grondtoestand zullen zijn en dus ook weer eerder met zichtbaar licht kunnen worden aangeslagen, waarna ze weer de keus hebben tot fluorescentie of naar het triplet gaan. Gemiddeld in de tijd betekent dit, dat nu niet 75% van de molekulen fluoresceren maar bijvoorbeeld 78% en de fluorescentieintensiteit (I_2) neemt iets toe ten opzichte van I_1. Dezelfde redenatie kunnen we houden als het verval wordt vertraagd, alleen neemt I_2 nu iets af t.o.v. I_1.

In het kort komt een FDMR experiment dan op het volgende neer. We bestralen het monster met zichtbaar licht van de juiste frequentie om een groot gedeelte van de molekulen in een aangeslagen toestand te brengen en we detecteren vervolgens de fluorescentie-intensiteit. Hierna laten we varierende radiostraling op het kristal vallen. Op een gegeven moment past de radiostraling precies tussen twee van de drie toestanden van het triplet, d.w.z. het 'radiofoton' is net zo groot als het energie-verschil van twee toestanden van het triplet en we zien een af- of toename van de fluorescentieintensiteit. In principe kan dit drie keer gebeuren, omdat we drie mogelijkheden hebben om het molekuul tussen twee van de drie toestanden van het triplet te laten trillen. Op deze manier kunnen we bijvoorbeeld het energieverschil tussen de triplet toestanden bepalen.

FLUORESCENTIE DOVINGS METHODE.

We weten nu wat het energieverschil tussen de drie toestanden van het triplet is, maar we willen ook graag weten hoe snel een molekuul uit elk van deze toestanden terug valt naar de grondtoestand. Een van de methodes om dit te bepalen is de fluorescentie dovings methode. Bij de FDMR methode hebben we het monster continu met licht bestraald, maar wat gebeurt er als we het licht snel aan en uit zetten. Op het moment dat het licht aan gaat, brengen we de molekulen naar een aangeslagen toestand en onmiddelijk zal het molekuul o.a. via fluorescentie terugvallen. Deze fluorescentie gaan we detecteren. Als het licht uit gaat, vallen alle molekulen heel snel terug en de fluorescentie is direkt afgelopen. De fluorescentie zal dus ook aan en uit gaan met precies dezelfde frequentie en direkt nadat het eerste lichtfoton het molekuul bereikt heeft. De intensiteit van de fluorescentie blijkt echter niet constant te zijn, maar neemt af. Uit dit afnemen kunnen we met behulp van een computer via een wiskundige berekening de tijd bepalen die het molekuul gemiddeld in elk van de drie toestanden van het aangeslagen triplet verblijft.

Met behulp van deze fluorescentie dovings methode en de reeds eerder genoemde FDMR methode zijn we zo vrij veel omtrent de aangeslagen triplet toestanden te weten gekomen.

Waarom doen we nu dit soort experimenten? We hebben in een vorig stukje gezien dat er onder andere energie overdracht in een plant optreedt. Nu blijkt deze vorm van energie transport vaak te snel te verlopen om efficient te kunnen zijn en daarom moet het proces vertraagd worden. Nu we weten dat een triplet aangeslagen toestand stabieler is dan een gewone aangeslagen toestand kunnen we begrijpen dat veel van dit soort processen in planten via een triplet aangeslagen toestand blijken te verlopen. Op deze manier kan een plant, gedurende een korte tijd, energie bewaren tot hij het gebruiken kan.

RESULTATEN.

De meeste metingen, die in dit boekje beschreven zijn, zijn gedaan met een molekuul dat bestaat uit twee modelmolekulen van chlorofyl, die door een 'touwtje' aan elkaar zijn geknoopt. We noemen een dergelijk molekuul een dimeer en het normale modelmolekuul een monomeer. Nu waren we in staat om de verbindingstouwtjes op verschillende plaatsen aan het modelmolekuul vast te knopen en we hebben hierdoor drie dimeren, die erg veel gelijke eigenschappen hebben, maar

ook een paar verschillende. Het blijkt dat in deze dimeren de afstand tussen de twee modelmolekulen en hun onderlinge orientatie verschillend zijn. We hebben nu enkele van die eigenschappen gemeten, die van deze afstand en orientatie afhankelijk zijn, o.a. met de technieken die in dit stukje beschreven zijn. Op deze manier zijn we in staat geweest om zeer gedetaileerde informatie te verkrijgen over de orientatie van de beide modelmolekulen, hun onderlinge beweeglijkheid en hun exacte afstand. Het is gebleken dat dit soort dimeren beschouwd kunnen worden als zeer, zeer eenvoudige modellen voor het gehele fabrieksproces, dat we de fotosynthese hebben genoemd en met de resultaten uit dit onderzoek kunnen we het model weer wat uitbreiden zodat we de werkelijkheid weer wat dichter benaderen en het echte proces weer wat beter begrijpen.

VERKLARENDE WOORDEN- EN BEGRIPPENLIJST.

chlorofyl - molekuulsoort in plantenbladeren, die de energie uit het zonlicht kunnen opnemen.

detector - apparaat dat een hoeveelheid licht omzet in een elektrische stroom.

dimeer - molekuul, bestaande uit twee (di) gelijke eenheden.

emissie - uitzenden van fotonen door molekulen bij het terug vallen naar de grondtoestand.

energie overdracht - overdragen van extra energie van molekuulsoort A naar molekuulsoort B.

FDMR - fluorescentie gedetecteerde magnetische resonantie.

fluorescentie - een vorm van emissie, waarbij het molecuul zichtbaar licht uitzendt.

foton - 'lichtdeeltje', kan ook van een onzichtbare vorm licht zijn.

fotosynthese - proces in een plant, waarbij zonlicht wordt opgenomen, wordt doorgegeven en gebruikt voor de aanmaak van bouwstoffen.

frequentie - aantal keren per seconde, bijvoorbeeld van een trilling.

intensiteit - hoeveelheid van licht.

kristal - vaste toestandsvorm van onze modelmolekulen.

modelmolekuul - eenvoudig molekuul met ongeveer dezelfde te bestuderen eigenschappen als een interessant, maar veel ingewikkelder soort molekuul.

molekuul - kleinste hoeveelheid (=deeltje) van een stof, dat nog net alle eigenschappen van die stof heeft.

monomeer - molekuul, bestaande uit een (mono) eenheid; deze term wordt gebruikt als onderscheid van een dimeer.

monster - de 'oplossing' van molekulen, waaraan de experimenten dedaan worden.

ODMR - optisch gedetecteerde magnetische resonantie.

spektrum - grafiek, getekent als funktie van de frequentie, waarmee de energie-inhoud van aangeslagen toestanden t.o.v. de grondtoestand bepaald kunnen worden.

toestand

aangeslagen - hogere energie toestand van een molekuul.

grond- - laagste energie toestand van een molekuul.

trilingsfrequentie - aantal trillingen per seconde.

triplettoestand - toestand, die uit drie aangeslagen toestanden bestaat.